DOCTORAL SCHOOL
UNIVERSITA' *MEDITERRANEA* DI REGGIO CALABRIA

DIPARTIMENTO DI INGEGNERIA DELL'INFORMAZIONE, DELLE INFRASTRUTTURE E DELL'ENERGIA SOSTENIBILE (DIIES)

PHD IN
INFORMATION ENGINEERING

S.S.D. ING-INF/02
XXXIII CICLO

NEW APPROACHES TO PHASELESS INVERSE SOURCE PROBLEMS IN ELECTROMAGNETICS

CANDIDATE
GIADA MARIA BATTAGLIA
Giada M. Battaglia
ADVISOR
Prof. Tommaso ISERNIA
Tommaso Isernia
COORDINATOR
Prof. Tommaso ISERNIA
Tommaso Isernia

REGGIO CALABRIA, APRIL 2021

Finito di stampare nel mese di **Aprile 2021**

Edizione CSdA Centro Stampa d'Ateneo

Quaderno N. 47
Collana *Quaderni del Dottorato di Ricerca in Ingegneria dell'Informazione*
Curatore *Prof. Tommaso ISERNIA*

ISBN 978-88-99352-44-8

Università degli Studi *Mediterranea* di Reggio Calabria
Salita Melissari, Feo di Vito, Reggio Calabria

GIADA MARIA BATTAGLIA

NEW APPROACHES TO PHASELESS INVERSE SOURCE PROBLEMS IN ELECTROMAGNETICS

The Teaching Staff of the PhD course in
INFORMATION ENGINEERING
consists of:

Tommaso ISERNIA (coordinator)
Pier Luigi ANTONUCCI
Giuseppe ARANITI
Francesco BUCCAFURRI
Salvatore COCO
Giuseppe COPPOLA
Lorenzo CROCCO
Claudio DE CAPUA
Francesco DELLA CORTE
Dominique DALLET
Aimè LAY EKUAKILLE
Giuliana FAGGIO
Fabio FILIANOTI
Patrizia FRONTERA
Sofia GIUFFRE'
Giorgio GRADITI
Voicu GROZA
Antonio IERA
Tommaso ISERNIA
Gianluca LAX
Giacomo MESSINA
Antonella MOLINARO
Andrea Francesco MORABITO
Giacomo MORABITO
Rosario MORELLO
Domenico ROSACI
Giuseppe RUGGERI
Domenico URSINO

"It is difficult to say what is impossible,
for the dream of yesterday is the hope of today
and the reality of tomorrow."
Robert H. Goddard

Acknowledgment

At the end of my PhD studies, an unforgettable journey that I will bring forever in my heart, thanks are due to those people that have allowed the drafting of this thesis.

First of all, I would like to express my greatest gratitude to Prof. Tommaso Isernia for the opportunity to work in his research group. Thanks for his continuous support, for teaching me so many things, and instill values such as perseverance and the spirit of overcoming any challenge. His guidance has been fundamental for achieving the results described in this thesis.

I would also extend my thanks to Dr. Andrea Morabito, for his sweetness, patience, and support. He has been a fundamental point of reference for my professional growth from the beginning. I am extremely thankful to Dr. Roberta Palmeri, an exemplary colleague, who has always helped me, providing valuable advices from both professional and personal perspectives. In covering all the LEMMA Research Group, my sincere thanks also go to my colleagues, Dr. Martina Bevacqua and Eng. Sabrina Zumbo, for the time we spent together.

Last but not least, I am thankful to Dr. Gennaro Bellizzi, for the time he dedicated to me during the Master thesis. Working with him has been a great starting point.

These acknowledgments would not be complete without mentioning the great members of Chemistry's Laboratory, Francesco, Angela, Emilia, Andrea, Chiara, and Antonio. I spent nice moments with them. Thanks a lot for everything.

I would like to thank my family source of constant, sincere, and unconditional support and love in my life. Last but not least, a special thank goes to my special colleague

and friend, Jaskirat, for always being close to me when I need and for pushing me to believe in myself.

"Now, this is not the end. It is not even the beginning of the end. But it is, perhaps, the end of the beginning."

Abstract

This Thesis deals with phaseless inverse source problems in electromagnetics.

In antenna applications, phaseless inverse source problems are strictly related to *synthesis problems*. In this case, the data are not measurements, but they are represented by some given specifications or constraints on radiated fields.

A strictly related problem, which is also of interest in antenna applications, is the so-called *Phase Retrieval (PR) problem*, whose aim is that of characterizing a source, or at least its radiated field, from amplitude-only measurements, i.e., by discarding any phase information about field. While dealing with simpler instrumentation, the adoption of phaseless data makes the problem still harder with respect to more usual solutions.

Main results presented in this Thesis concern new approaches developed for both the *synthesis* and the *PR* problems. The formulated methodologies are innovative with respect to the state of the art for different reasons, including the capability to deal with a reduced number of (auxiliary) unknowns in electromagnetic field shaping problems, and the capability to deal with single-surface data (for the *PR* problem).

Theoretical results include a new way of thinking to the retrieval or synthesis of sources generating a given (or mask-constrained) power pattern which leads to new effective solution approaches. In particular, the proposed methodologies for the two types of problems share a common focus. In fact, all problems, being difficult to be solved, will be considered as an assembly of solutions of simpler problems.

Finally, the developed approaches and procedures are validated through numerical experiments, including applications to hyperthermia treatment planning, satellite, cellular telecommunications as well as to array antenna design and reflector antennas surface deformations diagnostics.

Contents

List of Figures

List of Tables

List of Acronyms

AEP	Active Element Pattern
CP	Convex Programming
DoF	Degrees Of Freedom
DRR	Dynamic Range Ratio
FDTD	Finite Difference Time Domain
FF	Far-Field
FOCO	FOcusing via Constrained Optimization
GLO	Global Optimization
HFSS	Ansys High Frequency Structure Simulator
IN-FOCO	INtensity FOcusing via Constrained Optimization
LP	Linear Programming
mf-FOCO	multi-frequency FOcusing via Constrained Optimization
mt-FOCO	multi-target FOcusing via Constrained Optimization
Nf	Near-Field
NMSE	Normalized Mean Square Error
OES	Orchard-Elliott-Stern
PR	Phase Retrieval
PSL	Peak Sidelobe Level
PTR	Peak-To-Trough
SAR	Specific Absorption Rate
SF	Spectral Factorization
SLL	Sidelobe Level
SNR	Signal-to-Noise Ratio
sp-FOCO	sparsity promoted FOcusing via Constrained Optimization
SVD	Singular Value Decomposition
T-SVD	Truncated Singular Value Decomposition
WL	Woodward and Lawson

1

A GENERAL INTRODUCTION

1 A little bit of terminology: ill-posedness and ill-conditioning

A problem is said to be well-posed according to Hadamard [12] if:

- a solution exists;
- the solution is unique;
- the solution depends continuously on the data of the problem.

If even one of the above conditions is violated, the problem is said to be *ill-posed*.

It makes no sense to look for a solution of an ill-posed problem (as it stands). In fact:

- if a solution does not exist, then what are we looking for?
- if the solution is not unique, then what is the meaning/reliability of what is found?
- if the solution does not depend continuously on data, small modifications of (measured) data will involve "jumps" in the solution, so that the final result which is found cannot be considered to be reliable.

Therefore, this implies a lack of physical meaning.

A further concept of interest is "ill-conditioning". A problem is said to be *ill-conditioned* when "small variations" on data can produce "large variations" in the solution of the problem.

Because of the inherent instability, the solution of an ill-conditioned problem may not have a physical meaning in case of errors on data, that are simply unavoidable when a measurement process is in order.

It is worth to note that whenever the problem is ill-posed or ill-conditioned, one needs some regularization of the problem [12]. Such a regularization occurs by defining and finding a "generalized solution" to the problem that is usually defined as the optimum of some ad-hoc introduced cost functional.

2 Inverse source problems: basics

The source problem can be faced by considering two types of problem, the *forward source problem* and the *inverse source problem*. The former deals with the evaluation of the radiated field given the electromagnetic properties of the source. The latter copes with retrieving a radiating source distribution from knowledge of the field it generates outside its region of localization [13].

The forward and the inverse source problems are linked each other by a sort of duality. In fact, one problem can be obtained from the other by exchanging the role of the data and that of the unknowns: the data of one problem are the unknowns of the other one conversely.

In the literature, the forward problem is the most investigated one and a lot of work has been done in developing more and more efficient numerical methods and computational techniques. Conversely, the inverse source problem has deserved less attention, probably because of its much increased difficulty. In fact, even assuming one knows both amplitude and phase at the radiated field, it is very challenging because of two different reasons, i.e., ill-posedness (according to the Hadamard's definition [12]) and ill-conditioning. Obviously, a strong effort has been done by research groups in developing effective solution strategies which counteract both ill-posedness and ill-conditioning in order to solve the inverse problem at best.

Finding solution methods that allow to accurately solve the problem is an important task in a lot of application fields. Among all possible applications involving inverse source problems, it is worth to mention some of the most relevant area, which are:

- antenna characterization and diagnostics. In general, the aim is to check the behavior of a generic antenna under test [14–16];
- discover not working elements of a radar array [17,18];
- discover (and correct) deformations in large radio-telescopes [19–21];

As already stated, inverse source problems are of course of interest also in antenna synthesis as well as in more generic "electromagnetic field shaping" problems [1–3]. The mathematical formulation of the inverse source problem is given in the Section which follows.

3 The amplitude and phase inverse source problem: basic equations, difficulties and tools

By the sake of simplicity, let us suppose to deal with homogeneous background and sinusoidal regime ($e^{j\omega t}$ is assumed and dropped). Then, for a generic 2-D (z-invariant) electric source $J_z(\underline{r})$ the field can be expressed as follows:

$$E_z(\underline{r}) = \int_{\Omega} g(\underline{r} - \underline{r}^{'}) J_z(\underline{r}^{'}) dr^{'} \tag{1}$$

wherein

$$g(\underline{r} - \underline{r}^{'}) = -\frac{\omega\mu}{4} H_0^{(2)} \left[k|\underline{r} - \underline{r}^{'}|\right] \tag{2}$$

is the "impulsive response" (or "Green Function") of the relation amongst sources and fields[1], $H_0^{(2)}$ represents the zero-order second kind Hankel function [12][2], and Ω is the support of the source.

It is worth to note that expression (1) can be recast as:

$$E_z(\underline{r}) = \mathcal{A}(J_z) \tag{3}$$

Consequently, the inverse source problems amount to invert a linear operator [12] in our 2-D geometry.

3.1 Singular Value Decomposition (SVD) of $\mathcal{A}$

One of the most fruitful tools in the theory of inverse problem is the SVD of a matrix and its extension to certain classes of linear operators. Indeed, SVD is basic both for understanding the ill-posedness of inverse problems, and for describing the effect of the regularization methods.

[1] It can be interpreted as a cylindrical wave emanating from $\underline{r}^{'}$.

[2] Bessel function of integer order n are solutions of differential equation $\frac{1}{r}\frac{d}{dr} r \frac{dB_n}{dr} + \left(1 - \frac{n^2}{r^2}\right) B_n = 0$ which exhibits two independent solutions: the Bessel function of the first kind $J_n(r)$ and of the second kind $Y_n(r)$. A linear combination of these two solutions leads to *Hankel* functions of first kind and second kind, respectively: $H_n^{(1)}(r) = J_n(r) + jY_n(r)$ and $H_n^{(2)}(r) = J_n(r) - jY_n(r)$. For large value of the argument, one can use these simplified expressions $H_n^{(1,2)}(r) = \sqrt{\frac{2}{\pi r}} e^{\left[\pm j\left(r - \frac{n\pi}{2} - \frac{\pi}{4}\right)\right]}$.

Let A be a compact operator[3] such that [12]:

$$f \in X \rightarrow g \in Y,\ i.e.,\ g = \mathcal{A}(f) \tag{14}$$

Then, the SVD of $\mathcal{A}$ is the triplet $\{u_n, \lambda_n, v_n\}$

$$\mathcal{A}(u_n) = \lambda_n v_n \tag{15.a}$$

$$\mathcal{A}^{+}(v_n) = \lambda_n u_n \tag{15.b}$$

where "+" represents the adjoint operator, the left-hand singular function $\{u_n\}$ are orthonormal in X; the right-hand singular function $\{v_n\}$ are orthonormal in Y, and singular values $\lambda_n \rightarrow 0$ as $n \rightarrow \infty$.

In particular, the *truncated SVD* (T-SVD) is considered as a method for regularization of ill-posed problems [12]. To introduce this concept, let's go back to equation (9).

Compute the image of a ball (i.e., an (hyper)ellipsoid) (see Fig. 1.5) in order to solve the forward problem, requires the truncation of n. This is because in any measurement process, one has a measurement error. Therefore, it is useless to look for a representation accuracy finer than measurement accuracy. In particular, instruments accuracy determine to which value of N one has to truncate the SVD representation. Such a value can be defined as the "essential dimension" of the field.

It is worth to note that determining N parameters requires at least N measurements, that are also sufficient to determine the required N parameters provided the relationship amongst measurements and parameters is not ill-conditioned. If the relationship is well behaved, N determine the minimum while non-redundant number of measurements to perform to get the required accuracy. Finally, bandlimitedness properties of the field suggest measurements through sampling will lead to accurate determination of the required parameters.

Since to solve the inverse problem it is necessary to follow the reverse chain (eq. (10)), even a vanishingly small measurement error may have a dramatic impact (see Fig. 1.1).

[3] An operator $\mathcal{A}$ is compact if it maps any bounded set of X into a set having a compact closure of Y.

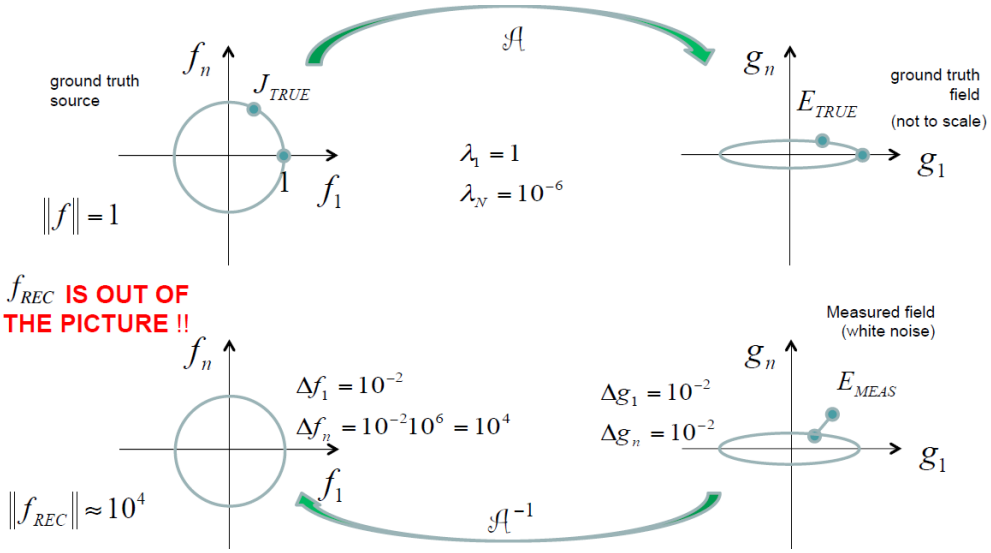

Fig. 1.1: Effect of a small measurement error on the reconstruction.

It is worth to note that for sufficiently large N, singular values decay exponentially fast. Moreover, for sources larger than a wavelength, and distances of at least a wavelength, singular values exhibit a step-like behavior.

Consequently, in case of 2-D sources enclosed in a circle with radius a, one has a "knee" around $M = 2ka$. Therefore, the larger the source, the steeper the knee. In particular, truncating to M the representation means to have an approximation error given by shaded area in Fig. 1.2, and it can be defined as the number of *Degrees of Freedom (DoF)* of the field on the considered observation surface. In fact:

- in case of larger value, it is useless to increase accuracy, as representation error is readily less than (any) measurement error;
- in case of lower value, it is wrong because possible significant variations of the field are lost.

In conclusion, we can summarize as follows:

- The inverse source problem is ill-posed because of the lack of uniqueness. In fact, 'non radiating sources' can exist, and there is no way to find them;
- The inverse source problem is also ill-posed because of the lack of continuity of solution with data. In fact, 'poorly radiating sources' having an ever increasing oscillating behavior imply an unbounded inverse;
- Because of the above, the discretized inverse source problem is ill-conditioned.

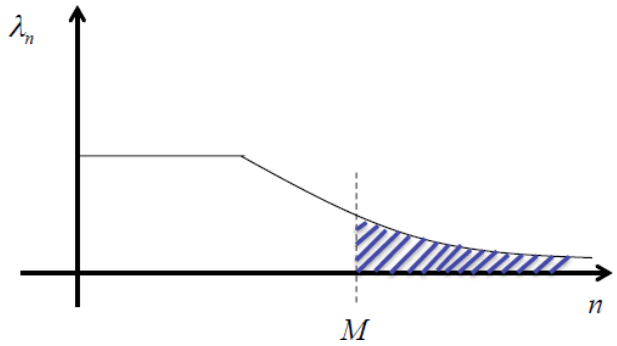

Fig. 1.2: The Degrees of freedom of radiated fields.

This is due to the fact that any source can be decomposed in terms of the "basis functions" $\{u_n\}$ (see Subsection 3.2):

$$J_z = \sum_{n=1}^{\infty} f_n u_n \tag{4}$$

and any radiated field can be decomposed in terms of the "basis functions" $\{v_n\}$:

$$E_z = \sum_{n=1}^{\infty} g_n v_n \tag{5}$$

where a simple relation hold true amongst f_n and the corresponding g_n coefficients. In fact:

$$E_z = \mathcal{A}(J_z) = \mathcal{A}\sum_{n=1}^{\infty} f_n u_n = \sum_{n=1}^{\infty} f_n \mathcal{A}(u_n) = \sum_{n=1}^{\infty} f_n \lambda_n v_n \tag{6}$$

This implies that:

$$g_n = \lambda_n f_n \tag{7}$$

Saying it in other words, the SVD setting "diagonalizes" the problem [12] (see Subsection 3.2). In fact:

- each u_n component only has an image $(\lambda_n v_n)$ onto v_n;
- each u_n source only produces a field $(\lambda_n v_n)$ of the kind v_n;
- each field v_n can be attributed to a source $\frac{1}{\lambda_n} u_n$.

Once the SVD of a radiation operator is known, in order to solve the forward problem is necessary to:

1. Decompose *J:z* into the left-hand singular functions

$$J_z = \sum_{n=1}^{\infty} < J_z, u_n > u_n = \sum_{n=1}^{\infty} f_n u_n \tag{8}$$

2. Compute the image

$$E_z = \sum_{n=1}^{\infty} \lambda_n f_n v_n = \sum_{n=1}^{\infty} g_n v_n \tag{9}$$

In the *inverse problem*, instead, one should follow the reverse chain, i.e., supposing one could define some "inverse" of $\mathcal{A}$:

$$J_z = \mathcal{A}^{-1} E_z = \sum_{n=1}^{\infty} \mathcal{A}^{-1} < E_z, v_n > v_n = \sum_{n=1}^{\infty} \mathcal{A}^{-1} g_n v_n = \sum_{n=1}^{\infty} \frac{g_n}{\lambda_n} u_n \tag{10}$$

But as $\lambda_n \to 0$, $\frac{1}{\lambda_n}$ is unbounded. Consequently, $\mathcal{A}^{-1}$ is also unbounded and not continuous, and the overall problem is *ill-posed* [12]. This is due to the so-called *non radiating sources* which cause the non-uniqueness of the solution (see Subsection 3.1).

Even not considering the ill-posedness (consequently, we assume that the non radiating sources are absent), the presence of the *poorly radiating sources* (see Subsection 3.1) makes the inverse source problem ill-conditioned. Therefore, by virtue of ill-posedness, measurement errors, and ill-conditioning, every attempt to get the truth is doomed to failure.

In this case, recovering some information on the source is much better than just knowing nothing. So, the basic idea is to just look for the source components which can be correctly (or almost correctly) retrieved.

3.2 Inverse source problems: difficulties

It is worth to note that two main difficulties about the inverse source problem:

1. the so-called *non radiating sources* (they do not leave any footprint on the radiated field at the measurement locations), Fig. 1.3. Let us see why they present a problem [12].

   Let us consider a generic function $f(\underline{r})$ having a compact support in a given region of space Ω, and continuous first derivatives. Starting from $f(\underline{r})$, let us consider the sources

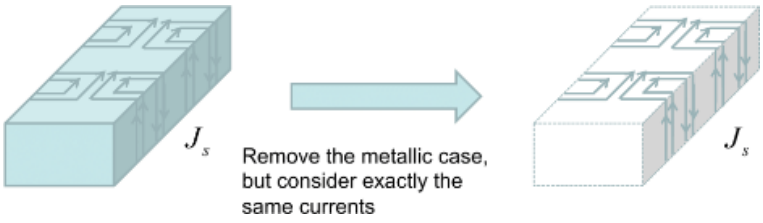

Fig. 1.3: Non radiating sources: an example.

$$J(\underline{r}) = \left(\nabla^2 + k^2\right) f(\underline{r}) \tag{11}$$

One easily proves that these sources produce a field which is confined in Ω, and thus they are not radiating outside Ω.

In this case:

$$E(\underline{r}) = \int_{\Omega} g(\underline{r} - \underline{r}^{'}) \left(\nabla^2 + k^2\right) f(\underline{r}^{'}) dr^{'} \tag{12}$$

and, integrating by parts two times, we obtain:

$$E(\underline{r}) = const \cdot f(\underline{r}) \tag{13}$$

and hence the field is compactly supported in Ω.

By adding a non radiating source to an already available solution, one has additional possible solutions. Therefore, the first Hadamard condition [12] is violated, and the inverse source problem is ill-posed.

2. the so-called *poorly radiating* sources. The latters are existing sources which leave a "nearly zero" footprint in the radiated field. Consequently, they cannot be determined from radiated field data unless "exact" measurements are available, and, even supposing non-radiating sources are absent, the inverse source problem is ill-conditioned, so that regularization is required.

   For example, by virtue of cancellation effects amongst the positive and negative parts of the source, fast oscillating source are "poorly radiating", Fig. 1.4. In particular, the faster the oscillations, the smaller their impact on radiated field, and harder the problem of correctly retrieving such a kind of source.

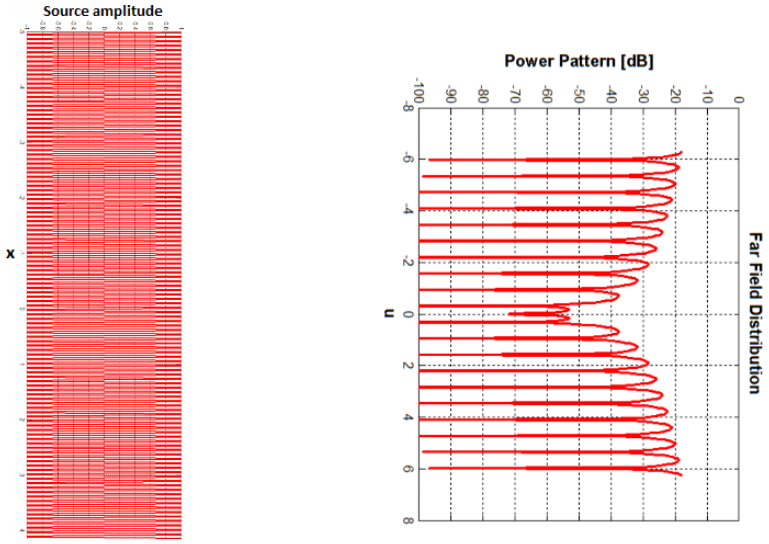

Fig. 1.4: Poorly radiating sources: an example.

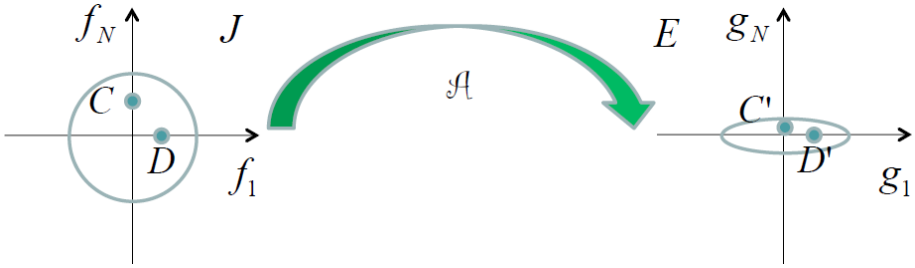

Fig. 1.5: Image of a ball

4 Phaseless problems

As already said, the Thesis concerns phaseless inverse source problems. It is worth to note that the adoption of phaseless data makes any problem very hard, since the solution is not unique (need to avoid "false solutions") [22, 23].

For this reason, phaseless measurements have been the subject of intensive research (see for instance [15, 24–28]). In fact, measuring a complex far-field (FF) pattern requires a stable phase reference and accurate positioning of the probe in each measurement point, so that measurements may become problematic [15, 27].

As a matter of fact, phaseless measurements have been proposed as an effective alternative to amplitude and phase measurements in applications ranging from array excitations retrieval [27], and on-site diagnostics of reflectors for radio astronomy [28].

Therefore, the Thesis proposes new approaches to both *synthesis* and *PR* problems by means of a small number of phaseless FF measurements.

5 Aims and contents of the Thesis, and the common ratio of the proposed strategies

The Thesis deals with both *synthesis* and *PR* problems. Needless to say, optimal synthesis of array antennas deserved interest especially in fields in which the human's health and safety are of interest, like hyperthermia treatment planning [29], as well as cellular telecommunications [30], satellite [31], radar [32], and very many further scenarios. Instead, PR methodologies play a key role in many fields of applied electromagnetics including inverse scattering [33], astronomy [34], as well as optics [35], crystallography, and so on.

During the years, the challenging nature of the problems have brought the inverse source community to develop more and more solution strategies for both *synthesis* and *PR* problem. In order to overcome the difficulties underlying inverse source problems, the Thesis proposes a new point of view to the problem. In fact, the proposed methodologies for the two types of problems share a common focus, which relies on somehow combining the solutions of simpler problems. Saying it in other words, all problems, being difficult to be solved, will be considered as an assembly of solutions of simpler problems.

The remainder of this Thesis is composed by two different parts (including five Chapters), Conclusions, and three Appendices (where mathematical details are deepened), and it is structured as follows.

In PART I, the array antenna synthesis problem is dealt with. In particular, the problem to determine the optimal excitations of an arbitrary fixed-geometry arrays generating a power pattern lying in a given mask (defined by an arbitrary upper-bound function plus an arbitrary lower-bound function) and optimizing some performance parameters is considered.

The starting point is the problem of maximizing the field intensity in a given point or direction ('target point') while satisfying arbitrary upper bounds elsewhere. In case of scalar fields, such a maximization problem, where excitations of given sources are considered as unknowns, has been solved by Italian researches since the nineties [36]. Notably, it is shown that the problem can be conveniently formulated as a Convex Programming (CP) problem, with the inherent advantages. Later, the approach, named 'FOCO' (Focusing via Constrained Optimization), has been successfully generalized and applied to 3-D complex scenarios and hyperthermia problems for the case where one component of the field is dominant [11].

However, this strategy cannot be trivially extended to the constrained focusing of the intensity of a vector field. In fact, when dealing with vector fields, the cost function to be optimized cannot be reduced anymore to a linear function of the unknowns and therefore suitable strategies are required to achieve the globally optimal solution of the arising non-convex problem. Therefore, in this Thesis a new approach able to address this issue is presented.

A second issue of interest in antenna synthesis problems is that of shaping the field within a given region ('target region'). In this case, one needs to develop a shaping strategy which is able to keep under control the sidelobes level (SLL) outside the target region while ensuring some uniformity (or some given shape) of the field intensity into it. Nonetheless, only a few shaping approaches can be found in the literature and none of them is able to fulfill the requirements in terms of SLL and field intensity into the target area.

By taking advantage from 'FOCO', the main contribution of Part I has been to delineate a general and unitary conceptual and mathematical framework identifying the causes of non-convexity (and hence difficulties) and to propose an effective way out. In this respect, novel synthesis procedures are presented in the first three Chapters.

In Chapter 2, after a brief summary of existing results, a first contribution is presented for the field shaping. By considering by the sake of simplicity scalar fields, one can fruitfully consider a set of 'control points' within the target region and fix the relationships amongst the corresponding amplitudes therein. In particular, the proposed technique combines the adoption of several target points with the FOCO method [36]. In such a way, one can exploit the inherent advantages of FOCO, and address both issues related to the occurrence of undesired side field peaks and to the field intensity uniformity in the target region. Consequently, the fields shaping can be interpreted as a combination of a number of focused fields. It is worth to note that, as long as enumerative technique is used, the computational complexity of the problem increases with the number of control points as well as with the number of phase-shift instances considered for each control point. Therefore, in order to limit the computational requirements, it is convenient to adopt this technique in case of generic 1-D arrays or 2-D arrays having a symmetric power pattern. In fact, as long as the given power mask is symmetric, one can limit computational requirements by enforcing the required symmetry in the expected complex pattern (which in turn translates into linear constraints on excitations). By so doing, as shown in the Chapter, one is able to design in a still reasonable time planar arrays composed of hundreds of elements as well as realizing fields with large footprints. Notably, although reducing

the DoF available to the designer, one is still able to design array solutions which favorably compare with the literature.

Chapter 3 propose a second approach for the synthesis of shaped beams by means of large and arbitrary arrays. With respect to the first approach presented in Chapter 2, the present one is based on nested optimizations, where the external global optimization (GLO) acts on the field's phase shifts over a minimal number of 'control points' located into the target region whereas the internal optimization acts instead on excitations. In fact, for any set of phase shifts the problem becomes essentially identical to FOCO (just more convex constraints are required), so that one just needs (but for some subtleties) to optimize the phase shifts. Then, the Chapter shows that as long as a given class of performance parameters (including ripple) is in order, the internal optimization reduces to a CP problem. Such a circumstance, along with the relatively small number of unknowns involved in the external GLO, allows a full control of the shaped beam's ripple and SLL in a number of cases (involving arrays having a large size and aimed at generating relatively large-footprint patterns), which cannot be solved in a globally-optimal fashion by the state-of-the-art techniques. In a nutshell, the proposed method identifies the phases of a few field samples as the actual reason for the non-convexity (and hence the difficulty) of the problem, and then elaborates on such a circumstance in order to deal with a GLO problem having a number of unknowns as small as possible.

In Chapter 4, after a brief summary of existing results, a third contribution is presented for the problem of focusing a vector field into a target area. When considering the field intensity problem, it can be easily argued that the problem can be conveniently formulated as an optimization over the possible polarizations of the field at the target point. In fact, for any given polarization the problem turns back to the basic 'FOCO' formulation. As a consequence, one can have the same kind of procedure as Chapter 3. Coming to details, the proposed method, named IN-FOCO (Intensity FOCO), is a hybrid approach based on nested optimizations, where the inner (convex) problem looks for the excitations corresponding to the optimal polarization which, in turn, is externally pursued through GLO. The IN-FOCO technique allows to improve the efficiency and the accuracy of a possible enumerative technique. Moreover, it is more efficient with respect to those approaches in which the GLO acts directly on excitations, resulting in a non-convex optimization on many variables and hence in the possibility of being trapped into local optima. Finally, the proposed synthesis tool has been successfully tested in case of near field (NF) focusing, complex scenario, and

hyperthermia treatment planning.

PART II of the Thesis is focused instead on the PR problem. Notably, in order to optimally solve the problem, essentially all approaches available in the Antennas & Propagation Community require data diversity, like two measurement surfaces, or two different probes, or two different defocus conditions [37–40]. Moreover, PR is often solved by using algorithms either having an exponentially-increasing computational burden with the unknowns, or being affected by the so-called 'false solutions'. Such circumstances are often induced by a number of difficulties intrinsic to the problem, e.g.: non-linearity [41]; non-availability of some antenna measurements [42]; non-uniqueness of the solution in both 1-D and 2-D cases due to trivial ambiguities [14,42]; non-uniqueness of the solution in the 1-D cases [2, 43]. Starting from these observations, the developed approaches to PR require only one measurement surface plus the knowledge of the source's support and very few additional information. Moreover, they deal with 2-D problems, i.e., with the retrieving of planar sources or excitations of planar arrays.

The proposed approaches are based on a proper combination of the solution of simpler problems, which are herein 1-D PR problems. Coming to details, the 2-D PR problem is decomposed into a number of 1-D PR problems and each of them can be solved through the well-known Spectral Factorization (SF) [2] method. Since 1-D PR problem does not admit unique solution (besides trivial ambiguities) [44], for each 1-D PR problem we have a collection of possible results. Hence, the final actual way out of the 2-D PR problem is gathered by following a procedure which resembles the solution of crosswords puzzles, where one has to guarantee the congruence amongst across and up-down possible words. In a more formal way, advantage is taken from the fact that a very effective procedure exists for the solution of 1-D PR problems for discrete signals, and it is able to give back all the (possibly very many) solution of the problems. These results become then possible 'words' to be allocated along the corresponding across, up-down (and oblique) solutions[4]. Finally, congruence considerations amongst the different possible 'words' along the crossing directions will possibly restore uniqueness of the solution (if any) for the 2-D scheme.

In Chapter 5, a first approach is proposed for the case of antenna arrays, and it is able to perform the 'crosswords' PR procedure by acting on horizontal, vertical and

[4] By virtue of bandlimitedness of $F(u)$ and $|F(u)|^2$, only a finite number of them has to be actually considered, and because of the periodicity of the involved functions, we just need to consider the portion of the spectral plane of vertices $(-\pi, -\pi)$, $(-\pi, \pi)$, (π, π), $(\pi, -\pi)$.

oblique cuts of the pattern in order to identify the correct field instances among all the ones provided by the SF.

In Chapter 6, the second proposed method considers circular continuous aperture sources instead of antenna arrays, and the first proposed solution procedure is improved by using concentric-ring (rather than vertical and oblique) cuts of the radiation pattern. By exploiting the multipole expansion of the FF (and of the corresponding power pattern), one will be able to perform the above 'crosswords' PR procedure by acting, this time, just on diameters and concentric-ring cuts of the pattern. Notably, this approach does not require any symmetry (e.g., a circularly-symmetric behavior) of the field in order to properly work. Finally, as a demonstration of the interest and effectiveness of the proposed approaches, applications to array diagnostics as well as to reflectors' surface deformations have been given.

Conclusions, including further developments, are finally drawn in Chapter 7.

Part I

PHASELESS INVERSE SOURCE PROBLEMS AND SOLUTIONS FOR ANTENNA SYNTHESIS

1 Preliminary remarks

The antenna synthesis problem is a very long-standing subject in Electromagnetics, with contributions dating back to [45–47]. It consists of designing a radiating system fulfilling a given set of requirements concerning:

- the FF pattern;
- the NF behavior;
- complex scenarios;
- the antenna structure and geometry;
- the feeding system.

With reference to the first point, a way to state the FF specifications is requiring to realize a power pattern lying in a given '*mask*'. In fact, one is usually interested in synthesizing an antenna satisfying given performances indices (f.i., level of secondary lobes, beam shape, and so on).

Concerning the last two points, in many instances, either the structure is fixed in advance, or the fulfillment of the FF requirements is sought by changing the geometry and/or electromagnetic structure of the antenna.

Depending on the kind of radiation pattern one is looking for, as well as from the available DoF, one can indeed identify a very large number of possible synthesis approaches.

Apart from very particular (and simple) cases, all the power synthesis techniques are optimization procedures, whose different solutions have a different degree of satisfaction with respect to the project requirement. The degree of optimality is measured through a '*cost function*', which is representative of the problem at hand. Mathematically speaking, the functional representing the problem can have many local minima. The goal of optimization is the identification of the optimal solution, i.e., of the *global minimum*.

A number of contributions ensuring the achievement of somehow globally 'optimal' solutions exist for the fixed-geometry case when looking for (unconstrained) excitations.

In particular, in case one is interested in a given component of the field, optimal solution strategies have been devised for the synthesis of pencil beams subject to arbitrary constraints on the sidelobes by means of arbitrary geometry arrays (including linear, planar, and conformal arrays). Notably, the approach in [36, 48–50] suggests that the problem of maximizing the field in a given point while keeping the field below given values can be conveniently reduced to a CP [36, 48, 49] or even to a Linear

Programming (LP) [50] problem, so that a unique global optimum exists for such a class of problems. As a consequence, these classes of canonical problems are somehow solved.

Optimal solution strategies, definitely solving another canonical problem, have been devised, in case of scalar fields, for the optimal synthesis of shaped beams by means of both uniformly-spaced one-dimensional arrays [2], and uniformly-spaced planar arrays having a quadrantal symmetry [51], as well as for the case of continuous sources exhibiting a circular symmetry [43, 52].

On the other hand, no simple and effective procedure guaranteeing the global optimality of the solution seem exist in the related problems of

- maximizing a vector field intensity in a given point;
- shaping a scalar field through generic array antennas having arbitrary layout and element patterns;
- shaping the field intensity in a given target region.

For the classes of problems above a large number of solution procedures essentially based on GLO approaches acting on excitations have recently appeared in literature. On the other side, by virtue of the so called 'No Free Lunch Theorem' (see [53]), these latter require a computational burden which grows exponentially with the number of unknowns, so that only a limited number of DoF can be dealt with in an actual global optimal fashion.

Then, the interesting theoretical question arises of how to tackle these classes of problems in such a way to achieve a kind of globally *optimal* solution to the design problem at hand, wherein by 'optimal' we mean
an array able to fulfill design goals by exploiting the minimum number of elements (or the minimum aperture size, or the minimum number of other resources or, equally, to optimize given performances for a fixed number of elements (or fixed aperture dimensions, or fixed other resources).

As a contribution towards the effective solution of more difficult synthesis problems, and motivated by the interest of such a kind of arrays in many fields of applied electromagnetics such as hyperthermia treatment planning [29, 54], NF focusing [55], wireless power transfer [56], this Part of the Thesis delineates possible solution strategies for both problems of maximizing the vector field intensity in a given point, and shaping the field in a target region, identifying their causes of non-convexity (and hence difficulties), and proposing effective ways out.

Notably, to achieve these goals, the proposed approaches take advantages from a well-assessed technique [36], which is briefly summarized in the Section 3.

More details are given in the following Chapters.

2 Convex and Non-Convex synthesis problems and the need to properly manage non-convexity

Optimization theory is a framework for selecting the best solution from feasible options. An optimization problem can be mathematically formulated as follows:

$$\min_x f(x) \tag{1.a}$$

subject to:

$$x \in X \tag{1.b}$$

where the vector x is a variable, f is an objective function, and X is a feasible set.

As previously said, apart from very particular cases, all the power synthesis techniques are optimization procedures. In particular, it is possible to identify two types of optimization problems:

- **Convex Optimization**. A convex optimization problem has a convex objective function and a convex feasible set. Convex optimization plays a significant role in mathematical optimization because it has several advantages. The first advantage is that a local optimal solution is also a global optimal solution in convex optimization problems, so that we can safely terminate optimization algorithms when we find a local optimal solution. Secondly, for convex optimization problems, theoretical convergence of gradient descent like is guaranteed.
- **Non-Convex Optimization**. A non-convex optimization problem has a non-convex objective function *f(x)* or a non-convex feasible set X in (1.b). Since non-convex problems can have lots of local minima, figuring out a global solution from lots of local minima is quite challenging. Due to the difficulty in solving non-convex optimization problems, people approached non-convex problems in many different ways such as: relaxing non-convex problems to convex problems, using convex optimization to find upper or lower bounds on non-convex problems, and further using the bounds to find a globally optimal solution. Since some practical problems are expressed as non-convex problems, research on various non-convex optimization methods has been widely conducted in [57]. Exploitation of GLO procedures (with the inherent limitations, see [58]) is also widespread.

The synthesis problems dealt with in this part of the Thesis are non-convex, and hence difficult to be solved. As the aim is the identification of the "optimal solution", by taking advantage from [36], we delineate in the following a possible way out for both focusing and shaping problems.

3 A review of a basic tool: FOCO (the scalar case)

In order to provide a basis for the approaches proposed in the following Chapters, it is useful to recall some results related to the case of scalar fields.

The component of interest of the FF of a generic N-elements array can be written as:

$$F(\underline{r}) = \sum_{n=1}^{N} I_n \Psi_n(\underline{r}) \tag{1}$$

wherein $\underline{r}$ is the coordinate spanning the observation space, $\Psi_n(\underline{r})$ is the complex *scalar* field induced by the unitary-excited *n-th* antenna in the region of interest Ω when all the other antennas are turned off, and I_n represents the complex excitation of the *n-th* element. As well known, the function $\Psi_n(\underline{r})$ represents the *n-th* Active Element Pattern (AEP), which takes into account possible mutual-coupling and mounting-platform effects [6].

If we denote by $\underline{r}_t \in \Omega$ the target point, the constrained focusing problem at hand can be formulated as follows [36]:

Determine the complex excitations coefficients I_n (n = 1,...,N) such to:

$$\max_{I_1,...I_N} |F(\underline{r}_t)|^2 \tag{2.a}$$

subject to:

$$|F(\underline{r})|^2 \leq UB(\underline{r}) \qquad \forall \underline{r} \in \Omega \tag{2.b}$$

where $UB(\underline{r})$ is a non-negative *arbitrary* function, say the *mask* function, of the coordinate $\underline{r}$ spanning the observation space Ω, which enforce the upper bound constraint on the power deposition outside the focal area. Notably, $UB(\underline{r})$ can be properly chosen depending on the specific application's requirements.

It is worth noting that the objective function is a non-negative quadratic polynomial with respect to the unknown coefficients. Hence, the overall optimization problem is in principle an NP-hard problems [53], and a specific strategy is required to cope with it.

However, fixing to zero the field phase in $\underline{r}_t$[1], the problem can be recast as [36]:

Determine the complex excitations coefficients I_n (n = 1,...,N) such to:

$$\max_{I_1,\dots I_N} \Re\{F(\underline{r}_t)\} \tag{3.a}$$

subject to:

$$\Im\{F(\underline{r}_t)\} = 0 \tag{3.b}$$

$$|F(\underline{r})|^2 \leq UB(\underline{r}) \qquad \forall \underline{r} \in \Omega \tag{3.c}$$

where $\Re$ and $\Im$, respectively, denote the real and imaginary parts of the complex arguments.

Notably, the cost function (3.a) and the constraint (3.b) are linear functions of the unknowns, while $|F(\underline{r})|^2$ is a positive semidefinite quadratic form. As the intersection of convex sets is still convex, the whole problem is equivalent to the maximization of a linear function in a convex set, and corresponds to a CP problem, with the inherent advantages in terms of solutions' optimality and computational burden.

Note that such a formulation includes synthesis of pencil beams through arrays of arbitrary structure and spacing. Moreover, if the observation domain Ω includes some NF observation domain, the technique is also able to tackle the upper bounds on the NF. Later, 'FOCO' is now under test in Clinical environments [29, 59].

Versatility, amongst all, is the more remarkable feature of FOCO. In the past years, indeed, the basic FOCO formulation has been modified in order to address different relevant needs. Specifically:

- **multi-frequency FOCO** (mf-FOCO) [54] is based on from the idea that hot-spot spatial collocations could change with frequency. Hence, exploiting such a feature, adopting multi-frequency applicators one could (in principle) avoid hot-spots occurrence (or lower their impact) [60].
- **multi-target FOCO** (mt-FOCO) [61] aims at uniformly shaping the Specific Absorption Rate (SAR) over an extended possibly with irregular contours target area (i.e., late stage tumors). Nowadays this task is not efficiently addressed by the clinically adopted algorithms [62].
- **sparsity promoted FOCO** (sp-FOCO) was introduced to address the need of 'optimally' selecting the active elements of a given applicator in a patient-specification [63].

[1] This assumption does not entail any lack of generality, as it is simply equivalent to fix the phase reference.

4 The common strategy

This part of the Thesis proposes a new point of view to the synthesis problem. In particular, the approaches introduced in the following Chapters share a common focus, that relies on the decomposition of the overall problems (difficulty to be solved) into an assembling of solutions of simpler problems. In fact, by taking advantages from "FOCO", PART I of the Thesis delineates a general mathematical framework, and proposes an effective way out.

In particular, in the following one will find a number of contributions, whose interest is witnessed by the recent publications [64–66], dealing with the development and discussion of solution approaches for:

i *the optimal synthesis of shaped beams for arbitrary arrays.* In order to solve this problem, the basic "FOCO" formulation can be extended to the shaping problem where, instead of a single "reference point", one combines the adoption of several "control points" arbitrary located into the target area. Therefore, the FOCO paradigm represents the starting point to initiate the overall procedure.

ii *the optimal focusing of vector fields intensity by means of arbitrary fixed-geometry one-dimensional arrays.* The aim is the extension of the "FOCO" formulation to the case of vector fields. To do this, the overall problem can be seen as a combination of a set of field polarizations with the FOCO method. In a nutshell, the field intensity focusing can be interpreted as an assembling (a proper combination) of a number of basic polarized fields.

2

OPTIMAL SYNTHESIS OF SHAPED BEAMS FOR ARBITRARY FIXED-GEOMETRY ARRAYS: THE BASIC IDEA AND A FIRST APPROACH

2.0 Summary

The optimal synthesis of shaped power patterns by means of generic array antennas having arbitrary layout and element patterns is addressed and solved. In particular, this Chapter proposes an approach to field shaping which combines the adoption of several "control points" with the basic "FOCO" method. In a nutshell, the field shaping can be interpreted as a complex superposition of a number of focused fields. Notably, opposite to [67], the approach is able to keep under control both the ripple inside the shaped area and the SLL. Moreover, as long as some condition is fulfilled, the proposed approach guarantees the achievement of the global optimum by using local optimization techniques, and a number of different excitation solutions all fulfilling the requires specifications are determined in a straightforward fashion. Numerical examples concerning applications of actual interest support the given theory and confirm the effectiveness of the developed solution procedures[1].

[1] Some contents of this Chapter have been published in references [2, 5, 6, 7, 8] of the "Publications List of G. M. Battaglia" reported at the end of the Thesis.

2.1 Some existing solution strategies

The synthesis of shaped-beam patterns is a canonical problem in antenna theory, as shown by the large number of both classical (e.g., [2, 3, 67–71]) and recent (e.g., [1, 4–6, 43, 52, 72–78]) contributions.

In this Chapter, some canonical strategies for shaped-beams pattern synthesis are briefly recalled in order to have a better insight of their possible usefulness.

A very popular approach has been given by Woodward and Lawson (WL) in [67]. In the latter, the shaped pattern is conceived as the superposition of many pencil beams which are steered, one by one, and then summed to achieve the desired shaping. While being intuitive and straightforward, the WL method suffers from a number of relevant drawbacks. In fact, the synthesized field is restricted within the class of *real* patterns, so that one is not exploiting all the DoF of the problem. Moreover, as already noticed in [71], this method does not guarantee the full control of the field in the shaped-beam zone in case of severe constraints.

By taking inspiration from [71], an approach similar to the WL technique has been recently proposed in [1]. In that paper, Taylor beams are superimposed in order to generate the desired shaped pattern. This approach allows some improvements in the control of SLL, but it still does not guarantee their full control. Moreover, and more important, the resulting patterns are still real, so that not all the DoF are exploited. Consequently, the approach is affected by essentially the same limitations of the WL method.

Some interesting approaches for the synthesis of shaped beams based on CP have been proposed in [5, 74, 79]. In [5], which deals with the case of sparse arrays, the problem is reduced to CP problems. However, in case of shaped-beams this is achieved by trying to fit a given complex field, rather than looking for a generic power pattern fulfilling given constraints. As a consequence, one is not exploiting again all the DoF which are eventually available. Paper [79] proposes an approach for the generation of shaped-beams by means of linear or planar arrays. In particular, conjugate symmetric beam-forming weights are looked for, so that the array factor becomes real, and the overall problem is also reduced to a CP one. By so doing, once again, the search space is limited to the case of real array factors, so that one is not exploiting all the DoF which are eventually available. A more general approach relies on the so called 'semidefinite relaxation' framework [74]. In fact, it both allows to deal with generic (fixed-geometry) arrays, as well as to enforce constraints on the power pattern. In such an approach, the products of the array excitations are used as auxiliary unknowns, so

that all power constraints become linear, and hence convex, in these new variables[2]. On the other side, this technique has a number of relevant drawbacks:

- the number of unknowns exhibits a quadratic growth with the number of array elements, thus possibly implying serious computational problems.
- at the end of the procedure only one solution is eventually found, so that a number of potentially-interesting solutions are lost.

Computational burden issues again come into play whenever the synthesis is tackled by recurring to global optimizers (see for example [72]).

In the last years, the SF method has proved to be an effective way to find meaningful solutions to the above drawbacks. As demonstrated by several contributions [2, 69, 70], this technique allows casting the synthesis as a mask-constrained one while still being computationally effective and not recurring to undesired limitations on the kind of field one is looking for. From the operative point of view, the array design is performed as a LP problem plus a polynomial factorization, with relevant advantages in terms of computational burden and global optimality of solutions. Interestingly, the approach is able to find all the different possible solutions to the problem at hand, so that the "most convenient" one can be selected according to some additional performance parameters. The above described peculiar features of SF has led to investigate such an algorithm also for the synthesis of 1-D arrays having even excitations [43] or high beam efficiency [78], 2-D rhombic arrays generating circularly-symmetric shaped beams [51], equispaced reconfigurable arrays [77], and continuous aperture sources [52] (in turn allowing the design of 1-D [75] as well as circular-ring [76] isophoric sparse arrays).

Another benchmark and well-assessed approach is the Orchard-Elliott-Stern (OES) one [3]. While previous to [2,69,70], this technique is similar in spirit to the SF method but for optimizing the zeroes (rather than the coefficients) of the polynomial underlying the sought power pattern.

Unfortunately, both SF and OES methods can be applied only if the FF can be written in terms of a 1-D trigonometric polynomials, i.e., in case of either equispaced 1-D arrays with identical element patterns, or circularly-symmetric fields, or u-v factorable planar arrays[3].

[2] By so doing, one needs however a coherence conditions amongst the auxiliary variables which is non convex (and somehow relaxed into a convex one).

[3] Such a limitation does not allow, for instance, considering 1-D arrays having an aperiodic layout and/or different elements' radiation patterns (where mounting-platform and mutual-coupling effects come into play) as well as generic planar or conformal arrays.

These issues and possible way to conveniently tackle them (as well as demonstrations of the usefulness of the developed tools) will be the subject of the following Sections. In particular, by taking advantage from the fact we know how to solve the basic "FOCO" problem, the Chapter elaborates and puts on the basic idea that shaping can be interpreted in terms of assembling of a number of focused fields. Starting from such a basic idea, and finding a way to enforce constraints directly on the overall field, the proposed approach is able to cast the synthesis in terms of a number of CP problems, with the inherent advantages in terms of both computational time and reliability of the obtained results.

Notably, the present approach is related to the WL one as it also adopts several properly-spaced 'control points' located in the shaped-beam zone. Similarities end however here. In fact, the proposed technique is able to exploit all the DoF of the problem by looking for complex patterns (rather than real patterns), look directly for a shaped pattern (rather than for a superposition of pencil beams), and take into account since from scratch the fulfillment of constraints on sidelobes. Moreover, the proposed method keeps many of the SF advantages while dealing with generic fixed-geometry arrays (including sparse, conformal, and planar arrays), and, exactly like the SF method, it allows identifying (if any) a multiplicity of substantially-different excitation sets all fulfilling the assigned power-pattern mask. It is worth to note that, unlike SF technique, the approach is able to take into account mutual-coupling and mounting-platform effects. The kind of outcomes of the proposed approach are exemplified in the subsequent Section with reference to cases of practical relevance. Some general comments and remarks follow.

2.2 An effective solution procedure

Let us recall the formulation of the FF radiated by a generic N-elements array:

$$F(\underline{r}) = \sum_{n=1}^{N} I_n \Psi_n(\underline{r}) \tag{1}$$

wherein $\underline{r}$ is the coordinate spanning the observation space, $\Psi_n(\underline{r})$ is the complex *scalar* field induced by the unitary-excited *n-th* antenna in the region of interest Ω when all the other antennas are turned off[4], and I_n represents the complex excitation of the *n-th* element.

[4] As well known, the function $\Psi_n(\underline{r})$ represents the *n-th* AEP, which takes into account possible mutual-coupling and mounting-platform effects [6].

More precisely, the problem at hand amounts to determine the optimal excitations such as to grant the desired shape and the minimum ripple of the pattern in the 'target' region Λ while fulfilling arbitrary upper-bound constraints in the 'sidelobes' region Ω.

To this end, we set the approach's basic bricks as follows:

i given the array layout and $\Psi_n(\underline{r})$ for $n = 1, \ldots, N$, let us consider the sampling of Λ into L 'control points', say $\underline{r}_{\Lambda i}, i = 1, \ldots, L$. [5]

ii by considering $\underline{r}_{\Lambda 1}$ as a 'reference' point, i.e., as the point wherein the phase of the synthesized field is fixed (to zero) once and for all, let us indicate with $\varphi_i \in [-\pi, +\pi]$ the field phase shift between $\underline{r}_{\Lambda i}$ and $\underline{r}_{\Lambda 1}$.

Then, for any fixed determination of the phase shifts $\varphi_2, ..., \varphi_L$, a convenient auxiliary problem can be conveniently set as:

Find the complex excitations $I_1, ..., I_n$ in such a way that:

$$\Re\{F(\underline{r}_{\Lambda i})\} = \alpha_i \cos\varphi_i \qquad i = 1, \ldots, L \tag{2.a}$$

$$\Im\{F(\underline{r}_{\Lambda i})\} = \alpha_i \sin\varphi_i \qquad i = 1, \ldots, L \tag{2.b}$$

$$|F(\underline{r})|^2 \leq UB(\underline{r}) \qquad \forall \underline{r} \in \Omega \tag{3}$$

where $\alpha_1, ..., \alpha_L$ are a-priori chosen real and positive numbers. In particular, while enforcing that the synthesized field is purely real in the first reference point[6], constraints (2) are equivalent to $|F(\underline{r}_{\Lambda i})| = \alpha_i$ and hence allow arbitrarily shaping the pattern at the control points. Also note that, once a sufficiently-fine discretization [80] is performed, constraints (3) allow enforcing arbitrary upper bounds on the sidelobes.

Notably, for fixed values of $\varphi_2, ..., \varphi_L$, constraints (2) are linear in the unknown excitations while, as the left-hand members in (3) are positive semi-definite quadratic forms, constraints (3) define, in each discretization point, a convex set [75]. Hence, the problem (2)-(3) can be solved in a fast and effective fashion as the search for the intersection (if any) amongst convex sets. Such a feature allows us solving the overall synthesis problem through the following procedure:

i. repeatedly solve the problem (2)-(3) for different fixed values of $\varphi_2, ..., \varphi_L$;

ii. pick, amongst the instances wherein step (i) admits a solution, the one corresponding to the minimum ripple inside Λ.

[5] The latter should be chosen in such a way to allow the full control of the pattern in the shaped zone while not being redundant. An obvious answer to such a question is the observation that FF patterns are bandlimited [80], so that the control points are conveniently chosen by sampling Λ at the Nyquist distance.

[6] Note this does not entail any lack of generality, as it is simply equivalent to fix the phase reference.

With respect to previous approaches, the proposed method presents a number of advantages:

- it is more powerful than [1, 67] as it allows dealing with complex fields and can guarantee since from scratch the fulfillment of constraints on the SLL;
- since different excitation sets corresponding to the same ripple can come out from step (ii), the method can allow identifying several different solutions to the problem.
- the proposed formulation is very general. In fact, no hypotheses have been given in (1)-(3) with respect to the array's layout and AEPs so that, opposite to SF [36], OES [3], and their derivations [43, 76–78], the procedure can be applied to whatever kind of uniformly and non-uniformly spaced linear, planar, and conformal arrays.

2.3 Assessment of the proposed procedure

In this Section, we report some numerical examples concerning the synthesis of linear and planar arrays. In particular, in Subsections 2.3.1 and 2.3.2 we provide comparisons with the SF and the OES methods. Then, in Subsection 2.3.3, we show that the presented method favorable compares with the one recently proposed in [1]. Finally, in Subsections 2.3.4 and 2.3.5, we consider instances where the OES and SF approaches cannot be applied, i.e., an aperiodic array with full-wave simulated AEPs (where the proposed technique is compared to the one in [6]) and two planar non-factorable arrays (where the outcomes are compared to the ones in [2, 7]).

Concerning the choice of the minimization algorithm, any *local* minimization algorithm could be exploited, but because we are looking for a constrained minimization the adoption of *fmincon* routine of MATLAB turns out to be convenient. Due to the numerical efficiency of these tools, all calculations were run on a PC equipped with the Intel i7-6700HQ processor and a 16GB RAM, with an average computational time, in 1-D test cases, equal to 0.7s per CP optimization.

For each trial solution, along with ripple we also evaluated the excitations' Dynamic Range Ratio, i.e.,

$$DRR = \frac{\max\limits_{n}|I_n|}{\min\limits_{n}|I_n|} \tag{4}$$

whose reduction leads to a simplification of the beam forming network and to an increase of the illumination efficiency [77].

In all experiments involving 1-D arrays we also evaluated the directivity and used the spectral variable $u = \sin\theta$ ($\theta \in [-\pi/2, \pi/2]$ denoting the angle between the observation and boresight directions) as the coordinate spanning the observation space. Consequently, the region Λ has been sampled as $u_{\Lambda 1}, ..., u_{\Lambda L}$. Finally, we considered $M = 20$ values of φ_i (uniformly-spaced in the range $[-\pi, +\pi]$).

By analogy, in the 2-D test cases, the observation space has been spanned by using the spectral variables $u = \sin\theta\cos\phi$ and $v = \sin\theta\sin\phi$ (θ and ϕ being the usual elevation and azimuth angles with respect to the boresight). Moreover, in order to keep low the computational burden of the solution procedure, the value of M (determining the phase shifts discretization) has been decreased up to 8. As it will be shown, such a reduction did not prevent the approach from achieving results which favorably compare with the literature.

In all examples, upper bound constraints were enforced in a number of spectral points proportional to the source dimensions (more precisely, ten points per wavelength). Finally, the number and locations of control points have been determined by finding, in the grid above, the closest sample to each of the points coming out from the Nyquist sampling of the region Λ.

2.3.1 Comparison with the SF method

In this Subsection, we report the outcomes of two synthesis problems wherein the proposed approach has been compared to the SF method published in [2]. To this end, we first considered the power goals depicted in Fig. 2.1 (c) and Fig. 2.2 (c), respectively, and solved them by exploiting the SF method (wherein the ripple minimization has also been added according to the guidelines in [43]), and then by using the proposed approach. In both problems, we considered an equispaced array composed of $N = 13$ isotropic elements with a $\frac{\lambda}{2}$ inter-element spacing (λ denoting the wavelength) and set $\alpha_i = 1\ \forall i$.

In the first synthesis problem, the goal was to minimize the ripple for $u \in [-0.19, +0.19]$ (while guaranteeing a maximum ripple of $\pm 1dB$) and to achieve a maximum sidelobe level lower than -15 dB for $u \leq -0.32$ and to -20 dB for $u \geq 0.32$. Fig. 2.1 (c) shows a comparison between the power patterns respectively achieved by exploiting the SF method and the proposed approach (wherein three equispaced control points inside the region $\Lambda \in [-0.19, +0.19]$, i.e., $u_{\Lambda 1} = -0.16, u_{\Lambda 2} = 0, u_{\Lambda 3} = 0.16$, have been used). Notably, the proposed procedure delivered exactly the same radiation performances as the SF method (corresponding to a ripple of ± 0.15 dB). Moreover, it turned out being able to provide multiple excitation sets giving rise to the same

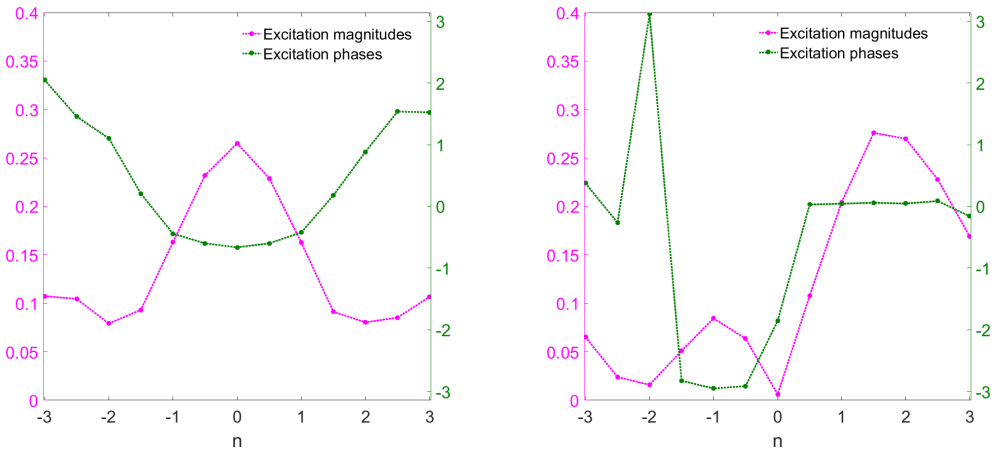

(a) (b)

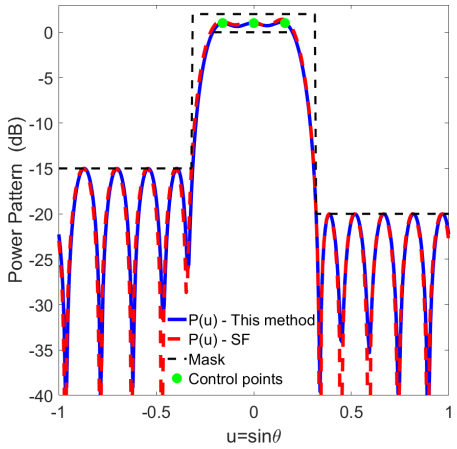

(c)

Fig. 2.1: First synthesis problem of Subsection 2.3.1. Two different excitation sets synthesized through the proposed method [(a) and (b)] and square-amplitude far-field distribution [denoted from now on by *P(u)*] corresponding to both of them (c): flat-top beam provided by the proposed procedure (blue line) as well as by the approach in [2] (red line), and adopted mask (black line).

square-amplitude FF distribution. For example, figures 2.1 (a) and (b) respectively depict two different excitation sets both delivering the pattern reported in Fig. 2.1 (c) (which provides a directivity of 6.32 dB, i.e., 0.87 dB lower than the one of a theoretical field being equal to 1 inside Λ and 0 elsewhere). For this mask, if DRR rather than ripple minimization is pursued then the DRR decreases from 3.3 to 2.7 while the ripple increases from ± 0.15 dB to ± 0.6 dB.

In the second synthesis problem, the goal was to minimize the ripple when dealing with a broader target area, i.e., $u \in [-0.32, +0.32]$, while guaranteeing that it does

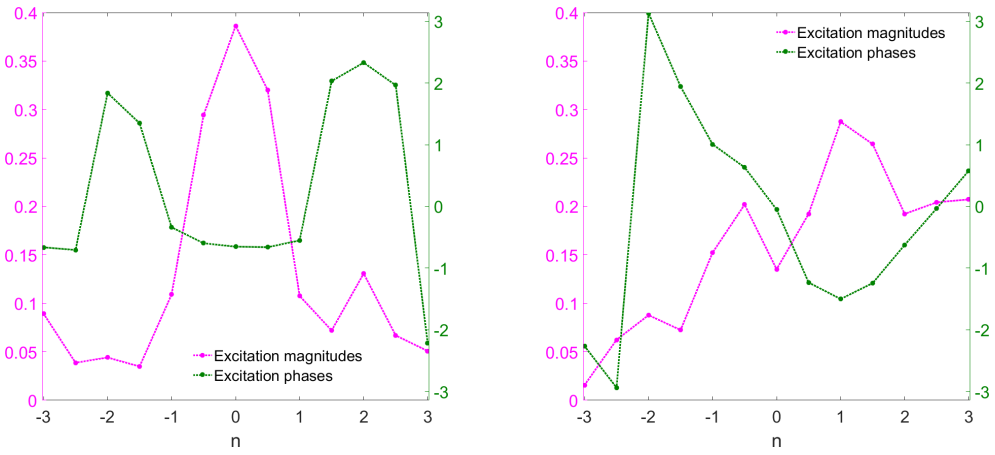

(a) (b)

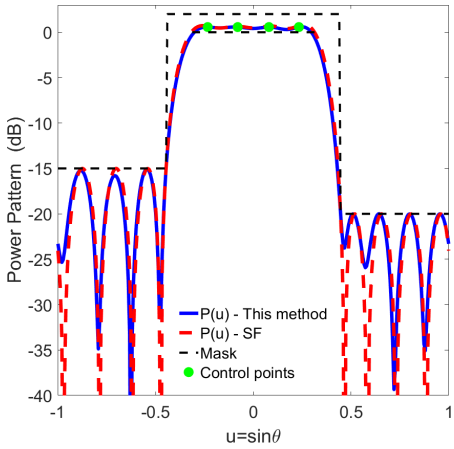

(c)

Fig. 2.2: Same as Fig. 1, but now with reference to the second synthesis problem dealt with in Subsection 2.3.1.

Table 2.1: Radiation performances achieved by the proposed method (comparison with the technique in [3]).

Performance Parameters	OES Method	This Method
Ripple [dB]	± 0.10	± 0.14
Directivity [dB]	9.31	9.15
Max SLL for $u < 0$ [dB]	-20	-23
DRR	9.27	9.23

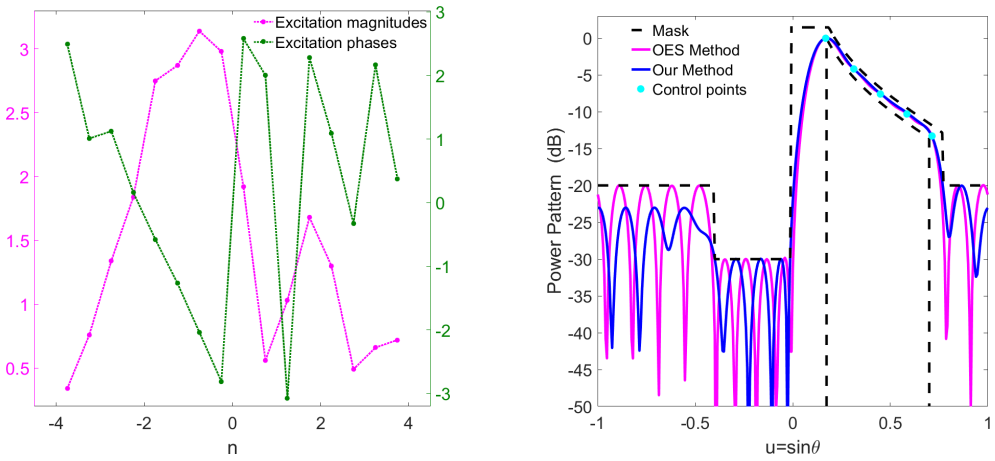

(a) (b)

Fig. 2.3: Comparison with [3]: excitations set synthesized through the proposed method (a) and comparison between the power pattern corresponding to them and the OES solution (b).

not exceed ± 0.5 dB and that a maximum sidelobe level lower than -15 dB for $u \leq -0.44$ and to -20 dB for $u \geq 0.44$ is achieved. Fig. 2.2 (c) depicts a superposition of the power patterns respectively delivered by the SF method and the proposed procedure. In this latter example, the four equispaced control points are located in $u_{\Lambda 1} = -0.23, u_{\Lambda 2} = -0.08, u_{\Lambda 3} = 0.08, u_{\Lambda 4} = 0.23$. The achieved directivity is equal to 4.54 dB, i.e., 0.39 dB lower than the one of a theoretical field being equal to 1 inside Λ and 0 elsewhere. Results again confirm the capability of the approach to achieve radiation performances as good as those of SF (wherein the achievement of the globally-optimal solution is guaranteed), i.e., ripple=± 0.06 dB, when both methods can be applied. Moreover, as in the previous example, the proposed approach has been also able to find a multiplicity of solutions. For example, figures 2.2 (a) and (b) depict two excitation sets both corresponding to the power pattern shown in Fig. 2.2 (c). For this mask, if DRR rather than ripple minimization is pursued then the DRR decreases from 11.1 to 6.5 while the ripple increases from ± 0.06 dB to ± 0.36 dB.

Due to the widely-recognized effectiveness of the SF method (see for instance [43, 52, 77, 78]), the results achieved in both test cases confirm the very good performances of the proposed architecture, and of the proposed approach to the synthesis.

2.3.2 Comparison with the OES method

In this Subsection, we challenge the proposed approach to provide performances similar to the ones achieved by the benchmark method published in [3]. To this end,

we considered an identical radiating system (i.e., an array composed of 16 isotropic elements with a constant $\frac{\lambda}{2}$ spacing) and set the power goals as the strictest ones reported in [3]. These latter consist in enforcing for $\theta \in [10°, 50°]$ a $cosec^2(\theta) \times cos(\theta)$ power-pattern behavior and strict upper-bound constraints on the sidelobes as shown in Fig. 4 (d) of [3], where the minimum possible ripple over the main-beam region was found to be ± 0.1 dB.

Table 2.2: Synthesized excitations for the power pattern shown in Fig. 2.3 (in the same format as in [3]).

n	$\lvert I_n \rvert$	$\angle I_n$
1	0.34	$-142.7°$
2	0.76	$-57.9°$
3	1.34	$-64.5°$
4	1.84	$-9.1°$
5	2.75	$33.0°$
6	2.87	$72.4°$
7	3.14	$116.7°$
8	2.98	$161.1°$
9	1.92	$-147.9°$
10	0.56	$-114.8°$
11	1.03	$176.3°$
12	1.68	$-130.8°$
13	1.30	$-62.4°$
14	0.49	$18.7°$
15	0.66	$-124.0°$
16	0.72	$-21.5°$

To perform the synthesis, we used $L = 5$ control points chosen according to the rules above, which result in $u_{\Lambda 1} = 0.17, u_{\Lambda 2} = 0.31, u_{\Lambda 3} = 0.45, u_{\Lambda 4} = 0.59, u_{\Lambda 5} = 0.71$. Moreover, we set $\alpha_1 = 1, \alpha_2 = 0.62, \alpha_3 = 0.42, \alpha_4 = 0.31, \alpha_5 = 0.22$. The key-performance parameters achieved by one of the solutions we found are summarized (and compared to the ones of [3]) in Tab. 2.1. Finally, Fig. 2.3 reports the achieved

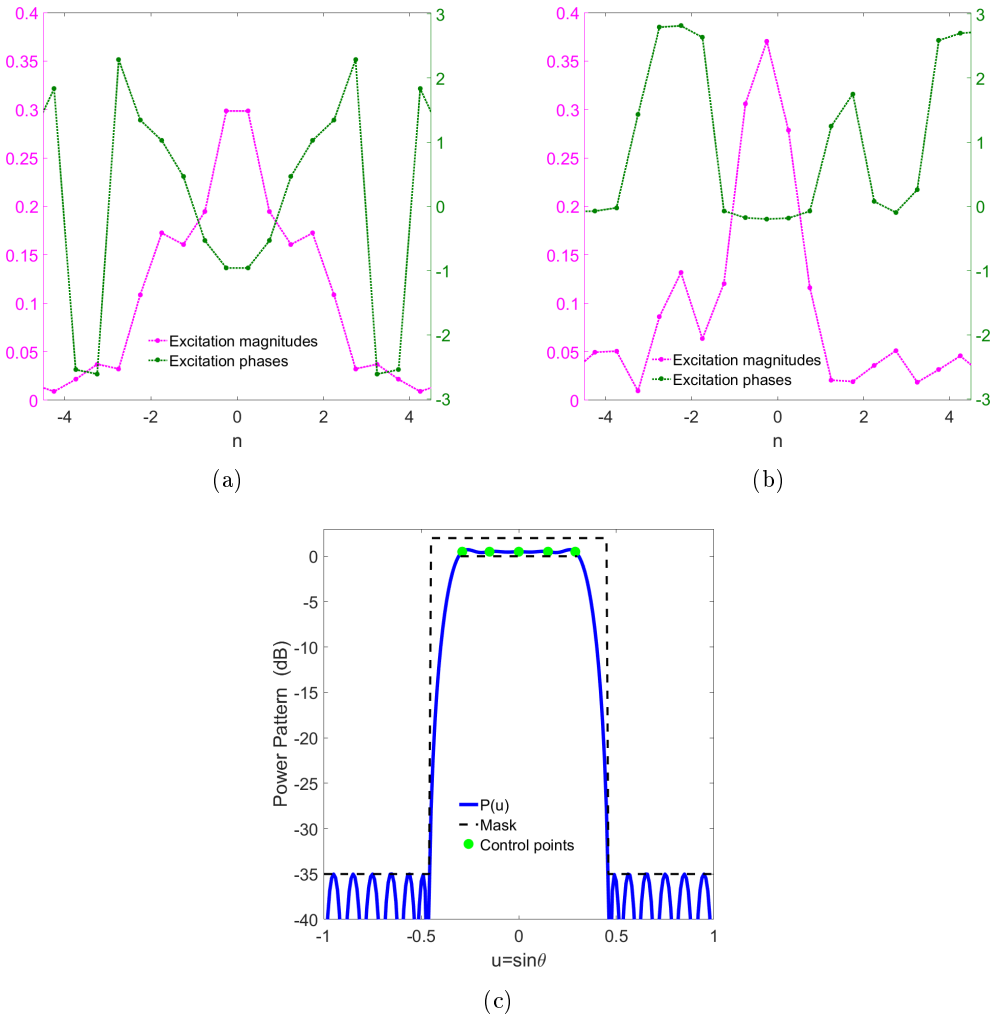

Fig. 2.4: Comparison with [1]: two different excitation sets synthesized through the proposed method [(a) and (b)], and power pattern corresponding to both of them (c).

excitations (which are also listed in Tab. 2.2) and a superposition of the corresponding power pattern with the exploited mask and the OES method's best solution.

Notably, the two techniques achieved very similar performances. In fact, the proposed approach allowed an improvement of both the sidelobe level (which decreased by 3 dB for $u < -0.4$ and $u > 0.9$) and the DRR (which decreased from 9.27 to 9.23) but, at the same time, provided a 0.16 dB lower directivity and a ± 0.04 dB higher ripple.

By considering the well known capabilities of the OES method, these results confirm the effectiveness of the proposed approach, whose performances can be eventually improved by a denser sampling of the space of phase shifts.

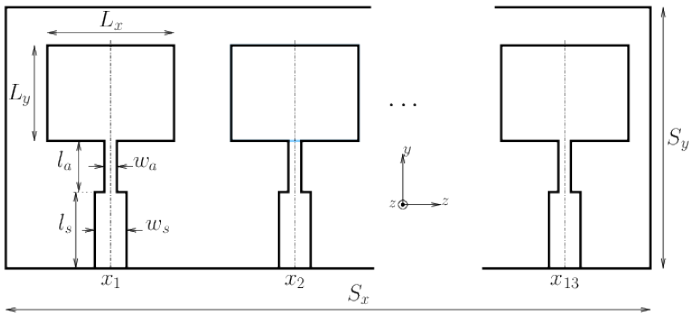

(a)

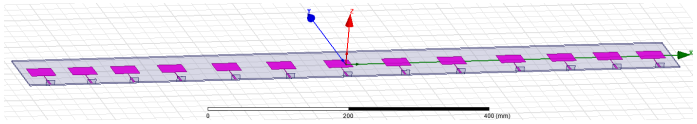

(b)

Fig. 2.5: Unequally-spaced array designed as in Subsection 2.3.4: layout (a) and 3-D HFSS view (b). The key parameters of the structure are listed in Tab. 2.3, while the patches' locations are reported in Tab. 2.4 and are the same as the ones published in [4–6].

2.3.3 Comparisons with the Taylor-based method [1]

We used the same reference array as in [1] (i.e., an array composed of 20 isotropic elements with a constant $\frac{\lambda}{2}$ spacing) and challenged the proposed method at lowering both the ripple value and the SLL. In this case $L = 5$ control points were set within $\Lambda \in [-0.29, +0.29]$, i.e., $u_{\Lambda 1} = -0.29, u_{\Lambda 2} = -0.15, u_{\Lambda 3} = 0, u_{\Lambda 4} = 0.15, u_{\Lambda 5} = 0.29$. Moreover, we set $\alpha_i = 1 \forall i$. Fig. 2.4 (c) reports the synthesized power pattern (which provides a directivity of 4.76 dB, i.e., 0.6 dB lower than the one of a theoretical field being equal to 1 inside Λ and 0 elsewhere) while figures 2.4 (a) and (b) respectively show two different excitation sets both corresponding to it. Notably, the proposed procedure favourably compares to the one in [1] by allowing a ripple reduction from 0.25 to 0.21 dB and, at the same time, a SLL reduction from -30 to -35 dB over the whole Ω region (i.e., $|u| \geq 0.45$).

2.3.4 Full-wave synthesis of an aperiodic array

We considered the same radiating structure and power-pattern constraints as in [6] in order to test the proposed approach in the full-wave synthesis of a non-ideal array which cannot be tackled by the SF and OES approaches. The latter is a non-uniformly spaced microstrip array composed of 13 elements (shown in Fig. 2.5) having the key

Table 2.3: Array design parameters referring to Fig. 2.5.

Parameter Name	*Value [mm]*	*Description*
L_y	27.7	Patch length (resonant)
L_x	36.87	Patch width
w_a	0.5	$\lambda/4$ strip width
l_a	16.78	$\lambda/4$ adapter strip length
w_s	2.92	50 Ω strip width
l_s	15.82	50 Ω strip length
h	1.57	substrate height
S_x	978.91	substrate length
S_y	92.9	substrate width

parameters and elements' locations respectively reported in Tab. 2.3 and Tab. 2.4. The single-element coordinates are reported also in Tab. 2 of [4] and have been used also in [5, 6]. The exploited power mask is the popular square-cosecant one depicted in Fig. 2.6 (c) and adopted also in [4–6, 68, 73].

As a first step, we computed the AEPs through the Ansys High Frequency Structure Simulator (HFSS) full-wave software [81] by setting $f = 2.45$ GHz and discretizing the u variable into 361 points. Then, $L = 5$ control points have been uniformly set within the target area $\Lambda \in [0.17, 0.83]$, i.e., $u_{\Lambda 1} = 0.17, u_{\Lambda 2} = 0.31, u_{\Lambda 3} = 0.45, u_{\Lambda 4} = 0.59, u_{\Lambda 5} = 0.73$. In order to achieve the desired cosecant pattern the amplitude coefficients have been set $\alpha_1 = 0.86, \alpha_2 = 0.48, \alpha_3 = 0.32, \alpha_4 = 0.23, \alpha_5 = 0.17$.

Fig. 2.6 reports three of the synthesized power patterns (whose maximum directivity is equal, in the average, to 13.9 dB) as well as one of the corresponding excitation sets and the related active driving impedances (compared with the self-impedances). Such impedance values, which are reported also in Tab. 2.4, actually differ from each other. This circumstance, combined with the heterogeneity of the AEPs (which are shown in Fig. 13 of [6]), testifies the actual presence of mutual coupling. On the other hand, the element-to-element self-impedance variations are not excessive and this can lead to a simple realization of the feeding network in a standard microstrip line technology.

In this case, the minimum DRR achievable while fulfilling the power mask turned out being equal to 1.4. Notably, for identical SLL performances, the proposed approach allowed decreasing the ripple with respect to [6] from ± 1.25 dB to ± 0.56 dB. Besides corresponding to improved radiation performances, the achieved result testifies a unique feature of the approach, i.e., the capability of providing a multiplicity of

Table 2.4: Aperiodic arrays's element locations referring to Fig. 2.5 and corresponding values of Z_{Dj} and $|Z_{Dj}/Z_{jj}|$ (see also Fig. 2.6).

Array element	x-Position [λ]	$\lvert Z_{Dj}\rvert$ [Ω]	$\angle Z_{Dj}$ [deg]	$\lvert Z_{Dj}/Z_{jj}\rvert$
1	-3.7487	34.46	11.8	0.75
2	-3.2394	44.27	9.4	0.95
3	-2.7173	47.67	4.6	1.03
4	-2.1410	47.15	1.5	1.02
5	-1.4688	46.17	5.9	1.00
6	-0.7949	46.59	2.9	1.01
7	-0.0912	46.64	5.7	1.01
8	0.6200	45.49	4.7	0.98
9	1.3009	45.35	3.3	0.99
10	2.0304	47.91	4.1	1.03
11	2.6541	46.53	6.8	1.00
12	3.2221	41.94	-2.4	0.91
13	3.7513	43.78	1.4	0.96

substantially-different excitation solutions even for aperiodic non-ideal arrays whose field cannot be expressed in terms of an array factor.

2.3.5 Synthesis of planar arrays

In the planar arrays case, the need of a larger number of control points implies an increased computational burden. As long as the given power mask is symmetric, one can limit computational requirements by enforcing the required symmetry in the expected complex pattern (which in turn translates into linear constraints on excitations). By so doing, as shown in the following, one is able to design in a still reasonable time planar arrays composed of hundreds of elements as well as realizing fields with large footprints. Notably, although reducing the DoF available to the designer, one is still able to design array solutions which favourably compare with the literature.

To show the reliability and effectiveness of the proposed method also in the 2-D case, in the following we compare its outcomes with the ones respectively achieved by the techniques in [2] and [7] in the synthesis of two planar arrays which cannot be tackled by the SF and OES techniques.

In the first test case, we considered the same array and power mask as the one adopted in [2], i.e., a 15×15 array with isotropic elements and a constant $\frac{\lambda}{2}$ spacing, as well as a mask enforcing a triangular footprint with a ripple and a peak SLL respectively equal to ± 0.5 dB and -29.4 dB. The enforced mask is shown in

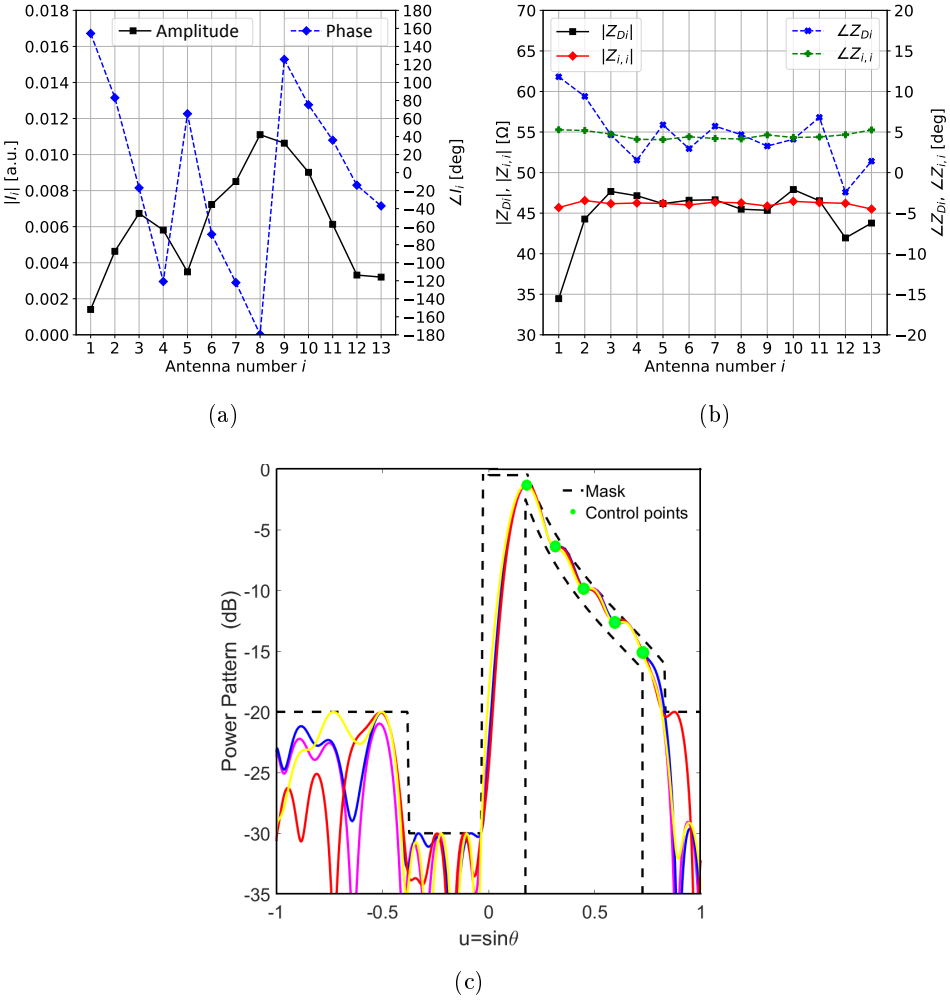

Fig. 2.6: Synthesis of a non-uniformly spaced microstrip array (full-wave HFSS simulation, comparison with [6]): one of the achieved equivalent excitation sets (a); comparison between the active driving impedance Z_{D_i} and the self-impedance $Z_{i,i}$ of the i-th element (b); multiplicity of synthesized power patterns (c).

Fig. 2.8 (c) (as well as in Fig. 10 of [2], where the footprint's vertices are also reported). By looking for a field symmetric with respect to the spectral plane's main diagonal, it has been possible to reduce the computational complexity of the synthesis. In particular, $L = 6$ control points have been uniformly set within half of the target area, corresponding to $(u_{A1},v_{A1})=(-0.85,-0.85)$, $(u_{A2}, v_{A2}) = (-0.25, -0.85)$, $(u_{A3},v_{A3})=(0.34,-0.85)$, $(u_{A4},v_{A4})=(0.85,-0.85)$, $(u_{A5},v_{A5})=(-0.25,-0.34)$, $(u_{A6},v_{A6})=(0.34,-0.34)$. Moreover, we set $\alpha_i = 1\ \forall i$.

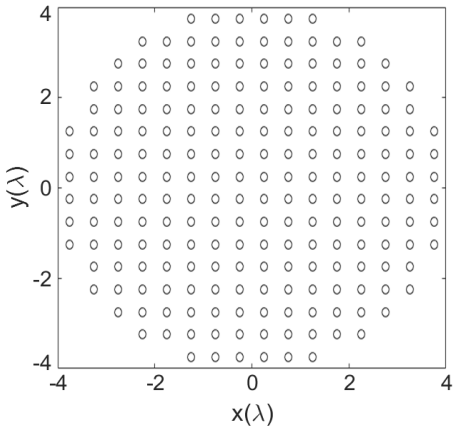

Fig. 2.7: Layout of the array with a circular boundary used in order to compare the proposed approach to the one in [7].

The square amplitude of the (complex) field synthesized through the proposed approach is shown in Fig. 2.8 (d) (2-D plot plus control points representation) and Fig. 2.8 (e) (3-D view), while figures 2.8 (a) and (b) report, respectively, the amplitude and phase of the excitation sets corresponding to it. The DRR turned out being equal to 16.2. It is worth noting that the achieved power-pattern distribution perfectly agrees with the one in [2] wherein, in turn, the application of the 'feasibility criterion' guaranteed that no array with a lower number of elements can equate those radiation performances.

In the second example dealing with planar arrays, we compared the outcomes of the proposed approach to the ones shown in [7]. In that paper, the authors exploited the 208-elements circular array layout shown in Fig. 2.7, which was designed by starting from a 16×16 square layout (with isotropic antennas and a $\frac{\lambda}{2}$ spacing) and then discarding the locations external to the circle of radius 4λ. The resulting radiating system was aimed at generating a flat-top beam guaranteeing a ripple equal to ± 0.15 dB for $|u| < 0.25$ and $|v| < 0.25$ as well as a peak SLL equal to -20.6 dB for $|u| > 0.3125$ and $|v| > 0.3125$.

The adopted mask is shown in Fig. 2.9 (c). In this case, we successfully performed the synthesis by looking for fields having a quadrantal symmetry, so that control points can be located in just a quarter of the shaped region. In particular, the adopted control points covering such a surface (and fulfilling the Nyquist criterion) correspond to $u, v \in [-0.25, 0.25]$, i.e., $(u_{\Lambda 1}, v_{\Lambda 1}) = (0.84,\text{-}0.08), (u_{\Lambda 2}, v_{\Lambda 2}) = (0.24,\text{-}0.24), (u_{\Lambda 3}, v_{\Lambda 3}) = (0.08,\text{-}0.08), (u_{\Lambda 4}, v_{\Lambda 4}) = (0.08,\text{-}0.24), (u_{\Lambda 5}, v_{\Lambda 5}) = (0, 0)$. Moreover, we set $\alpha_i = 1 \forall i$.

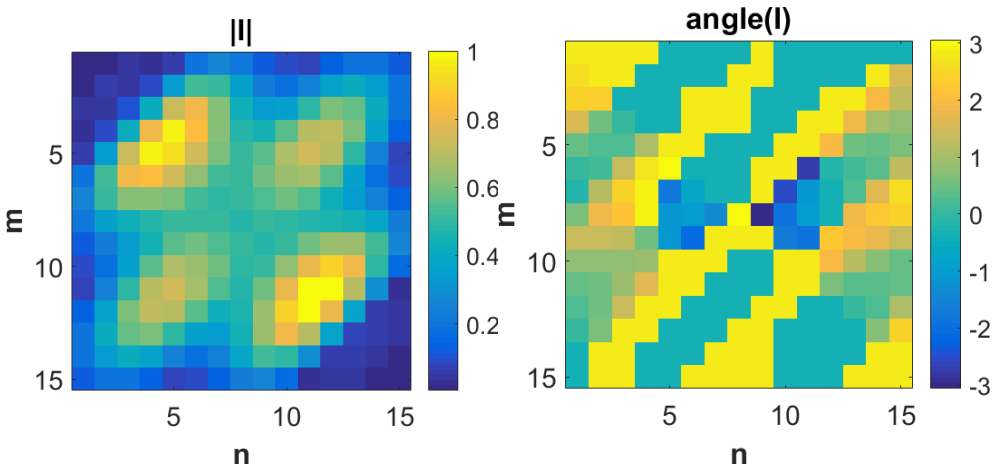

(a) (b)

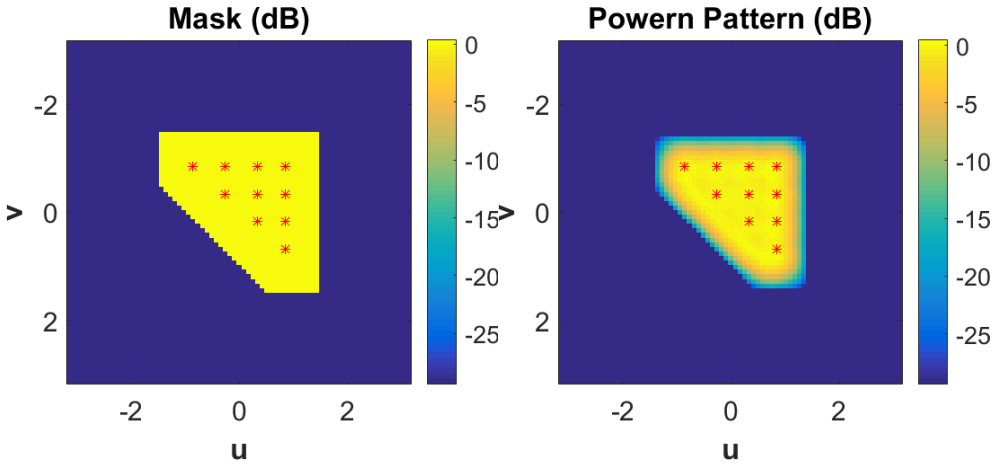

(c) (d)

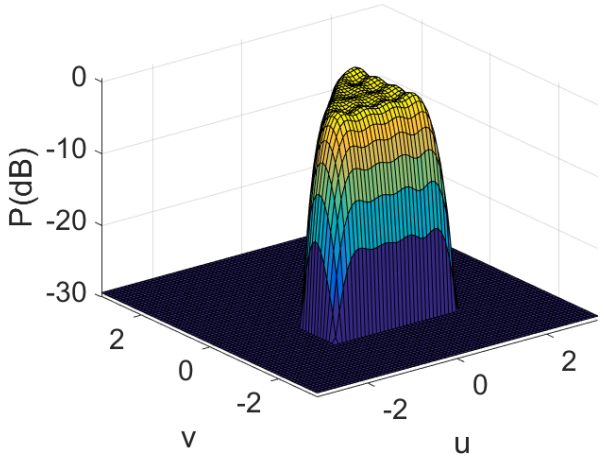

(e)

Fig. 2.8: Synthesis of a triangular contoured beam (comparison with [2]): amplitude and phase of the excitation sets synthesized through the proposed approach [(a) and (b)]; prescribed power mask and control points (c); 2-D and 3-D power-pattern representations [(d) and (e)].

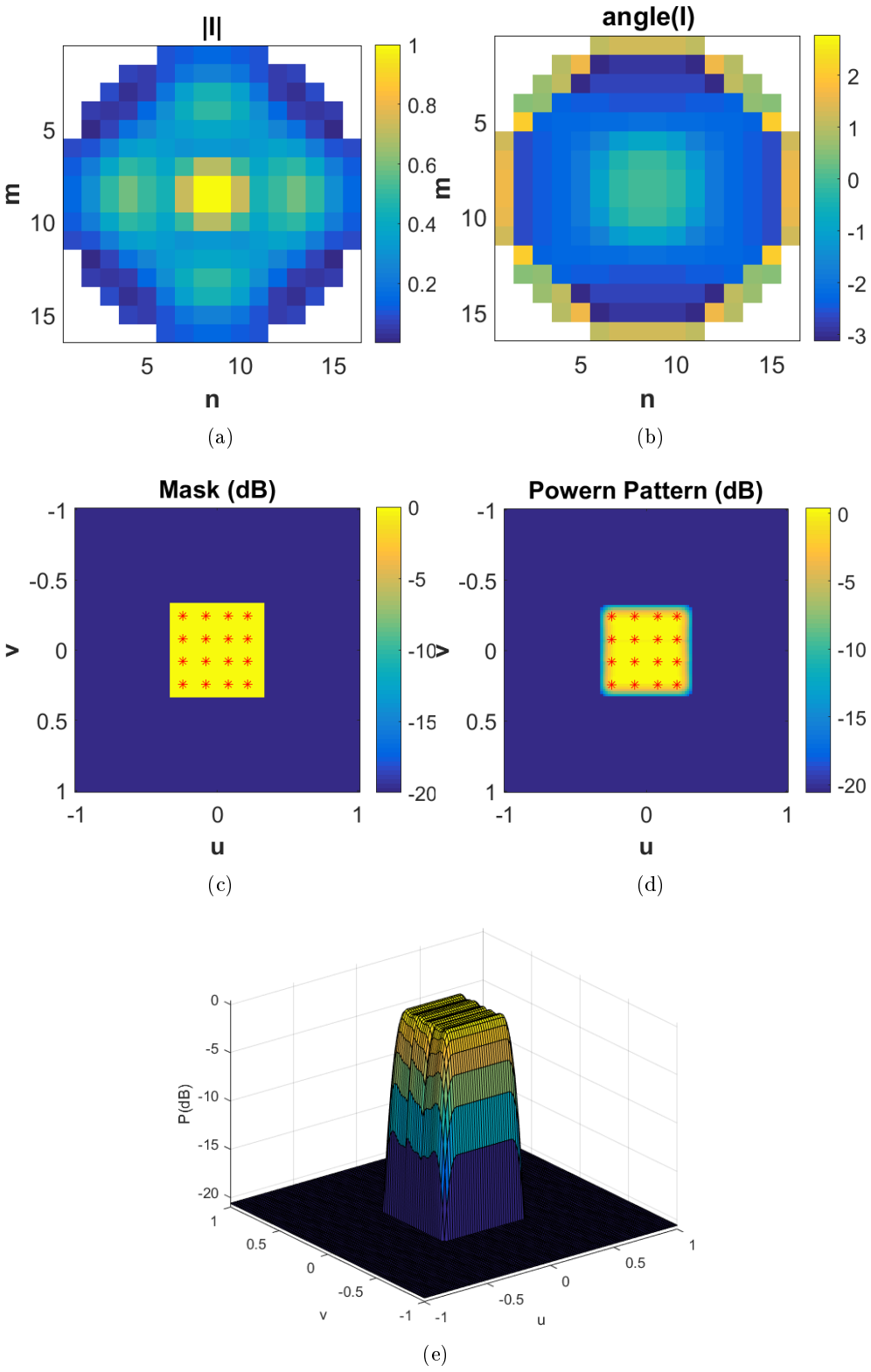

Fig. 2.9: Synthesis of a power pattern having a large square footprint (comparison with [7]): Amplitude and phase of the excitation sets synthesized through the proposed approach [(a) and (b)]; prescribed mask and control points (c); 2-D and 3-D views of the achieved power pattern [(d) and (e)].

Figures 2.9 (d) and (e) respectively show the 2-D and 3-D plots of the power-pattern distribution associated to the synthesized (complex) field, while figures 2.9 (a) and (b) report, respectively, the amplitude and phase of the excitation sets corresponding to it. Notably, the proposed method favourably compares to the one in [7] by allowing, for equal SLL performances, a ripple reduction from ± 0.15 dB to ± 0.1 dB and, at the same time, a DRR reduction from 24.4 to 20.

2.4 Comments and remarks

In this Chapter, by taking advantage from the basic "FOCO" formulation, the problem of shaping a field into a region of interest has been solved as an assembling of solutions of simpler problems. Results achieved in benchmark problems as well as in the case where the array factor cannot even be defined confirm the interest and validity of the approach.

Notably, the proposed method presents a number of interesting features.

First, differently from a large body of literature, it is not formulated in terms of GLO of the excitations, and it allows casting the overall design as a finite number of CP optimizations.

Second, which is a novelty with respect to all of the state-of-the-art methods, it is engineered in such a way to provide a multiplicity of excitation solutions even in those cases where it is not possible to reason just in terms of the array factor (and 1-D polynomials).

Third, by using the "reduced radiated field" concept [82], the approach can also be used to perform the pattern shaping on a NF surface (rather than in the FF zone).

Lat, but not least, the approach seems to be the first one able to grant, at the same time, all the above features plus the capability of dealing with completely-arbitrary array layouts and element patterns (including aperiodic planar and conformal arrays where mounting-platform and mutual-coupling effects are present). Notably, this is done without resorting to simplifying (yet common) assumptions such as dealing with symmetric array locations and AEPs [83], restricting the fields to the class of real ones [1, 67, 84], operating just in terms of the array factor [2], or pursuing (in the non-sidelobe region) a nominal field pattern synthesis rather than a power mask-constrained one [67, 85, 86].

Unfortunately, as long as enumerative techniques are used, the computational complexity of the problem increases with the number of control points. In particular, if M is the number of different φ_i values being considered ($\forall i = 2, ..., L$) in step (i),

the overall number of CP problems pertaining to step (i) will be equal to M^{L-1}. In case of need, a smart exploitation of the space of the phase shifts (including tabu search [87] for a-priori excluding unsuitable sets of values[7], or analytical derivations for restraining the search around given values) will allow reducing considerably the computational burden.

While having a computational complexity exponentially growing with the number of unknowns, the proposed method still implies a computational burden comparable or even lower than the one of GLO techniques acting on excitations (see for instance [72]) and semidefinite-relaxation approaches (see for instance [74]). In fact, the number of elements of an array is generally much larger than the number of phase shifts to be considered. Also, approaches based on semidefinite relaxation imply a number of unknowns which quadratically grows with the number of array elements, and the relaxation from a non-convex problem to a convex one can induce non-trivial and possibly-detrimental effects.

Therefore, the next Chapter proposes a possible way out for the synthesis of shaped beams by means of large and arbitrary arrays.

[7] For example, in the case of two control points, $\varphi_1 = \pi$ implies a negative interference at the midpoint between them, with detrimental effects on the ripple.

3

OPTIMAL SYNTHESIS OF SHAPED BEAMS AS A PROPER COMBINATION OF FOCUSED FIELDS AND LOW DIMENSIONAL GLOBAL OPTIMIZATION

3.0 Summary

The Chapter presents an innovative effective technique to the optimal power synthesis of shaped beams through fixed-geometry antenna arrays. In particular, the proposed formulation, which can take into account mutual coupling and mounting platform effects, is a hybrid approach based on a nested optimization, where the external GLO acts on the field's phase shifts over a minimal number of 'control points' located into the target region whereas the internal optimization acts instead on excitations. Notably, in line with the previous approach, the starting point is the basic "FOCO" formulation that is herein exploited in order to solve a more difficult problem. As the internal optimization of the ripple is shown to result in a CP problem and the external optimization deals with a reduced number of unknowns, a full control of the shaped beam's ripple and SLL is achieved even in case of arrays having a large size and aimed at generating large-footprint patterns. In a nutshell, the proposed method identifies the phases of a few field samples as the actual reason for the non-convexity (and hence the difficulty) of the problem, and then elaborates on such a circumstance in order to deal with a global optimization problem having a number of unknowns as small as possible. Numerical examples concerning applications of actual interest are given to assess the effectiveness of the proposed synthesis strategy[1].

[1] Some contents of this Chapter have been published in references [3, 9, 10, 12] of the "Publications List of G. M. Battaglia" reported at the end of the Thesis.

3.1 Motivation and state of the art

As discussed in [2,3,36,43,51,52,67,77,84,88–95] as well as in the previous Chapter, the optimal synthesis of array antennas plays a key role in many fields of applied electromagnetics including radar [32], satellite [31], and cellular [30] telecommunications, as well as electrical-energy [78] and medical [29] applications.

In this respect, the synthesis of *shaped* [3] beams still represents an unsolved canonical problem. In fact, as already stated in the previous Chapter, the problem has been solved in a globally-optimal fashion only in the case where the sought power pattern is (or can be reduced to) a 1-D trigonometric polynomial. In all the (very many) remaining instances, e.g., conformal arrangements of elements as well as arrays generating element-dependent radiation patterns, only sub-optimal solutions seem to be available. In fact, the problem is usually tackled by resorting to a GLO of either the excitations or all the field samples (see for instance [93–95]). Hence, since in most cases the computational complexity of GLO procedures is expected to exponentially grow with the number of unknowns [96], it can prevent (in case of arrays composed by a large number of elements) the actual attainment of the global optimum.

A very recent approach partially overcoming the above difficulties is the one presented in the previous Chapter. However, since the field's phase shifts are explored in an enumerative fashion, the computational burden of that approach grows very rapidly with the number of control points, so that it is expected to be unpractical and/or not effective in case of large-footprint power patterns and large arrays. Moreover, the sampling of the phase shifts' space which is needed for enumeration could be inadequate, thus possibly missing the global optimum.

As a contribution towards effective solutions strategies for such a problem, this Chapter proposes a nested optimization procedure where the external GLO acts on the field's phase shifts over a minimal number of 'control points' located into the target region whereas the inner convex optimization acts instead on excitations. Such a circumstance allows a full control of the shaped beam's ripple and SLL in a number of cases (involving arrays having a large size and aimed at generating relatively large-footprint patterns) which cannot be solved in a globally-optimal fashion by the state-of-the-art techniques.

Finally, it is worth to note that, in line with the previous Chapter, the proposed approach takes advantage from the basic "FOCO" formulation [36] that represents the key to our solution. Comparisons with the approach presented in the previous Chapter and many other methods confirm the effectiveness of the proposed method.

In the following, Section 3.2 is aimed at presenting the devised synthesis procedure, while Section 3.3 shows a number of results supporting to the given theory and reports the final remarks ending the Chapter.

3.2 The proposed synthesis approach

The component of interest of the FF of a generic N-elements array can be written as:

$$F(\underline{r}) = \sum_{n=1}^{N} I_n \Psi_n(\underline{r}) \tag{1}$$

wherein $\underline{r}$ is the spatial variable, I_n is the excitation of the *n-th* element, and $\Psi_n(\underline{r})$ represents the complex *scalar* field induced by the unitary-excited *n-th* antenna in the region of interest Ω when all the other antennas are turned off. As well known, the function $\Psi_n(\underline{r})$ represents the *n-th* AEP [97], which takes into account the possible heterogeneity amongst the radiating elements as well as mutual coupling and mounting platform effects.

The goal is to determine the optimal excitations generating a power pattern lying in a given mask [defined by an arbitrary upper-bound function UB($\underline{r}$) plus an arbitrary lower-bound function LB($\underline{r}$)] and optimising some performance parameter. In order to fix ideas, let us suppose we are interested in minimizing the shaped-beam ripple in the region Λ. To this end, we set the approach's basic bricks as follows:

i given the array layout and AEPs, let us sample Λ into L 'control points' $\underline{r}_{\Lambda i}$,...,$\underline{r}_{\Lambda L}$ at the Nyquist distance [80][2];

ii let us indicate with $\phi_i \in [-\pi, +\pi]$, $i = 1,...,L$, the field phase shift between $\underline{r}_{\Lambda i}$ and $\underline{r}_{\Lambda 1}$, and fix to 0 the phase value attained by of the field in the point $\underline{r}_{\Lambda 1}$ (which acts in the procedure as a 'reference' point)[3];

iii note that the square of the power pattern's ripple inside the shaped-beam region Λ can be expressed as:

$$R(I_1, ..., I_n, \phi_1, ..., \phi_L) = [P(\underline{r}) - \bar{P}(\underline{r})]^2 \tag{2}$$

[2] While this criterion will allow avoiding any redundancy, other choices (such as involving the so-called 'self-truncating' sampling series [98] — see also Appendix A) are possible.

[3] This assumption does not entail any lack of generality, as it is simply equivalent to fix the phase reference.

where $P(\underline{r}) = |F(\underline{r})|^2$ and $\bar{P}(\underline{r}) = [UB(\underline{r}) - LB(\underline{r})]/2$. Therefore, for any fixed L-tuple $\phi_1, ..., \phi_L$, R is a fourth-order polynomial of the unknowns $I_1, ..., I_n$. This notwithstanding, we show in Appendix A that, by a proper choice of the sampling points (and sampling representations), such a function can be considered to be substantially convex with respect to the field samples (and hence to the excitations, which linearly depend on them).

Under these assumptions, and by denoting as $|F|_i^{desired}$ the desired value for the field amplitude at the *i-th* control point, one can consider the following auxiliary synthesis problem:

$$\min_{\phi_1,...,\phi_L} \left\{ \min_{I_1,...I_N} \int_{r \in \Lambda} R(\underline{r}) dr \right\} \tag{3}$$

where the internal problem is subject to the following constraints:

$$\Re\{F(\underline{r}_{\Lambda i})\} = |F|_i^{desired} cos\phi_i \qquad i = 1, ..., L \tag{4}$$

$$\Im\{F(\underline{r}_{\Lambda i})\} = |F|_i^{desired} sin\phi_i \qquad i = 1, ..., L \tag{5}$$

$$|F(\underline{r})|^2 \leq UB(\mathbf{r}) \qquad \forall \underline{r} \in \Omega \setminus \Lambda \tag{6}$$

$$\bar{P}(\underline{r}) + \sqrt{R} \leq UB(\underline{r}) \qquad \forall \underline{r} \in \Lambda \tag{7}$$

where, by virtue of the definition of $\bar{P}$, the constraint (7) also entails that $|F(\underline{r})|^2 \geq LB(\underline{r})$.

A number of comments are now in order. As already discussed, for any fixed value of $\phi_1, ..., \phi_L$, constraints (4)–(5) are equivalent to enforce $|F(\underline{r}_{\Lambda i})| = |F|_i^{desired} \forall i$, and hence a proper choice of $|F|_1^{desired}, ..., |F|_L^{desired}$, and the use of constraints [36], allows shaping the power pattern inside the region of interest. Also, constraint (6) allows keeping under control the sidelobes' behavior outside Λ. Hence, in summary;

- *inside the target region* Λ, constraints (4) and (5) are used to ensure that the field amplitude attains a precise value on each of the control points while constraint (7) allows ensuring that its ripple does not exceed a given threshold;
- *outside the target region* Λ, constraint (6) allows keeping under control the sidelobes' behavior.

Notably, constraints (4)–(5) and (6) respectively are linear forms and a positive semi-definite quadratic form of the excitations. Then, provided R can be considered to be quadratic (which can be eventually enforced by a smaller spacing among control points, see the Appendix A), constraints (7) and the objective function (3) are also convex, so that the overall problem is a CP one, with the inherent advantages in terms

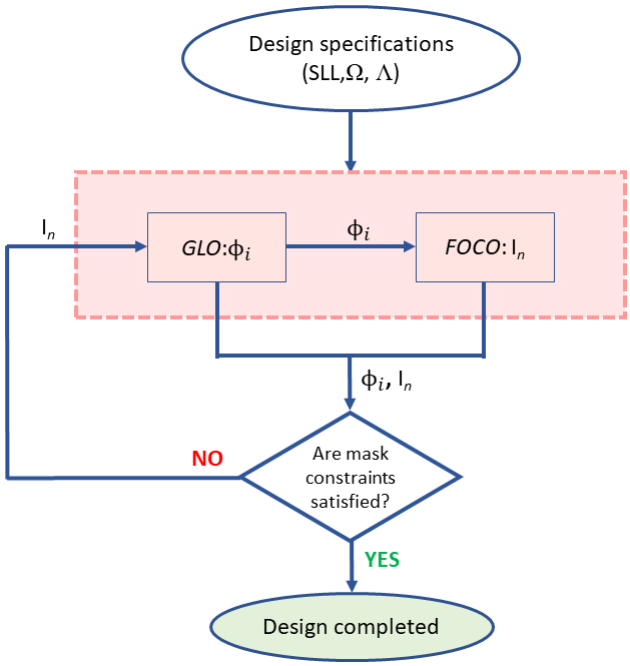

Fig. 3.1: Flowchart summarizing steps of the proposed approach to shaping the fields into the target area.

of solutions' optimality and computational burden. In particular, for any fixed value of $\phi_1, ..., \phi_L$ and $|F|_1^{desired}, ..., |F|_L^{desired}$, it admits a single minimum (if any), which is therefore the global optimum.

In (3) the external minimization will require a GLO tool on a reduced number of unknowns, whereas the internal minimization can be solved by means of a fast local-optimization. In summary, the synthesis is conveniently decomposed into two nested parts, i.e., a GLO on L variables and a CP optimization of the N excitations. It is also worth noting that the cost function (3) can be eventually substituted by other convex cost functions such as for instance the maximum value of R(r) [i.e., using a *minimax* criterion on the ripple rather than the one in (3)] or the overall radiated power (which would optimize directivity) without affecting the CP nature of the overall problem.

The overall procedure is summarized in the flowchart of Fig. 3.1, and it has been conceived in such a way that the GLO deals with the minimum number of unknowns (i.e., just with the ones responsible for non-convexity), with a beneficial impact on both the computational time and the reliability of the obtained results.

The proposed approach exploits the partial convexity[4] of the overall synthesis problem with respect to the excitations in order to reduce the dimensionality of the GLO problem. In fact, as long as the number of control points keeps reasonably

[4] By 'partial convexity' we mean here convexity for the case of fixed phase shifts.

small, the GLO algorithm must deal only with the few (auxiliary) variables in which the overall problem is not convex, i.e., the phase shifts, with a decisive, beneficial effect on both the computational time and the reliability of the obtained results. In fact, the exploitation of a GLO on just the 'non-convex part' of the problem will allow avoiding sub-optimal solutions, i.e., local minima of the objective function. Moreover, since the required value of L is generally much lower than N, the computational burden of the proposed synthesis procedure will be lower than the one of any GLO algorithm acting on either all of the field samples or the array excitations. Finally, possible discretization errors arising in the enumerative technique presented in the previous Chapter are also avoided. As a consequence of all the above, the proposed strategy is much more effective than the previous enumerative technique which, however, was able to identify a multiplicity of solutions.

3.3 The proposed approach at work

In this Section, we report some numerical examples concerning the synthesis of large planar arrays. In particular, in Subsection 3.3.1 we provide comparisons with the procedures respectively published in [2, 7], and [8], while in Subsection 3.3.2 we consider a realistic array of truncated waveguides with full-wave simulated AEPs.

In order to deal with a number of unknown phase shifts as small as possible, we basically consider a Nyquist sampling for the choice of the control points. Smaller displacements have been anyway used in some cases (as indicated) in order to get a better matching with the mask requirements.

The internal and external part of the minimization (3) have been respectively performed thorough the *fmincon* and *ga* routines of MATLAB (version R 2016B). Also note that an optimal choice of the external global optimization procedure is outside of the scope of the proposed general approach.

In all experiments, the radiating system has been set as an equispaced planar array composed by an eventually different number of elements along the x and y axes, and the $\underline{r}$ coordinate has been expressed through the usual spectral variables u and v, i.e., $u = \beta d_x sin\theta cos\phi$ and $v = \beta d_y sin\theta sin\phi$ [where $\beta = 2\pi/\lambda$ denotes the wavenumber (λ being the operative wavelength), (d_x,d_y) are the element spacings along the x and y axis, and (θ, ϕ) respectively denote the elevation and azimuth aperture angles with respect to boresight). Moreover, we set $|F|_i^{desired} = 1 \forall i$.

The radiation performances have been evaluated by means of the 'peak-to-trough' ripple (PTR) (defined as the ratio between the maximum and the minimum value

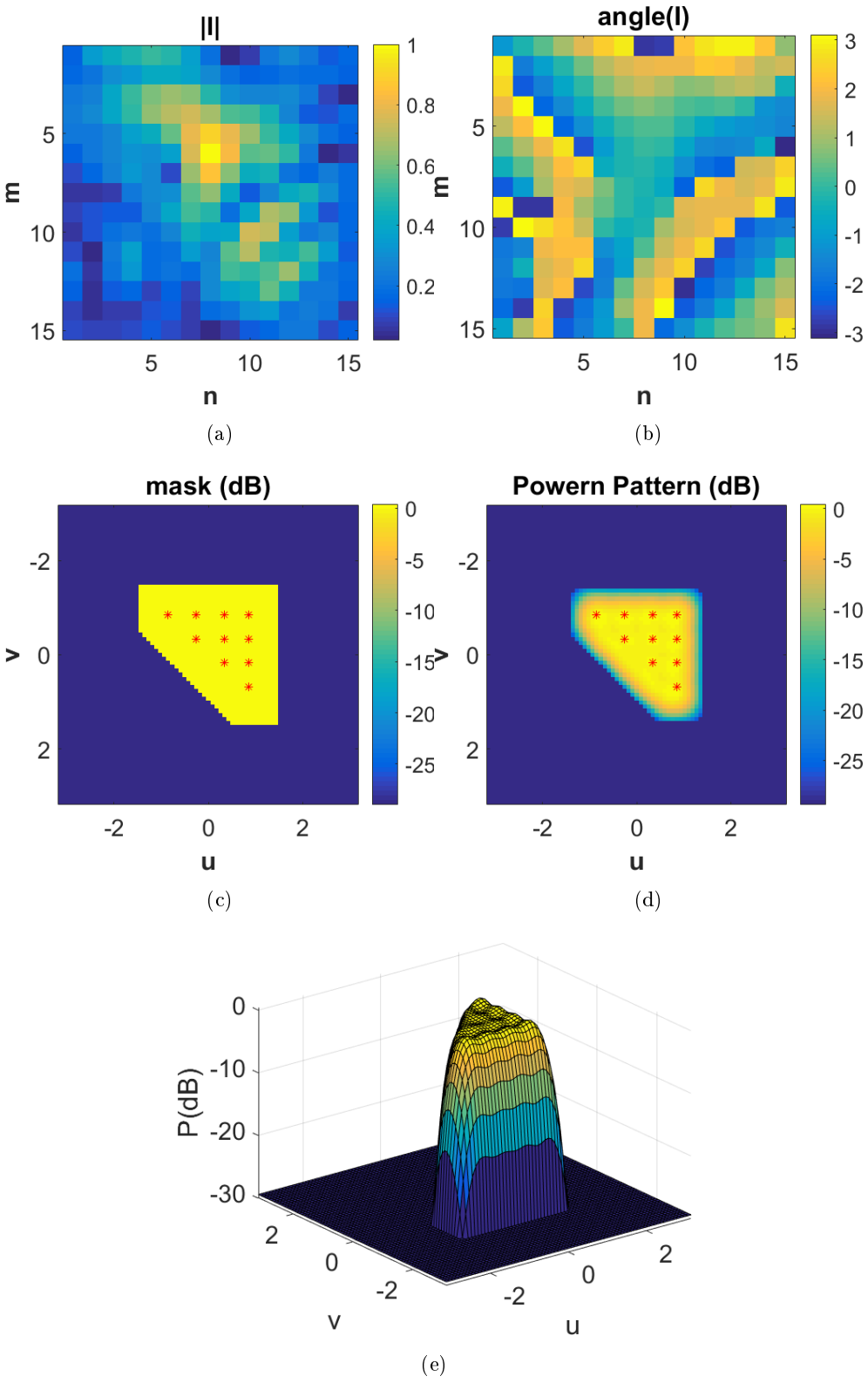

Fig. 3.2: Synthesis of a triangular contoured beam (comparison with [2]): amplitude and phase of the excitation sets synthesized through the proposed approach [(a) and (b)]; prescribed power mask and control points (c); 2-D and 3-D power-pattern representations [(d) and (e)].

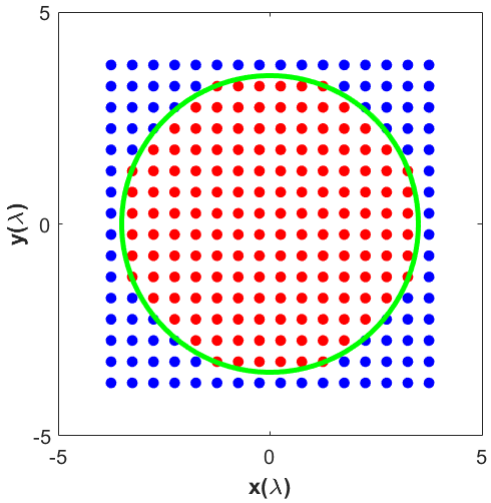

Fig. 3.3: Array layout (comparison with [7]), where only the elements internal to the circle of radius 3.5λ (i.e., depicted in red color) are used.

attained by the power pattern $\forall \underline{r} \in \Lambda$), the 'peak' sidelobe level (PSL) (defined as the ratio between the maximum value attained by the power pattern $\forall \underline{r} \in \Omega \setminus \Lambda$ and the power pattern's absolute maximum), and the DRR (defined as the ratio amongst the maximum and minimum amplitudes of the excitations). In particular, for each example, we report the achieved values for these parameters in two different cases, i.e.:

- case (a), when using the basic formulation of the synthesis problem;
- case (b), when adding to the stopping rule of *ga* an upper-bound constraint on DRR and turning off (i.e., erasing) the antennas having a very-small excitation amplitude.

3.3.1 Comparison with Some Existing Approaches

In the first example, we considered the same array and power mask as the ones adopted in [2] and in the previous Chapter, i.e.:

- a square equispaced array with $N = 225$ isotropic elements located along the x and y axes with a 0.5λ spacing;
- the power mask shown in Fig. 10 of [2], which enforces a triangular footprint with PTR = 1 dB.

In order to get the desired shaping, $L = 10$ control points have been located inside the region Λ as described by fig. 3.2 (c). Figures 3.2 (d) and (e) respectively show the 2-D and 3-D plots of the power pattern distribution associated

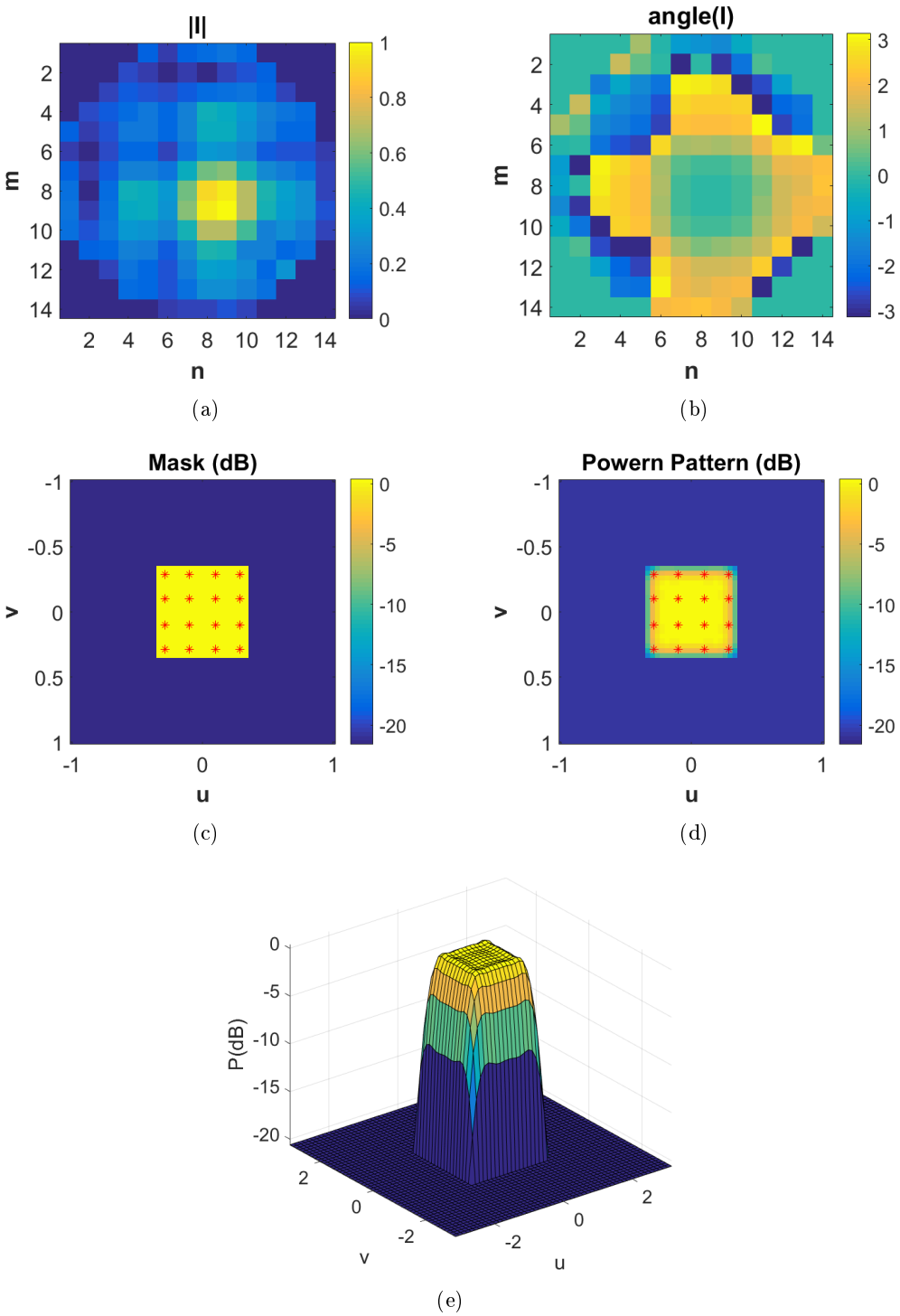

Fig. 3.4: Synthesis of a 156-elements array generating a flat-top power pattern having a square footprint (comparison with [7]): Amplitude and phase of the excitation sets synthesized through the proposed approach [(a) and (b)]; prescribed mask and control points (c); 2-D and 3-D views of the achieved power pattern [(d) and (e)].

Fig. 3.5: Map of China (courtesy of the authors of [8])

to the synthesized (complex) field, while figs 3.2 (a) and (b) report, respectively, the amplitude and phase of the excitation sets corresponding to it. The presented method provided $\{DRR = 144, PTR = 1dB, PSL =-29.4dB\}$ in the case (a), and $\{DRR = 97, PTR = 1dB, PSL =-29dB\}$ in the case (b) by erasing the 7 elements having the lowest excitation amplitude. Therefore, in the latter case, as compared to the results in [2] (i.e., $DRR = 20, PTR = 1dB, PSL =-28dB$) the approach provided a lower PSL but a larger DRR. Since it allows the straightforward determination of the array excitations, the present approach is both much easier to implement and much faster than the one in [2]. Finally, the computational burden was considerably reduced with respect to the technique presented in the previous Chapter, where, in fact, we needed to enforce some symmetry on the complex pattern in order to halve the number of control points (with a consequent loss of DoF).

In the second test case, we compared the proposed technique to the one in [7] by pursuing similar power-pattern goals through an array composed of a lower number of elements. In particular, starting from a 16×16 grid (with $d_x = d_y = 0.5\lambda$), an array composed by $N = 208$ elements has been considered in [7] by erasing all the antennas external to the circle of radius 4λ. Conversely, by starting from the same uniform grid but using a circle of radius 3.5λ (see fig. 3.3) in order to discard some elements, we achieved a layout composed of 156 elements. All the element patterns have been set as isotropic and, in the same way as in [7], the mask has been designed in such a way to generate a flat-top beam with a square footprint covering the region ($|u|<0.25$, $|v|<0.25$) and guaranteeing a $PSL =$-20.6dB for ($|u|>0.3125$, $|v|>0.3125$).

The $L = 16$ adopted control points are depicted in fig. 3.4 (c). Figures 3.4 (d) and (e) respectively show the 2-D and 3-D plots of the power pattern distribution associated to the synthesized (complex) field, while figs 3.4 (a) and (b) report, re-

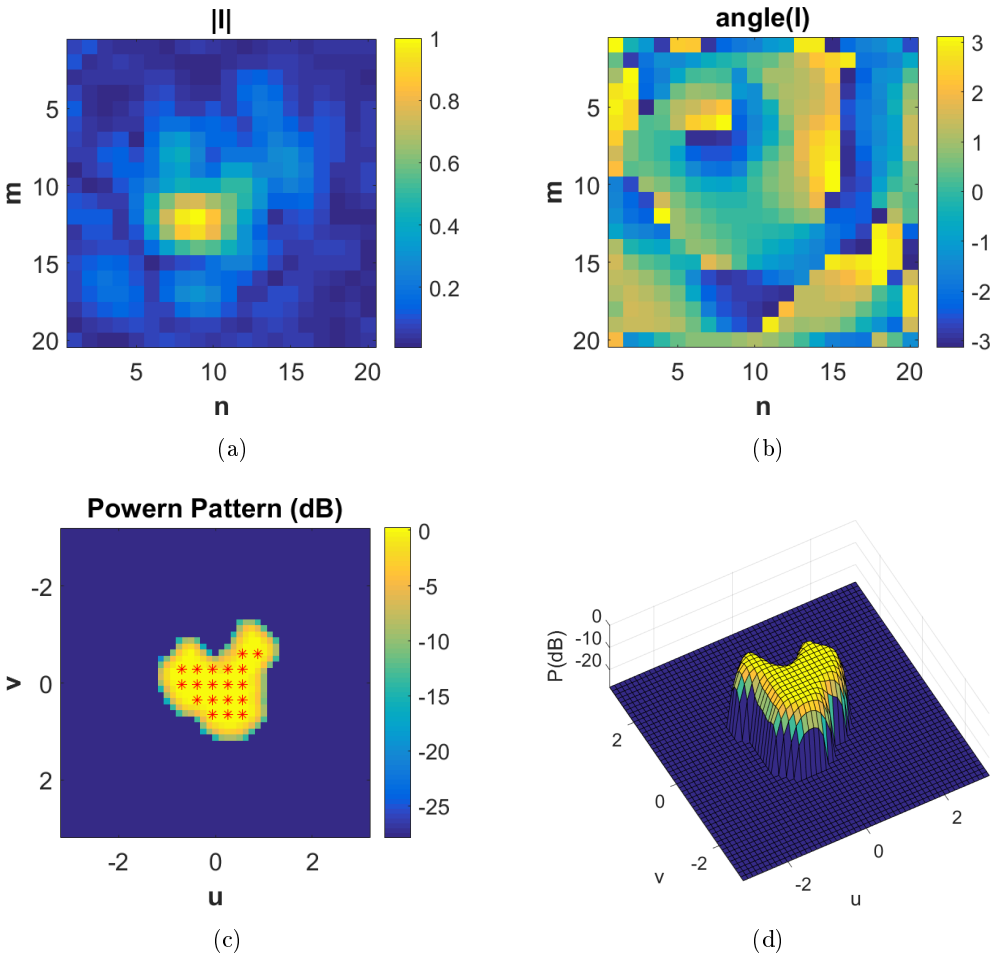

Fig. 3.6: Synthesis of a 400-elements array devoted to covering the mainland of China (comparison with [8]):Amplitude and phase of the excitation sets synthesized through the proposed approach [(a) and (b)]; 2-D and 3-D views of the achieved power pattern [(c) and (d)].

spectively, the amplitude and phase of the excitation sets corresponding to it. The presented method provided $\{DRR = 174, PTR = 0.3dB, PSL$ =-20.6$dB\}$ in the case (a), and $\{DRR = 19, PTR = 0.45dB, PSL$ =-20.6$dB\}$ in the case (b) by erasing the 6 elements having the lowest excitation amplitude. Therefore, in the latter case, as compared to the best results in [7] (i.e., $DRR = 24.4, PTR = 0.3dB, PSL$ =-20.6 dB), the proposed approach allowed to save the 22.5% of elements while guaranteeing the same PSL and beam footprint, a slightly lower DRR, and a slightly larger PTR. As in the previous test case, the adopted mask and the synthesis goals resulted unaffordable by the approach presented in the previous Chapter.

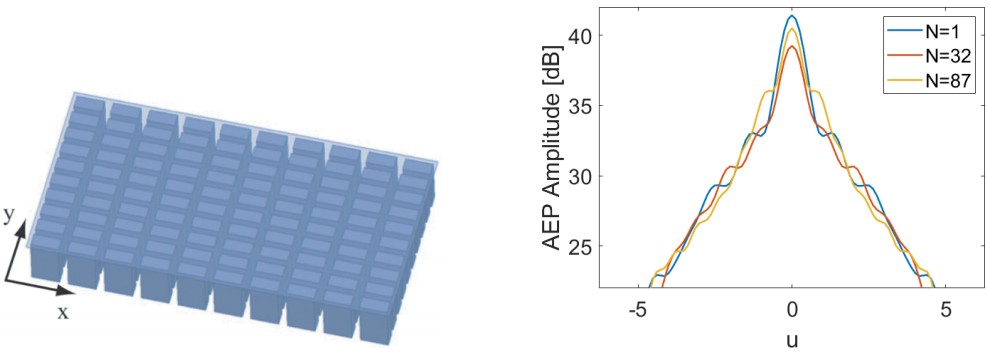

(a) (b)

Fig. 3.7: Full-wave synthesis of a realistic array generating a flat-top beam having an elliptical footprint: (a) llustration of the 100 WR90 open-ended waveguide array simulated through CST [(c) subplot, figure taken from [9]); (b) a sample of AEPs.

As the third test case, we provide a comparison with the method recently published in [8]. In particular, we considered the same array and specifications as the ones adopted therein, i.e., a $N = 400$ elements square array (composed by 20×20 isotropic antennas located on the x and y axes with a constant 0.5λ spacing) as well as a mask pursuing a uniform coverage of the mainland of China (see fig. 3.5, and also Fig. 7 of [8]).

To get the desired shaping, $L = 19$ control points have been uniformly set within the target area as reported in fig. 3.6 (c). The 2-D and 3-D plots of the achieved power-pattern distribution are respectively shown in fig. 3.6 (c) and fig. 3.6 (d). The amplitude and phase of the corresponding excitations are depicted in fig. 3.6 (a) and fig. 3.6 (b), respectively.

The presented method provided $\{DRR = 10000, PTR = 0.12dB, PSL =-27.9dB\}$ in the case (a), and $\{DRR = 198, PTR = 1dB, PSL =-27.9dB\}$ in the case (b). Therefore, in the latter case, it favorably compares to one in [8] by allowing equal PSL performances, a PTR reduction from 1.4 to 1.0 dB and, at the same time, a DRR decrease from 1000 to 198. Finally, it is worth noting that the number of control points required to realize the China coverage definitively excludes the enumerative technique developed in the previous Chapter.

3.3.2 Full-wave Synthesis of a Realistic Array

As a final numerical experiment, we tested the proposed technique for the full-wave synthesis of a $N = 100$ elements planar array equal to the one considered (for different purposes) in [9,16], i.e., composed by 10×10 truncated waveguides uniformly

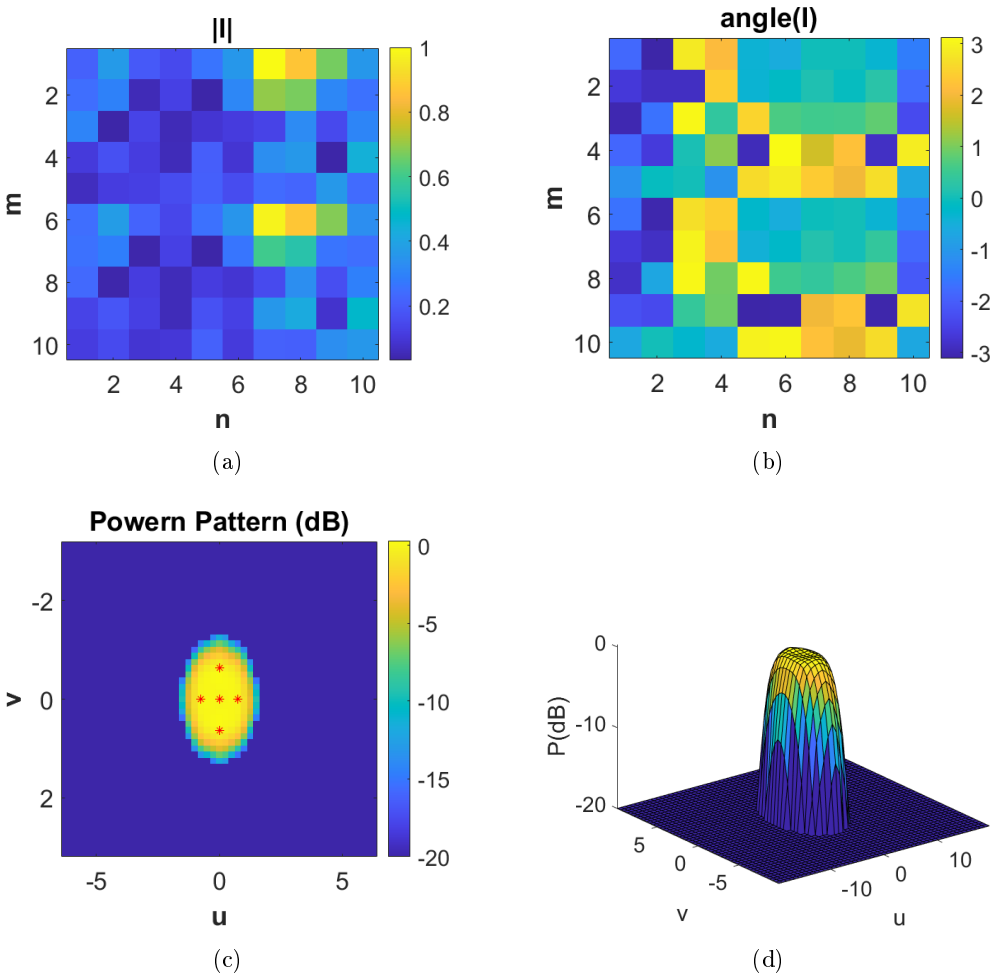

Fig. 3.8: Full-wave synthesis of a realistic array generating a flat-top beam having an elliptical footprint: Amplitude and phase of the excitation sets synthesized through the proposed approach [(a) and (b)]; 2-D and 3-D views of the achieved power pattern [(c) and (d)].

spaced with $d_x = \lambda$ and $d_y = 0.5\lambda$. In particular, WR90 waveguides having a size of $22.86 \times 10.16\ mm^2$, operating at 10 GHz, truncated without any flaring, and mounted on an infinite ground plane were used [see fig. 3.7 (a)].

First, in order to perform the synthesis, the AEPs have been computed by CST Microwave Studio full-wave simulations. Some of them, whose heterogeneity prevents one from using any technique relying on the array factor concept or trigonometric polynomials, are reported in fig. 3.7 (b).

Then, the ripple has been minimized within the ellipsoidal shaped target area of axes $(sin\theta cos\Phi, sin\theta sin\Phi) = (0.22, 0.42)$ while pursuing a PSL =-20dB outside the

ellipsoidal area of axes $(sin\theta cos\Phi, sin\theta sin\Phi) = (0.45, 0.86)$. To this end, $L = 5$ control points have been uniformly set within the target area as reported in fig. 3.8 (c).

Figures 3.8 (c) and 3.8 (d) respectively show the 2-D and 3-D plots of the synthesized power pattern, while amplitude and phase of the corresponding excitations are depicted in fig. 3.8 (a) and fig. 3.8 (b), respectively. The PTR and DRR turned out being equal to 0.28 dB and 32.2, respectively.

3.4 Comments and remarks

A contribution has been given to the synthesis of shaped beams patterns subject to arbitrary sidelobe bounds by means of generic fixed-geometry arrays. Results achieved in benchmark problems confirm the interest and validity of the approach.

In particular, the proposed method represents the natural extension of the enumerative technique introduced in the previous Chapter. In fact, it is based on the exploitation of some hidden convexity property, auxiliary variables, and nested optimization.

In particular, it has been shown that the problem of shaping the field into a target area can be recast as an optimization with respect to two sets of unknowns, that is the field's phase shifts and the arrays' excitations (when considering a fixed-geometry array). While the enumerative technique is based on the solution of several CP problems (with respect to the array's excitations) associated with each field's phase shift, the hybrid approach relies on performing the GLO in the phase shifts' space.

As discussed and validated through examples, the approach is very effective even in those cases where the previous methods based on either enumerative strategies or GLO on all the excitations (or field samples) result too heavy under the computational point of view. In fact, the GLO is here performed on a minimal number of unknowns (which are conveniently identified as the field phase in a low number of control points). By so doing, the computational burden required for optimizing the synthesis is reduced as much as possible.

The new approach is also very general and overcomes the limitations of the WL related techniques (which do not exploit the DoF arising from the field's phase shifts) as well as of all methods requiring that the field is expressible as a 1-D trigonometric polynomials.

4

OPTIMAL FOCUSING OF VECTOR FIELDS IN A 3-D SPACE AS A COMBINATION OF BASIC POLARIZED FIELDS

4.0 Summary

This Chapter aims at outlining, discussing, and assessing a new hybrid effective approach to focus the intensity of a vector field generated by an arbitrary fixed-geometry array antenna into a target point and keep it bounded elsewhere. To overcome the complexity of the underlying non-convex problem involving a possibly large number of unknowns, the proposed solution deals with a nested procedure which jointly relies on an (external) global optimization of the field polarization on the target point plus an (internal) convex optimization of the array excitations. Notably, in line with the shaping problem, the starting point is the basic "FOCO" formulation that is extended in order to solve a more difficult problem. As a matter of fact, by so doing, one can not only focus the target point, but also obtain a field distribution that better accommodates some other requirements (e.g., minimization of sidelobe level). Numerical examples concerning applications of actual interest support the given theory and confirm the effectiveness of the developed solution strategies[1].

[1] Some contents of this Chapter have been published in references [4, 11, 14] of the "Publications List of G. M. Battaglia" reported at the end of the Thesis.

4.1 Introduction

Focusing a field into a target point while controlling its intensity level elsewhere has a considerable interest in areas as different as: activation of chemical [99] or biological [100] processes, array antenna synthesis [36, 88, 101], deep tissue hyperthermia treatments planning [29], radio frequency identification (RFID) systems [102–104], medical systems for microwave imaging [105], gateway control system [55], or wireless power transmission [56]. In all of these applications, the goal is designing the excitations of an array antennas able to induce a selective field concentration.

More precisely, the problem at hand amounts to find a source such to maximize the field intensity in the target point, while ensuring elsewhere a prescribed upper mask for the sidelobes.

In a first instance, one can consider two different cases, i.e., the case where one is interested in focusing a scalar field (or a single component of a vector field) and the case where one pursues instead the focusing of the overall intensity of the vector field at hand. A further element leading to different focusing problems is whether or not one is interested in controlling the level of the field intensity outside of the target region (which leads to a constrained optimization problem).

Last, but not least, in an eventual classification of the different problems, one also has to consider the DoF at disposal for synthesis. In fact, one can consider the amplitude and the phase of the excitations of an array [43], or just the phases of these latter [89], or the aperture-field distribution [106], and many other cases including the case where locations of the array are unknown.

Some interesting solutions applicable to scalar fields are already available in literature such as the one in [56], where the focused field at a target point located in the NF zone is obtained by an iterative algorithm ensuring that the radiated field lies in a specific mask. In case focusing of a single component is of interest, the technique allows full control of the depth of focus, spot diameter, and SLL.

An elder overlooked approach dealing with the focusing of scalar fields with constrained SLL is the one in [36][2]. This latter has been then generalized and applied to 3-D complex scenarios and hyperthermia problems [59] for the case where one component of the field is dominant. However, this strategy cannot be trivially extended to the constrained focusing of the intensity of a vector field. In fact, in this case suitable strategies are required to achieve the globally optimal solution of the aris-

[2] Although written for the FF case, which is the reason while it has been overlooked in the NF literature, [36] explicitly notes the applicability to the cases of NF constraints and NF focusing.

ing non-convex problem [58]. Hence, some alternative strategy has to be devised to preserve the capability of achieving the global optimum, while controlling side power deposition.

An attempt to solve the field intensity focusing problem has been made in [107] where, however, the formulated optimization problem (acting directly on excitations) results in a non-convex optimization on many variables, so that solution procedures may still get stuck at local optima.

A recent general approach partially overcoming the above difficulties has been introduced in [108]. In the latter, exploiting [36], the overall problem is tackled as the solution of a sequence of convex problems. In fact, one can solve the convex problem corresponding to any possible field polarization into the target point and then select the solution which guarantees the best focusing performances. Unfortunately, the overall optimization procedure is very time consuming and/or affected by errors deriving from an insufficiently-fine discretization of the space of polarizations.

Due to the above reasons, the development of new approaches to the focusing of vector fields has always represented a field of research in Electromagnetics [62, 108, 109]. To this end, this Chapter presents a hybrid approach, for a generic fixed-geometry set of sources, based on nested optimizations where the inner (convex) problem looks for the excitations corresponding to the optimal polarization which, in turn, is externally pursued through GLO. Consequently, the optimal focusing problem is reduced to a GLO of a cost functional which just depends on the field polarization.

It is worth to note that, in line with the previous approaches developed for the shaping problem, the proposed technique takes advantage from the basic "FOCO" formulation [36] that represents the starting point to initiate the overall procedure.

Notably, the exploitation of GLO algorithms is obviously not a novelty in the antenna synthesis community. However, differently from [110] (where other antenna problems are considered), the GLO-based problem only has to deal with a very reduced number of parameters (i.e., the five parameters identifying the field polarization at the target point – see Appendix B). Such a feature plays a decisive role in order to get actually optimal solutions to the problem at hand. In fact, although still dealing with a non-convex problem, the approach is much more effective than all the ones where the excitations of the array (which can have very many elements) are directly looked for.

The Chapter is organized as follows. The next Section presents the basic idea and the corresponding procedure, while Section 4.3 reports a representative set of results. Conclusions follow.

4.2 The synthesis approach

The proposed approach, which will be referred in the following as IN-FOCO is aimed at maximizing the intensity of a *vector* field in a given point or direction (subject to arbitrary upper bounds elsewhere) by exploiting the excitations of a generic (fixed-geometry) array antenna as DoF.

As recalled in Section 4.1, the vector nature of the field induces a further difficulty to the focusing problem. Therefore, by taking advantage from the FOCO's underlying theory [36], in the following a possible solution strategy relying on the identification (and isolation) of the reason for non-convexity has been presented. Once again, similarly to the methods proposed for the shaping problem, the basic "FOCO" formulation represents the starting point to initiate the overall procedure.

To this end, given an arbitrary set of N sources with given locations, the total radiated field can be written as:

$$\mathbf{F}(\underline{r}) = \sum_{n=1}^{N} I_n \boldsymbol{\Psi}_n(\underline{r}) \tag{1}$$

wherein $\underline{r}$ and I_n denote the coordinate spanning the observation space and the *n-th* complex excitation coefficient, respectively, while $\boldsymbol{\Psi_n}(\underline{r})$ is the complex *vector* field induced by the unitary-excited *n-th* antenna in the region of interest Ω when all the other antennas are off. As such, the function $\boldsymbol{\Psi}_n(\underline{r})$ represents the *n-th* AEP and includes possible mutual-coupling and mounting-platform effects [97].

If we denote by $\underline{r}_t \in \Omega$ the target point, i.e., the point in which we want to focus the field intensity, the constrained focusing problem can be formulated as follows:

Determine the complex excitations set such to maximize $|\boldsymbol{F}(\underline{r}_t)|^2$ *while enforcing arbitrary upper bounds elsewhere [i.e.,* $\forall \underline{r} \notin B(\underline{r}_t), B(\underline{r}_t)$ *indicating a given neighborhood of* $\underline{r}_t$ *and identifying the 'target' region].*

Unfortunately, the cost function, i.e., $|\mathbf{F}(\underline{r}_t)|^2$, is a non-negative quadratic polynomial with respect to the unknowns. As such, the overall optimization problem is non-convex [58], so that one can be eventually trapped into sub-optimal solutions when solving it.

In order to develop a method robust with respect to such an issue, we will first (re)consider an auxiliary preparatory case, and then we will turn back to the original general problem.

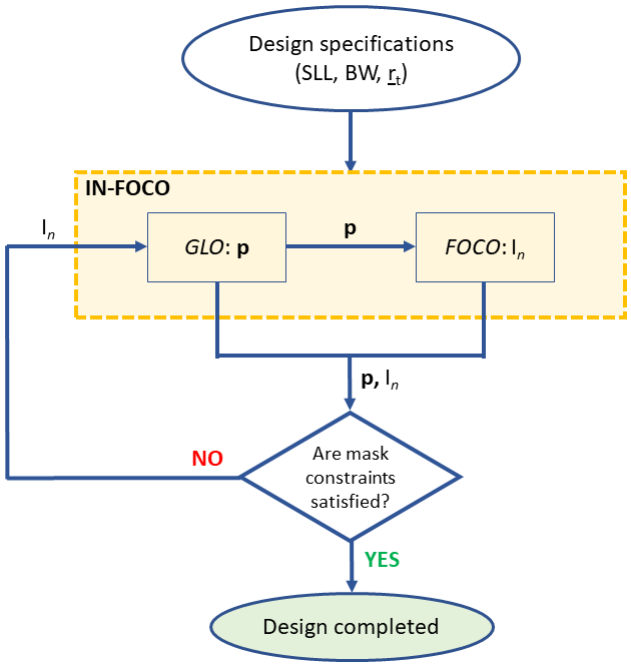

Fig. 4.1: Flowchart summarizing steps of the proposed approach to focusing the field intensity of vector fields.

For the first (and auxiliary) case, let us initially consider the (still unknown) polarization plane of the field at the target point. In such a point the total vector field can be written as [111]:

$$\mathbf{F}(\underline{r}_t) = \sum_{n=1}^{N} I_n \langle \boldsymbol{\Psi}_n(\underline{r}_t), \mathbf{p} \rangle \mathbf{p} + \sum_{n=1}^{N} I_n \langle \boldsymbol{\Psi}_n(\underline{r}_t), \mathbf{q} \rangle \mathbf{q} = \sum_{n=1}^{N} I_n \psi_{pn}(\underline{r}_t) \mathbf{p} + \sum_{n=1}^{N} I_n \psi_{qn}(\underline{r}_t) \mathbf{q} \tag{2}$$

where $\mathbf{p}$ and $\mathbf{q}$ are the unit vectors associated to two generic orthogonal polarizations of the field.

If the polarization which guarantees the most convenient $|\mathbf{F}(\underline{r}_t)|^2$ value (say $\widehat{\mathbf{p}}$) were a-priori known, then the corresponding field into the target point would be equal to:

$$\mathbf{F}(\underline{r}_t) = \sum_{n=1}^{N} I_n \langle \boldsymbol{\Psi}_n(\underline{r}_t), \widehat{\mathbf{p}} \rangle \widehat{\mathbf{p}} = \sum_{n=1}^{N} I_n \psi_{\widehat{\mathbf{p}}n}(\underline{r}_t) \widehat{\mathbf{p}} \tag{3}$$

Therefore, the focusing problem could be formulated as a CP one (as in the introductory paragraph 3), i.e.:

Find the complex excitations I_n (n=1,...,N) such to:

$$\max_{I_1,...I_N} \Re\left\{\sum_{n=1}^{N} I_n \psi_{\widehat{\mathbf{p}}n}(\underline{r}_t)\right\} \tag{4}$$

subject to:

$$\Im\left\{\sum_{n=1}^{N} I_n \psi_{\widehat{\mathbf{p}}n}(\underline{r}_t)\right\} = 0 \tag{5}$$

$$|\mathbf{F}(\underline{r})|^2 \leq UB(\underline{r}) \qquad \forall \underline{r} \notin B(\underline{r}_t) \tag{6}$$

where $\Re$ and $\Im$, respectively, denote the real and imaginary parts of the complex arguments, and $UB(\underline{r})$ is a non-negative arbitrary function (say the *mask* function) enforcing the upper bound constraint on the field intensity outside $B(\underline{r}_t)$.

Unfortunately, in actual cases, one does not know a-priori the optimal polarization $\widehat{\mathbf{p}}$.

In a first instance, the overall problem could be tackling as an enumeration of convex problems, by exploiting [36]. In fact, we know from the preparatory problem (4)-(6) that, for any fixed polarization, the problem reduces to a CP one, and we also know how to solve it. Consequently, one can solve the convex problem corresponding to any possible field polarization into the target point and then select the solution which guarantees the best focusing performances. From a different point of view, the field intensity focusing can also be interpreted as a proper combination of basic properly polarized focused fields.

On the other side, since the polarization of a field is determined by only five parameters (see Appendix B), the simple idea proposed in this Chapter is to introduce an optimization procedure looking for the best polarization $\widehat{\mathbf{p}}$. To this aim, the overall problem can be formulated as a nested optimization wherein one looks for externally (by means of a GLO procedure) the most convenient polarization while the internal optimization looks for the optimal excitations set corresponding to the polarization at hand. Accordingly, the new formulation will be as follows:

Find $\mathbf{p}$ and the corresponding I_n (n=1,...,N) in such a way that:

$$\max_{\mathbf{p}}\left\{\max_{I_1,...I_N} \Re\left\{\sum_{n=1}^{N} I_n \psi_{\widehat{\mathbf{p}}n}(\underline{r}_t)\right\}\right\} \tag{7}$$

subject to:

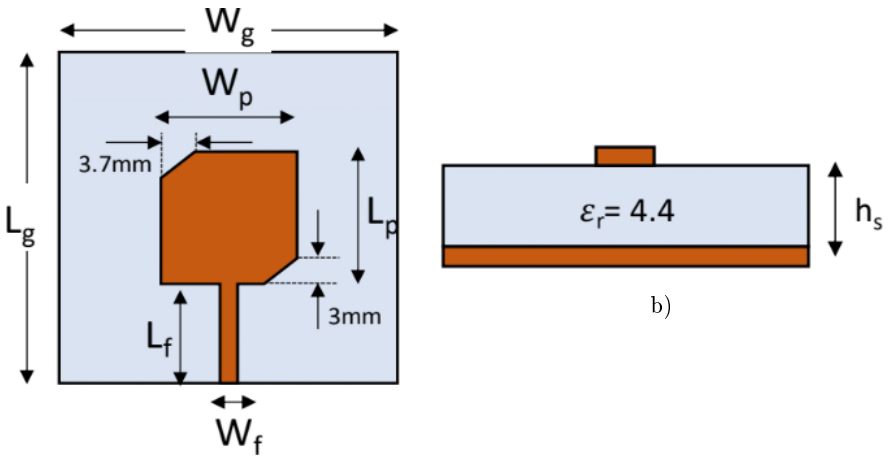

Fig. 4.2: Single radiating element for array considered in the first numerical example (see also Fig. 12 of [10]): (a) top view; (b) side view.

$$\Im\left\{\sum_{n=1}^{N} I_n \psi_{\widehat{\mathbf{p}}n}(\underline{r}_t)\right\} = 0 \tag{8}$$

$$|\mathbf{F}(\underline{r})|^2 \leq UB(\underline{r}) \qquad \forall \underline{r} \notin B(\underline{r}_t) \tag{9}$$

$$\|\mathbf{p}\|_2^2 = 1 \tag{10}$$

wherein $\mathbf{p}$ is the unknown encoding the specific polarization [see the Appendix B, where a discussion of constraint (10) is also included].

By virtue of the above discussion, in (7) the external minimization will require a GLO tool, whereas the internal minimization, by virtue of its CP nature, can be conveniently solved by means of a fast local-optimization. As the external GLO acts on polarization, while the internal one identifies the value of the cost function along with the corresponding optimal excitations for the trial polarization at hand, we are indeed optimizing simultaneously polarization and excitations in a nested fashion.

The overall procedure is summarized in the flowchart of fig. 4.1, and it has been conceived in such a way that the GLO deals with the minimum number of unknowns (i.e., just with the ones responsible for non-convexity), with a beneficial impact on both the computational time and the reliability of the obtained results.

From a physical point of view, we can finally state that *the original problem can be interpreted as a global optimization in the space of the possible polarizations.* This is a key point of the proposed method if we compare it with the method in [110] or many other ones where 'brute force' GLO-based strategies are generally adopted and one has to deal with a number of real unknowns at least twice the number of antennas. Conversely, the present approach deals with a GLO procedure having only

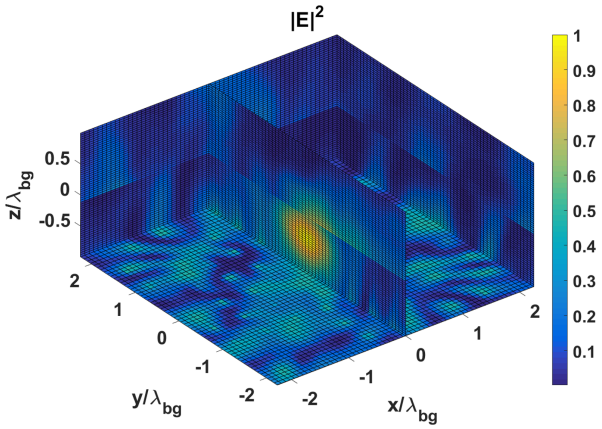

(a)

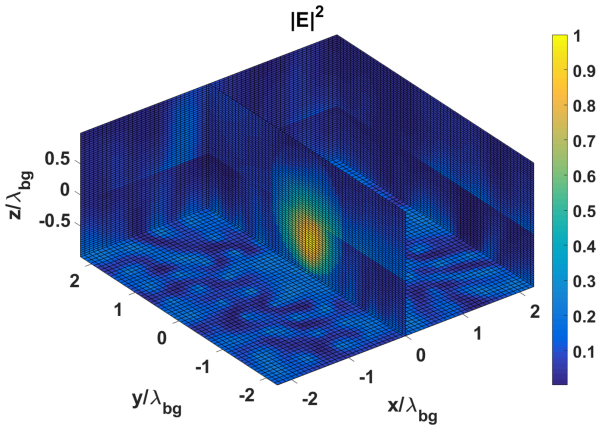

(b)

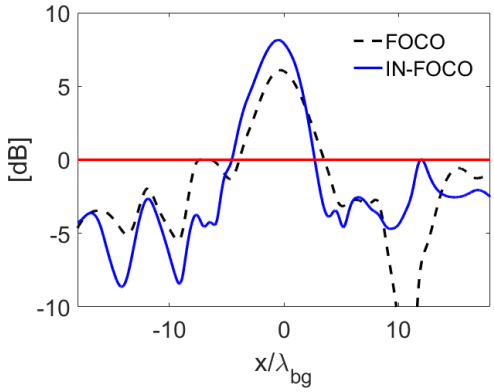

(c)

Fig. 4.3: Focusing in a complex scenario - Power distribution synthesized by the standard FOCO technique and the new IN-FOCO approach [$\underline{r}_t$=(-0.3051,-0.3051,-4.9888)λ_{bg}]: (a) normalized to maximum power deposition when only the *y-component* of the field is optimized; (b) normalized to maximum power deposition granted by the proposed technique; (c) superposition of the x-cuts of the two power distributions normalized to their maximum sidelobe level.

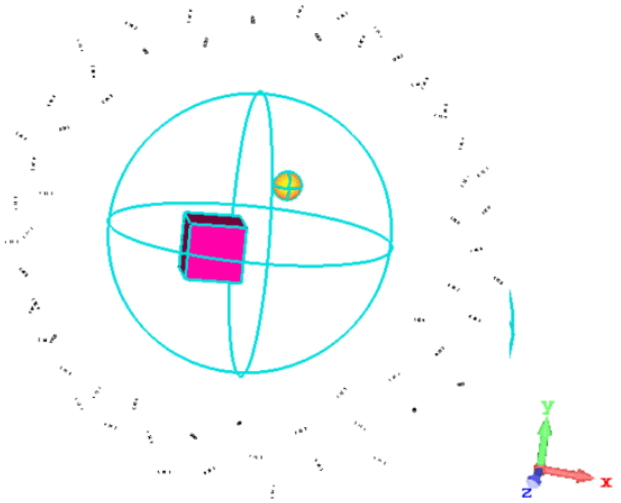

Fig. 4.4: Reference inhomogeneous 3-D scenario adopted in the second numerical example.

five unknowns[3] and, although the convergence to the global optimum is not ensured in a deterministic sense, this problem is generally believed to be effectively solvable by state-of-the-art global optimization procedures.

4.3 Numerical results

In order to prove the actual feasibility and generality of the proposed IN-FOCO technique, as well as to test its performance in actual cases, we report three numerical examples dealing with the problem of focusing the radiation pattern of a planar array in the NF zone of the antenna, and within two complex inhomogeneous scenarios, respectively. In all cases, the achieved results are compared with the FOCO approach [36] which optimizes just a single (dominant) component of the field.

The internal and external parts of the minimization (7) have been respectively performed through the *fmincon* and *ga* routines of MATLAB (version R2016B), while the AEP were obtained through a FDTD full-wave commercial software.

In the first example, we tested the proposed focusing approach in the NF. The volume Ω is $4.5\lambda_{bg} \times 4.5\lambda_{bg} \times 2\lambda_{bg}$ large (λ_{bg} being the wavelength in the background medium) and located in the NF zone of a $\lambda_{bg}/2$ spaced array of 9×9 microstrip patch antennas working at 2.4 GHz and printed on a FR4 substrate with a relative permittivity equal to 4.4 and a thickness equal to 1.6 mm. The dimensions of the patch have been set as in [10]. In particular, by referring to fig. 4.2, it is: $W_p = 29$ mm, $L_p =$

[3] More precisely, they belong to a zero-measure set of a five-dimensional space.

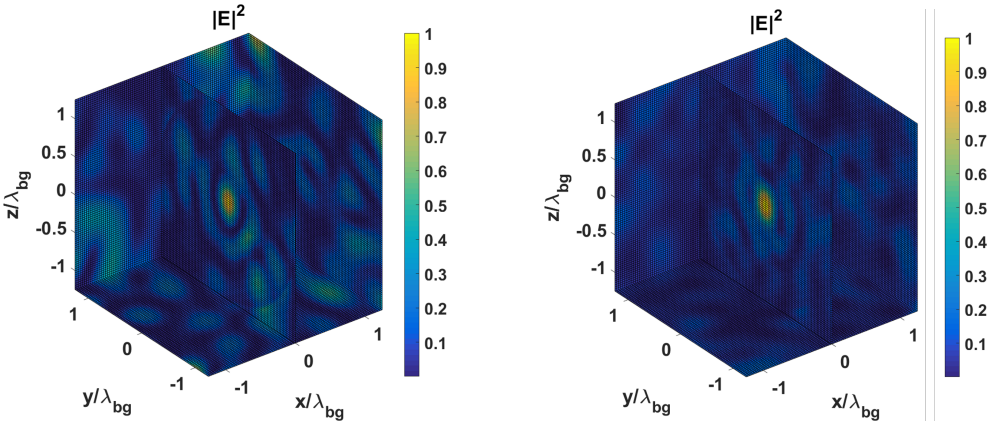

(a) (b)

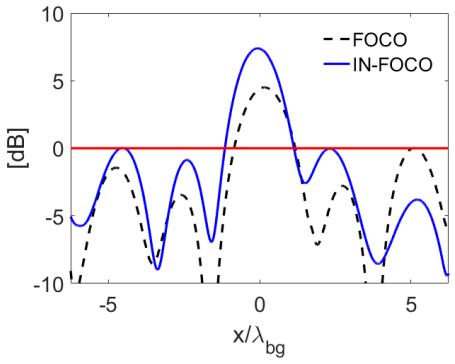

(c)

Fig. 4.5: Focusing in a complex scenario-Power distribution synthesized by the standard FOCO technique and the new IN-FOCO approach [$\underline{r_t}$=(-0.0687,-0.0687,-0.0687)λ_{bg}]: (a) normalized to maximum power deposition when only the *z-component* of the field is optimized; (b) normalized to maximum power deposition granted by the proposed technique; (c) superposition of the x-cuts of the two power distributions normalized to their maximum sidelobe level.

29 mm, W_g= $\lambda_{bg}/2$, L_g = $\lambda_{bg}/2$, W_f = 3 mm, L_f = $L_g/2$ - $L_p/2$. The target region is an ellipsoidal volume $2\lambda_{bg}$ far from the array aperture and whose semi-axes are $0.8\lambda_{bg}$ × $0.8\lambda_{bg}$ × λ_{bg}. The outcomes of the proposed IN-FOCO approach are reported in fig. 4.3 (b). By comparing these results with those achieved by the standard FOCO procedure [see fig. 4.3 (a)] optimizing just the *y (dominant)* component of the field, it can be seen that better focusing performance are granted by the novel approach. As a matter of fact, undesired 'hot spots', i.e., high field intensity outside the target region, are suppressed with the present approach, as also witnessed by the field cuts in fig. 4.3 (c). Moreover, IN-FOCO provided a higher separation between the main

(a) (b)

Fig. 4.6: Reference inhomogeneous 3-D scenario used for validation (a) and antenna array configuration (b) (see also Fig. 1 of [11]).

beam and the SLL than the basic FOCO technique. Notably, we were not able to achieve similar performance by means of the enumerative approach in [108].

In the second example, we dealt with the complex non-homogeneous 3-D scenario depicted in fig. 4.4, in which the region of interest Ω is a sphere of radius about $2\lambda_{bg}$ filled with air and embedding two dielectric objects, i.e., a cube and a sphere. The cube has a side of $\lambda_{bg}/2$ and a dielectric permittivity equal to 4, whereas the sphere has a radius of $\lambda_{bg}/4$ and a dielectric permittivity equal to 3. A cylindrical array of radius $4\lambda_{bg}$ and made up by 65 unitary-excited infinitesimal dipoles working at 1.5 GHz surrounds Ω. The array elements are arranged (with a random tilt angle) over 5 equally-spaced circumferences along the z-direction. Finally, the considered focusing target area is a sphere with a radius equal to $\lambda_{bg}/3$.

As in the previous test case, the results achieved by the new IN-FOCO approach have been compared with the ones attained by the original FOCO one optimizing just the *z (dominant)* component of the field. As it can be observed from fig. 4.5, the proposed approach led to a better-focused (narrower) field granting a higher separation amongst the focused beam and sidelobes.

In the last example, we dealt with the complex non-homogeneous 3-D scenario depicted in fig. 4.6. In particular, it consists of two dielectric objects (a cube and a sphere) hosted in free space into the cubic region of interest Ω. This domain has a side $l \simeq 2\ \lambda_{bg}^4$, while the cube has a side equal to $\lambda_{bg}/2$ and a dielectric permittivity equal to 2, and the sphere has a radius equal to $\lambda_{bg}/4$ and a dielectric permittivity equal to 3. The antenna is also equal to the one used in [11], i.e., it is a hemispherical-shaped array having a radius equal to $4\lambda_{bg}$ and composed of 92 small dipoles (see fig. 4.6). Finally, the considered focusing target area is a sphere with radius $\lambda_{bg}/3$.

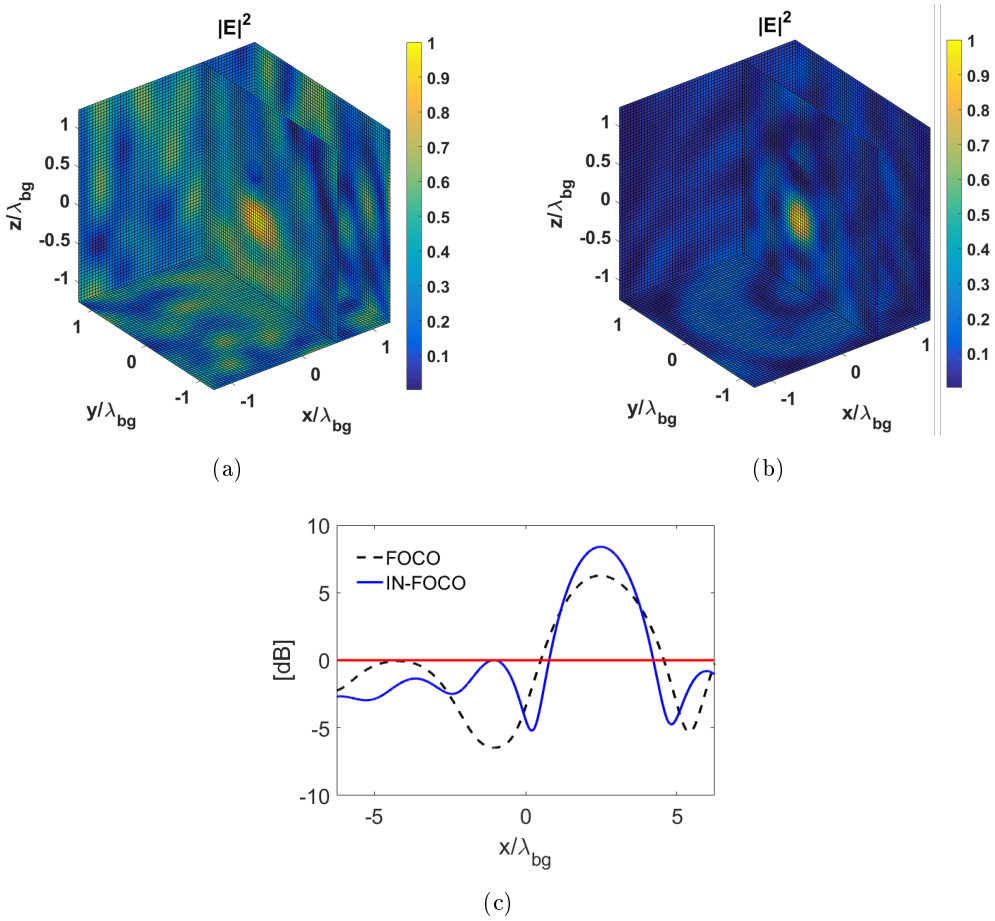

Fig. 4.7: Focusing in a complex scenario - Power distribution synthesized by the standard FOCO technique and the new IN-FOCO approach [$\underline{r}_t$=(-0.1000,-0.0400,-0.0667)λ_{bg}]: (a) normalized to maximum power deposition when only the *z-component* of the field is optimized; (b) normalized to maximum power deposition granted by the proposed technique; (c) superposition of the x-cuts of the two power distributions normalized to their maximum sidelobe level.

The outcomes of the proposed IN-FOCO approach are reported in fig. 4.6. By comparing these results with those achieved by the standard FOCO procedure (in which only the *z (dominant)* component of the field has been optimized), it can be seen that better focusing performances are granted by the novel approach. In particular, a reduced field intensity is granted outside the target region [see fig. 4.7 (c)].

The achieved results are coherent with expectations as when a single given component of the field is taken into account the other components do not cooperate for the field intensity-focusing phenomenon. They also prove the capability of the approach to take actual advantage of the vector nature of the field.

4.4 Final remarks

In this Chapter a new approach for focusing the intensity of a vector field into a target point while keeping it bounded elsewhere has been proposed. In particular, it has been shown that, when dealing with vector fields, the non-convex focusing problem at hand can be re-interpreted as the optimization of the polarization of the field at the target point. This is due to the fact that one can univocally associate a set of optimal excitations[4] to any given polarization, so that the field polarization becomes, in a certain sense, the actual unknown of the problem.

This circumstance led to the development of a new solution strategy relies on performing the global optimization in the polarization's space.

It is worth to note that, the proposed technique is inspired by the basic "FOCO" formulation, that represents the starting point to initiate the overall procedure. In particular, this is the common point shared with the previously-proposed approach for the shaping problem. In a nutshell, if we compare the two inserted optimizations, we have that in both cases the internal optimization looks for the optimal excitations, while the external one looks for the optimal polarization/phase shifts.

Accordingly, a very general problem (including situations as different as FF, NF, and 3-D non-homogeneous regions of space, mutual coupling, mounting platform effects) has been reduced to an external GLO in the space of polarizations nested with an internal CP optimization of the excitations guaranteeing, for any fixed polarization, the achievement of the unique (and hence globally-optimal) solution.

Although the approach still requires the exploitation of GLO techniques, such an optimization just deals with a zero-measure set of a five-dimensional space, with the inherent advantages with respect to the cases where the GLO directly looks for the array excitations.

[4] Strictly speaking, one could have a convex set of solution all having the same performances.

Conclusions of Part I

As a first problem involving phaseless data, Part I of this Thesis dealt with antenna synthesis (or more generally, with field shaping problems). In particular, the case of a set of elementary radiators (i.e., an array of antennas or applicators) is considered, and the goal is to determine the optimal arrays' excitations able to satisfy some given specifications.

In this area, it is well known that a number of canonical problems has been successfully solved during the years [2, 3, 5, 6, 36]. This is not however the case for the two canonical problems of focusing in a globally optimal fashion a vector field, as well as for the globally optimal shaping of a scalar field radiated by arrays other then linear and uniformly spaced. In PART I, these two problems have been successfully turned into an assembling of simpler problems. In this way, by taking advantage from FOCO, it is possible to identify the causes of non-convexity (and hence difficulties) of the problems at hand and propose an effective way out.

An obvious possible development is using sinergically the two approaches above for the optimal shaping of the intensity of vector fields, that still represents an unsolved canonical problem.

Once again, the common strategy is that of identifying the causes of non-convexity of the problem and formulate its solution in such a way that the (required) GLO procedures only have to deal with a strongly reduced number of unknowns. In such a way, GLO procedure deal with a minimal number of unknowns, with the inherent benefits.

Part II

PHASELESS INVERSE SOURCE PROBLEMS FOR ANTENNA CHARACTERIZATIONS: A "X-WORDS LIKE" SOLUTION PROCEDURE

Preliminary remarks

PR problems play a key role in many fields of applied electromagnetics ranging from power pattern antenna synthesis [2] to inverse scattering [33] to antenna characterization [37], with particular emphasis on the diagnostics of reflectors [28].

The aim of a PR problem is that of retrieving a source from amplitude-only data, i.e., by discarding any phase information about the field. While allowing the advantages of dealing with simpler instrumentation in real world applications (f.i., in case of antenna diagnostics), the adoption of phaseless data makes the problem still harder.

By virtue of its relevance, very many different approaches have been proposed during the years for solving PR problems. In antenna diagnostics, in order to optimally solve the problem by avoiding 'false solutions' [23], all methods require data diversity, like two measurement surfaces, or two different defocus conditions in case reflectors are dealt with [112].

In order to overcome the above drawbacks, this Part of the Thesis presents two approaches to PR problem which require only one measurement surface plus the knowledge of the source's support and a few additional information. They deal with 2-D problems, i.e., with the retrieving of planar sources (or excitations of planar arrays).

In particular, the proposed methods are based on a proper combination of the solution of 1-D PR problems so that each of them can be solved through the well-known SF [2] technique. Hence, if one is able to identify and store the different solutions along different strips, the final actual solution of the 2-D PR problem can be gathered by following a procedure which resembles the solution of crosswords puzzles, where one has to guarantee the congruence amongst the possible intersecting words.

First of all, let us understand the meaning of 'crosswords-like'. When you start off a new crossword puzzle, the best way to do this is to look for the clues that are easiest to solve first. By solving one or two of the latters, you will have some letters that will be useful in the puzzle and that will reduce the search space for subsequent words.

We can see the crossword exactly like the FF matrix that needs to be retrieved. As previously said, the proposed approach requires knowledge of the field' phase in a couple (or slightly more) of sampling points. This is equivalent to know some letters of the puzzle in order to reduce the number of combinations to be explored and giving us the momentum to keep going.

Crosswords' solver knows that the next thing one could conveniently do is look for answers that have the fewest number of letters. In our case, this is equivalent to

start from a line where many zeroes are present in order to reduce the number of ambiguities on the corresponding 1-D PR problems. Once you have scanned through the clues and solved some of the easiest ones, it is time to start working through systematically. Completion of the scheme implies considering additional horizontal, vertical, oblique or concentric-ring cuts of the radiation pattern in order to identify the correct field behavior (i.e., the correct 'words') amongst the very many possible ones.

Starting from this basic idea, Chapter 5 presents the first proposed approach and considers the case of the characterization of array antennas. The aim is to retrieve the unknowns excitations starting from the knowledge of the source' support and eventually of the field' phase in very few sampling points. Coming to details, the proposed technique is able to perform the 'crosswords' PR procedure by acting on horizontal, vertical and oblique cuts of the pattern. In order to identify the correct field instances among all the ones provided by the SF, it will be sufficient considering the intersections between three strips. In fact, while a proper choice of the corresponding phase constant will allow any oblique candidate field to correctly intersect the candidate vertical field, at the other intersection the phase of the oblique field will generally be different from the one of the horizontal field. As a consequence, one will be able to discard a number of possibilities and hopefully identify the correct triple of words (or at least to considerably reduce the number of possibilities).

Differently, the second proposed approach, introduced in Chapter 6, relies on the aperture antenna theory. If one considers circular continuous aperture sources instead of array antennas, the previous strategy can be improved by using concentric-ring (rather than vertical and oblique) cuts of the radiation pattern. In this case, the aim is to retrieve the unknown source starting from the knowledge of the source' support.

By exploiting the multipole expansion of the far field (and of the corresponding power pattern), one will be able to perform the above 'crosswords' PR procedure by acting, this time, just on diameter and concentric-ring cuts of the pattern. In this case, in order to identify the correct field instances among all the ones provided by the SF, it will be sufficient considering the intersection between two field values. In particular, while a proper choice of the corresponding phase constant will allow any diameter field cut to correctly intersect the candidate concentric-ring field cut, at the other intersection the phase of the same concentric-ring field cut will generally be different from the one of the diameter field cut. The need of just two intersections in order to discard the unsuitable field distributions will lead to a considerably reduced computational burden with respect to the first approach.

5

PHASE RETRIEVAL OF SCALAR FIELDS: A CROSSWORDS-LIKE PROCESSING

5.0 Summary

This Chapter aims at outlining, discussing, and assessing a new approach to the phase retrieval of 2-D radiated scalar fields. The technique takes advantage of fundamentals results available for the recovery of a 1-D discrete complex signal from the intensity of its Fourier Transform. The problem is solved by following a simple yet effective philosophy resembling the solution of crosswords puzzles and allowing (if any) the identification of all the different solutions. Differently from the state-of-the-art approaches, the proposed technique exploits only one measurement surface (plus the knowledge of the support of the source) and, despite the inherent difficulties of the inverse problem at hand, it results completely deterministic and does not exploit GLO algorithms in order to achieve the global optimum. Numerical examples concerning planar array-antenna sources support the given theory and confirm the effectiveness of the developed solution strategies[1].

[1] Some contents of this Chapter have been published in references [16, 17] of the "Publications List of G. M. Battaglia" reported at the end of the Thesis.

5.1 Introduction

PR problems have a considerable interest in areas as different as: optics [35], crystallography, inverse scattering [33], interferometry [113], astronomy [34], lithography [112], electronic microscopy [114], holography [28], testing through UAV [115], THz far-field prediction [116], as well as in antenna diagnostics [14–16], and synthesis [2, 27, 51]. Problems of this kind occur every time the full knowledge of a complex signal is needed but phase measurements are either unavailable or not convenient.

By denoting with *f(**x**)* and T, respectively, an arbitrary and eventually multidimensional signal and an operator such that:

$$F(\mathbf{u}) = T[f(\mathbf{x})] = |F(\mathbf{u})|e^{j\phi(\mathbf{u})} \tag{1}$$

wherein $\mathbf{x}$ ans $\mathbf{u}$ are real vector variables spanning either mono-dimensional or multi-dimensional spaces, a PR problem can be formulated as:
*determine f(**x**) starting from the knowledge of |F(**u**)| plus some additional information.*

In the literature, large attention has been devoted to the case where T is a Fourier Transform, which this Chapter considers in the following. As well known, solving such a problem requires tackling a number of difficulties, which are briefly recalled below.

First, in both the one-dimensional and two-dimensional cases (as well as for higher dimensional problems) the solution of the problem is not unique. In fact, the so-called trivial ambiguities, i.e.,

- a constant phase on *F(**u**)*;
- a linear phase on *F(**u**)* (resulting in a shift on *f(**x**)*);
- conjugation of *F(**u**)* (resulting in a reversal of *f(**x**)* with respect to the axes plus a conjugation);

and any combination of the above, resulting in an identical $|F(\mathbf{u})|^2$ distribution, come into play.

Things are even worse in the 1-D case. In fact, in such a case, by denoting with u a one-dimensional instance of $\mathbf{u}$, $|F(u)|^2$ can be written (but for a constant) as the product of (infinite) factors of the kind $e^{ju} - z_i$, with roots z_i organized in couples such that if one of them is relative to $F(u)$, the companion one determines a factor of $F^\star(u)$. Then, unless the two elements of a couple have a unitary amplitude, any 'zero flipping' within any couple generates a new solution[2]. Such a difficulty is readily

[2] By virtue of the Weierstrass Factorization Theorem [117], which may be viewed as an extension of the Fundamental Theorem of Algebra, every entire function can be represented as a (possibly infinite) product involving its roots.

understood in the case of discrete signals having a finite length, where $|F(u)|^2$ can be seen a polynomial in the $z = e^{ju}$ variable [2].

Notably, the last cause for non-uniqueness above is not likely to occur in the 2-D case, as two-dimensional polynomials (for the discrete-signal case) or entire functions of the exponential type (for the continuous source case) are not factorable (but for a zero-measure set of cases). As a consequence, in the 2-D case (which is the one we deal with in the remaining part of the Chapter) the PR problem has a unique solution but for trivial ambiguities and a zero-measure set of cases.

Such a last situation is not likely to occur in the 2-D case, as two-dimensional polynomials (for the discrete signal case) or entire functions of exponential type (for the 2-D case) are not factorable (but for a zero-measure set of cases). As a consequence, 2-D PR problem this Chapter is dealing with is known to have a unique solution but for trivial ambiguities and a zero-measure set of cases.

As one can get rid of the first two ambiguities by a-priori fixing, respectively, a phase reference and the support of the source, in the recovery of a 2-D signal from the amplitude of its Fourier transform one has to deal with the (unavoidable) ambiguity amongst the 'true' $|F(\mathbf{u})|$ and its conjugate as well as with the zero-measure set of cases where, due to the fact that $|F(\mathbf{u})|^2$ can be decomposed into further factors, additional ambiguities do exist. Hence, even in the 2-D case, some additional a-priori information is necessary in order to get a theoretically unique solution.

Even assuming a theoretically unique solution exists in case of ideal data, two further difficulties come into play:

- a solution to the problem may not exist at all in cases of actual (i.e., error affected) data, so that the problem keeps ill-posed. This is due to the fact that in the 2-D case the (measurement-error-affected) square amplitude distribution may be such that the data do not belong to the range of the quadratic operator relating the unknown signal $f(\boldsymbol{x})$ to the actual $|F(\mathbf{u})|^2$ distribution [118]. As a possible countermeasure to such an issue, a generalized solution is usually looked for as the global minimum of some cost functional enforcing the best possible fitting amongst the actual and the tentative intensity distributions. Such a functional can be complemented by some penalty function enforcing some expected property of the solution;
- even if the available a-priori information theoretically ensures the uniqueness of the solution, the iterative procedure minimizing the cost function may be trapped into local minima, actually different from the ground truth [119], thus resulting into 'false solutions' of the problem.

Notably, additional difficulties may arise in the particular problem one is dealing with. In antenna testing, for example, even assuming the antenna is a uniformly spaced array (so that the spectrum is periodic), depending on the element spacing one may not be able to collect the whole square amplitude distribution of the Fourier Transform of the unknown signal in the basic periodicity cell (see [42] for details).

By taking into account all the above, this Chapter proposes and tests a new approach to recovery of 2-D discrete signals from the square amplitude of its Fourier Transform. Motivated by the last circumstance above, the approach will be tested with reference to the case of antenna arrays (where the array excitations and the square-amplitude far-field distribution play the role, respectively, of the signal to be recovered and of the known data). By the sake of simplicity, we will start by considering the noiseless case, where effective solution procedures are anyway still lacking, and then we will consider the noisy case at a later stage.

The key idea of the proposed procedure is to recast the 2-D problem at hand as the combination of a number of auxiliary 1-D PR problems. Then, as all the possible solutions of each 'auxiliary' 1-D problem are identified in a fast and effective fashion by using the SF technique [2], the final solution of the 2-D PR is identified by enforcing congruence amongst them. In a nutshell (see below), the procedure resembles the solution of crossword puzzles, where one has to guarantee the congruence amongst across and up-down possible words.

The proposed approach differs from the large variety of existing techniques under many points of view:

- at least for the noiseless case, it is able to deterministically and uniquely solve the PR problem by exploiting an amount of information coincident with the one theoretically needed to ensure uniqueness of the solution. Note this is a far from trivial capability, as to avoid false solutions one is generally forced to exploit further information[3];
- it is based on a very precise deterministic procedure, thus avoiding expensive random searches while still guaranteeing the achievement of the globally optimal solution. Differently, the other techniques available in literature use GLO techniques [120] in order to get the actual solution with the minimal information. However, these latter are based on a stochastic search, and they have a computational burden growing exponentially with the number of unknowns [96].

[3] For example, in antenna testing one needs either *two* measurement surfaces, or *two* different probes, or *two* different defocus conditions [40, 119].

- in those cases where the problem at hand admits multiple different solutions, the proposed technique allows identifying all of them. Instead, one of the approaches currently used in literature, the so-called 'Phase Lift' strategy [121]. Roughly speaking, it amounts to introduce a number of auxiliary unknowns equal to the square of the number of the original problem and on the relaxation of an inherent non-convex constraint into a convex one. As it may be easily understood, the computational complexity of such a technique also grows very rapidly with the number of unknowns (just like in global optimization so that it is mainly adopted for 1-D problem). Moreover, which is often overlooked in the literature, Phase Lift-based procedures just find a solution of the problem whereas in some instances (e.g., the 1-D case) the problem may have very many different solutions.

The Chapter is organized as follows. The next Section presents[4] the basic idea and the corresponding procedure, while Section 5.4 reports a representative set of results. Conclusions follow.

5.2 2-D Phase Retrieval as a combinatorial problem in 1-D instances

By the sake of simplicity, let us consider the case where our unknown 2-D discrete complex signal $f(\mathbf{x}) = f(x, y)$ is arranged over a uniformly spaced rectangular grid[5]. Also, let us consider the case where the discrete signal is centered around the origin of its domain, and the number of elements along the x and y coordinates are respectively equal to $2\tilde{N}+1$ and $2\tilde{M}+1$. In such a case[6], by denoting with u and v the spectral variables in the Fourier transform domain, one will achieve:

$$F(\mathbf{u}) = F(u, v) = \sum_{n=-\tilde{N}}^{\tilde{N}} \sum_{m=-\tilde{M}}^{\tilde{M}} C_{n,m} e^{jnu} e^{jmv} \tag{1}$$

By simple computation, the square amplitude of (1) can be written in terms of auxiliary variables $D_{p,q}$ as:

[4] The basic idea, resumed in Subsection 5.2.2, has been presented as a conference contribution in [122, 123]. The present contribution gives new insights on actual capabilities and suggests new ways to overcome limitations both in case of antenna problems as well as for other cases of general interest.

[5] In antenna problems, that would be a planar array over a rectangular grid.

[6] Similar reasonings hold true in case the number of elements is even.

$$|F(u,v)|^2 = \sum_{p=-2\tilde{N}}^{2\tilde{N}} \sum_{q=-2\tilde{M}}^{2\tilde{M}} D_{p,q} e^{jpu} e^{jqv} \tag{2}$$

where, because of the fact the left-hand member is a real quantity, $\{D_{p,q}\}$ is a Hermitian sequence of complex coefficients.

Notably, the choice of the indices in (1) [as well as and the corresponding outcomes in (2)] emphasize that the square amplitude distribution has a (spatial) bandwidth which is (obviously) twice the one pertaining to the corresponding complex signal.

Notably, by denoting with $A^2(u,v)$ the measured *square-amplitude* data (which is assumed to be known over all its domain):

$$A^2(u,v) = \sum_{p=-2\tilde{N}}^{\tilde{N}} \sum_{q=-2\tilde{M}}^{\tilde{M}} D_{p,q} e^{jpu} e^{jqv} \tag{3}$$

with $u = [u_1, u_2, ..., u_J]$, $v = [v_1, v_2, ..., v_K]$, and assuming that measurements are properly taken according to the rules in [80], the $\{D_{p,q}\}$ sequence can be found in a fast and effective fashion by expanding the measured $A^2(u,v)$ into a truncated Fourier series, where the spectral variables belong to the range $[-\pi, \pi]$. If some oversampling is used in collecting data, in such a step a filtering of measurement errors on the acquired data is also performed.

5.2.1 The basic idea

As anticipated above, the proposed procedure resembles the solution of crossword puzzles, where one has to guarantee the congruence amongst solutions across and up-down possible words. In actual facts, advantage is taken from the fact that a very effective procedure exists for the solution of 1-D PR problems for discrete signals, and it is able to give back all the (possibly very many) solution of the problems. These solutions become then possible 'words' to be allocated along the corresponding across, up-down, and eventually oblique directions[7]. Finally, congruence considerations amongst the different possible 'words' along the crossing directions will possibly restore uniqueness of the solution (if any) for the 2-D scheme.

A first possible solution procedure, which works nicely for the noiseless case, is given in the Subsection 5.2.2. Then, in order to counteract the effect of both noise and an increased size of the discrete signals, some alternative solution procedures

[7] By virtue of bandlimitedness of *F(u)* and $|F(u)|^2$, only a finite number of them has to be actually considered, and because of the periodicity of the involved functions, we just need to consider the portion $[(-\pi, \pi), (-\pi, \pi)]$ of the spectral plane.

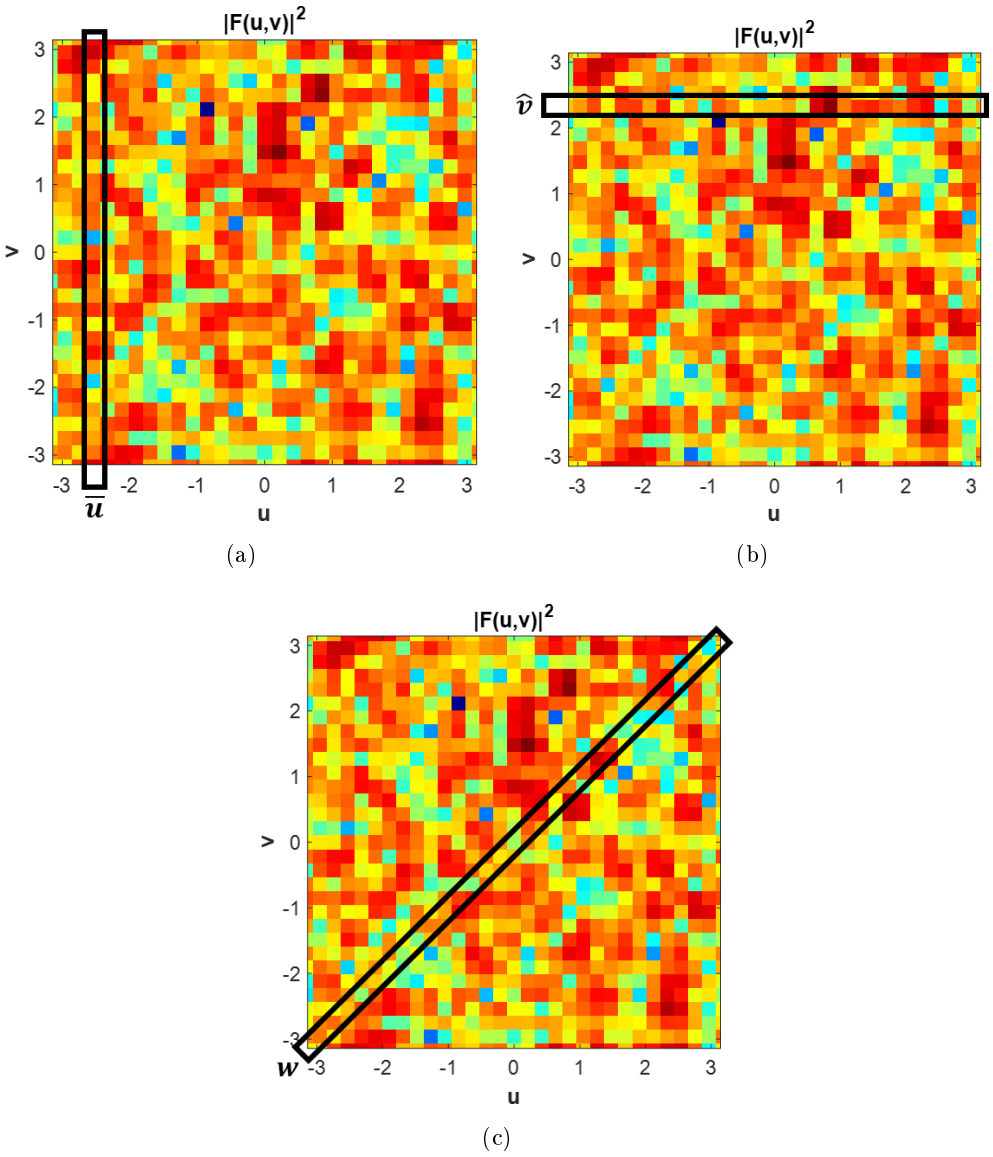

Fig. 5.1: Pictorial representation of the crosswords-like procedure described in Subsection II.B. The square amplitude of a random 2-D sequence is considered: (a) vertical, (b) horizontal and (c) oblique line of the spectral plane selected for the solution of the 1-D PR problem via SF for the identification of all possible signal solutions.

(implying a minimal additional a-priori information) are given in Subsection 5.2.3. Finally, in Subsection 5.2.4 a very effective solution procedure is proposed for the case of interest in [44, 124] where the unknown function is known to be *real* or *real and positive*.

5.2.2 A first possible solution procedure

In the noiseless case, and assuming in the following that the $\{D_{p,q}\}$ sequence is known, the proposed approach can be conceptually split into a first part initializing the solution of the 'crosswords' puzzle plus a second part where the subsequent completion of the scheme is performed. The first part (in the following referred to as initializing part) is the most difficult one, and it can be separated in two sub-steps. In particular, in the first sub-step of the *initializing part* one aims to identify all the (very many) possible complex fields along three intersecating lines (see fig. 5.1).

In order to get a better understanding of the overall procedure, let us consider for instance a *vertical* line of the u-v plane (restricted to the $[-\pi, \pi]$ portion) as depicted in fig. 5.1(a). By following [2] it is easy to identify all possible $F(\bar{u}, v)$ behaviors corresponding to the measured power pattern along that line. In fact, along the line $u = \bar{u}$, such a 'dictionary' of signals will be determined by applying to the corresponding square amplitude data, i.e.,

$$|F(\bar{u}, v)|^2 = A^2(\bar{u}, v) = \sum_{q=-2\tilde{M}}^{2\tilde{M}} \bar{D}_q(\bar{u}) e^{jqv} \tag{4.a}$$

the SF technique introduced in [2], where the inherent coefficients are given by [122, 123]

$$\bar{D}_q(\bar{u}) = \sum_{p=-2\tilde{N}}^{2\tilde{N}} D_{p,q} e^{jp\bar{u}} \tag{4.b}$$

By so doing, a multiplicity of functions defined as:

$$F(\bar{u}, v) = \sum_{m=-\tilde{M}}^{\tilde{M}} \bar{C}_m(\bar{u}) e^{jmv} \tag{5.a}$$

is achieved, where:

$$\bar{C}_m(\bar{u}) = \sum_{n=-\tilde{N}}^{\tilde{N}} C_{n,m} e^{jn\bar{u}} \tag{5.b}$$

Contemporarily, by following an identical procedure, one can also determine all possible$F(u, \widehat{v})$ behaviors corresponding to the measured square amplitude data along a *horizontal* line of the u-v plane [see fig. 5.1(b)]. For instance, along the coordinate $v = \widehat{v}$, one will achieve:

$$|F(u,\widehat{v})|^2 = A^2(u,\widehat{v}) = \sum_{p=-2\tilde{N}}^{2\tilde{N}} \widehat{D}_p(\widehat{v}) e^{jpu} \tag{6.a}$$

where

$$\widehat{D}_p(\widehat{v}) = \sum_{q=-2\tilde{M}}^{2\tilde{M}} D_{p,q} e^{jq\widehat{v}} \tag{6.b}$$

so that the SF technique [2] can be again applied in order to get a multiplicity of possible behaviors:

$$F(u,\widehat{v}) = \sum_{n=-\tilde{N}}^{\tilde{N}} \widehat{C}_n(\widehat{v}) e^{jnu} \tag{7.a}$$

with:

$$\widehat{C}_n(\widehat{v}) = \sum_{m=-\tilde{M}}^{\tilde{M}} C_{n,m} e^{jm\widehat{v}} \tag{7.b}$$

Obviously, in the same manner, one can also determine all possible field behaviors along an *oblique* line of the *u*-*v* plane. For instance, by considering the main diagonal *u*=*v* (see fig. 5.1(c)) and denoting by w the coordinate spanning it, one will achieve:

$$|F(\mathrm{w})|^2 = A^2(\mathrm{w}) = \sum_{h=-2(\tilde{N}+\tilde{M})}^{2(\tilde{N}+\tilde{M})} \widetilde{D}_h e^{jh\mathrm{w}} \tag{8}$$

and

$$F(\mathrm{w}) = \sum_{h=-(\tilde{N}+\tilde{M})}^{\tilde{N}+\tilde{M}} \tilde{C}_h e^{jh\mathrm{w}} \tag{9}$$

where $\widetilde{D}_h$ and $\tilde{C}_h$ denote suitable auxiliary sequences. Again, one can deal with an auxiliary 1-D PR problem and, by solving it, he/she will be able to find all the possible F behaviors along the line *u*=*v*. The only additional difficulty is that along such an oblique line the number of terms of summations (and hence the number of zeroes to be considered in the procedure [2]) grows.

Note in case $\bar{u} = 0$, or $\widehat{v} = 0$, or for any line passing through the origin, one may also refer to the above 1-D functions (5.b) and (7.b) as to the so-called 'collapsed distributions' [125], which are also related to the Fourier slice theorem [126].

The reason for such a terminology is that expression (5.a) (as well as (7.a)) can be seen as the array factor of a linear array where, for any given *n(m)*, all coefficients $C_{m,n}$ sum up (collapse) into the single excitation $C_m(0)\ C_n(0)$, and similar reasonings apply to all other cuts passing through the origin.

In the second sub-step of the *initializing part*, one can considerably reduce the dictionary of possible words, hopefully getting a single combination amongst the three dictionaries of possible signals, by checking congruence or lack of congruence amongst the different possible combinations of signals.

Actually, one can examine any possible combination of horizontal and vertical retrieved signals and, for each couple, looking for the existence of an oblique signal correctly intersecting them. In fact, while a proper choice of the corresponding phase constant will allow any oblique candidate signal to correctly intersect the candidate *vertical* (*horizontal*) one, at the other intersection the phase of the *oblique* signal will generally be different from the one of the *horizontal* (*vertical*) signal (see fig. 5.1). As a consequence, one will be able to discard a number of possibilities and hopefully identify the correct triplet of words (or at least to considerably reduce the number of possibilities).

The second and final part of the procedure, i.e., the completion of the scheme, is rather obvious for crosswords solvers. One has to consider additional horizontal, vertical and oblique lines intersecting the ones already considered and determine the corresponding signals by proceeding to SF along each line, and then pruning the tree of possible solutions by means of congruence arguments.

The approach is very different from all existing procedures. In fact, once 1-D factorizations are produced, it is a kind of combinatorial problem. As such, it can be computationally heavy. On the other side, its similarity with crossword puzzles still comes to help by suggesting useful strategies.

For example, in order to reduce the number of combinations to be explored one can start from a line where many zeroes are present. In fact, this reduces the number of ambiguities on the corresponding 1-D PR problems [2]. Hence, a clever choice of the first three lines depicted in fig. 5.1 will be of help. In this respect, care must be taken in avoiding that they intersect at a null of $A^2(u,v)$ (wherein phase would make no sense).

As a distinguishing characteristic, if the solution is not unique (which is for instance the case when one deals with *u-v* factorable patterns [2]) then the approach is able to find in a deterministic fashion all the different solutions of the problem.

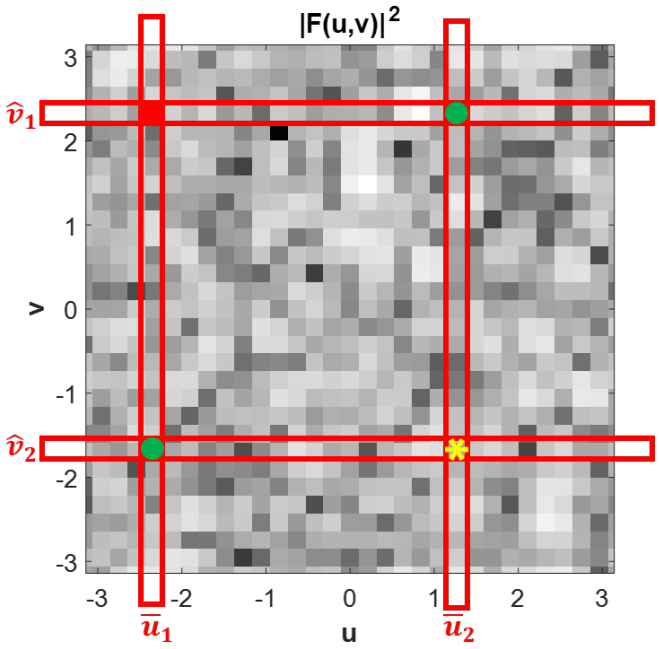

Fig. 5.2: Pictorial representation of the crosswords-like procedure described in Subsection 5.2.3 as a possible way out for limitations. The square amplitude of a random 2-D sequence is considered. The red square and green circular markers represent the three a-priori known complex data. In particular, the red point $(\bar{u}_1, \widehat{v}_1)$ is used to set a reference phase for all the signals along line ($v = \widehat{v}_1$ and $u = \bar{u}_1$, while the yellow star marker is used as discrimination point to discard the unsuitable solutions and hopefully retrieve the correct signal along the considered lines.

5.2.3 Limitations, and a second possible solution procedure for noisy or large-sized signals

The above approach set a deterministic procedure for the noiseless case, which, to the best of our knowledge, was anyway lacking. On the other side, as one can easily understand, limitations arise in case of noisy data and/or large 2-D sequences. In fact, as noisy data imply approximate solutions along the considered lines, some tolerance has to be used at the discrimination points when checking congruence amongst the possible 'words', so that more candidate solutions become eventually admissible. Also, the problem becomes harder and harder with increasing dimensions. In fact, under the actual noisy conditions, the existence of very many candidate words implies that more signals may become 'admissible' at the discrimination points. Accordingly, with increasing dimensions a (possibly exponentially) increasing number of candidate words enter into play, thus negatively affecting the pruning of the tree of possible solutions.

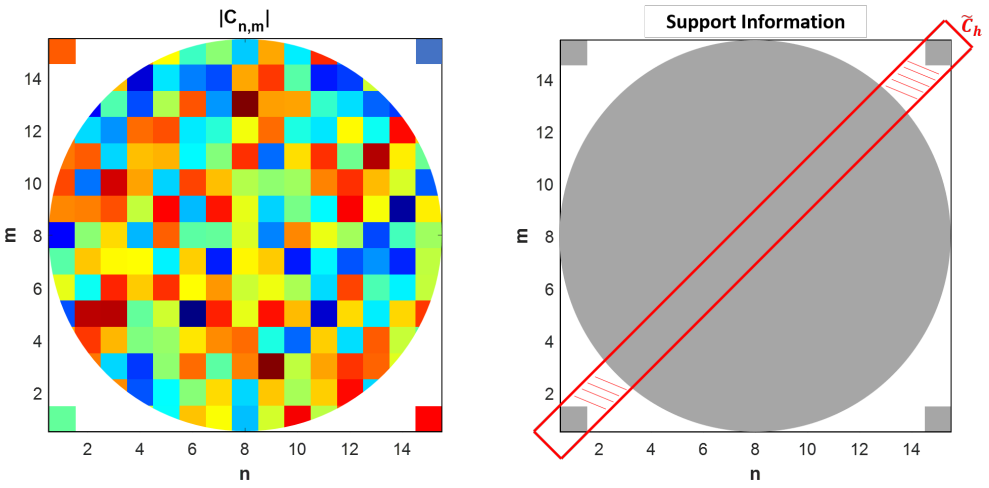

(a) (b)

Fig. 5.3: Pictorial representation of the crossword like procedure described in Subsection 5.2.4 for special case of actual interest: (a) amplitude of a random 2-D signal; (b) support information about the signal in (a) which can be supposed a-priori known to simplify the recovery of the collapsed distribution $\tilde{C}_h$ since null coefficients are expected in correspondence of red-lined regions.

Again, one possible way out comes from the similarity to crossword puzzles. In fact, in those cases, the schemes can be simplified by the availability of some letters in given crossings of rows and columns. In a corresponding fashion, the basic scheme of Subsection 5.2.2 can take advantage from a reduced number of amplitude and phase measurements; in such a way, one can conveniently and effectively initialize the solution of the overall scenario.

One possible strategy, represented in fig. 5.2, takes advantage from just three amplitude and phase measurements disposed on three vertexes of a rectangle, while the fourth vertex point is used to enforce congruence amongst possible words. By so doing, one can hopefully have an initial pruning of the possible solutions along the two corresponding rows and columns. Also, by means of congruence arguments one can establish the values of $F(u, v)$ along the four lines determining the rectangle, so that from now on one will have (at least) a couple of amplitude and phase known values of $F(u, v)$ along any row and column.

Obviously, the same statement also holds true in case the fourth vertex can be also considered an a-priori known point, which allows for a significant reduction of the complexity of the initializing step. Also note that PR along diagonals is not anymore strictly required.

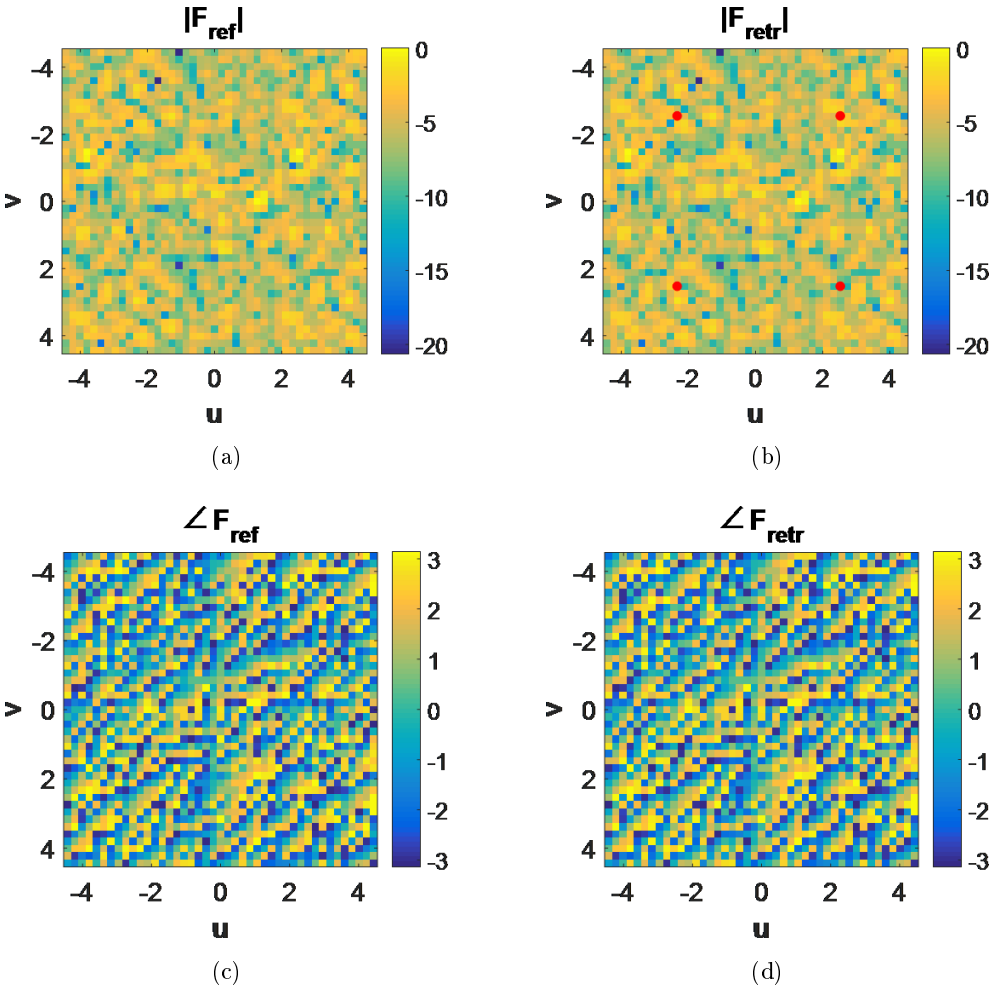

Fig. 5.4: Example 1: (a) Amplitude of the reference field; (b) Amplitude of the retrieved field; (c) Phase of the reference field; (d) Phase of the retrieved field. The red circle markers are those point wherein the complex field is supposed a-priori known (in amplitude and phase), and correspond to $(u_1, v_1) = (-2.33, -2.54)$, $(u_2, v_2) = (2.54, -2.54)$, $(u_3, v_3) = (-2.33, 2.54)$, $(u_4, v_4) = (2.54, 2.54)$.

As it can be easily understood, the initialization of the procedure is the most difficult part, as once the phase distribution along three or more rows and columns has been correctly retrieved, the pruning of solutions along the remaining rows and columns becomes easier and easier.

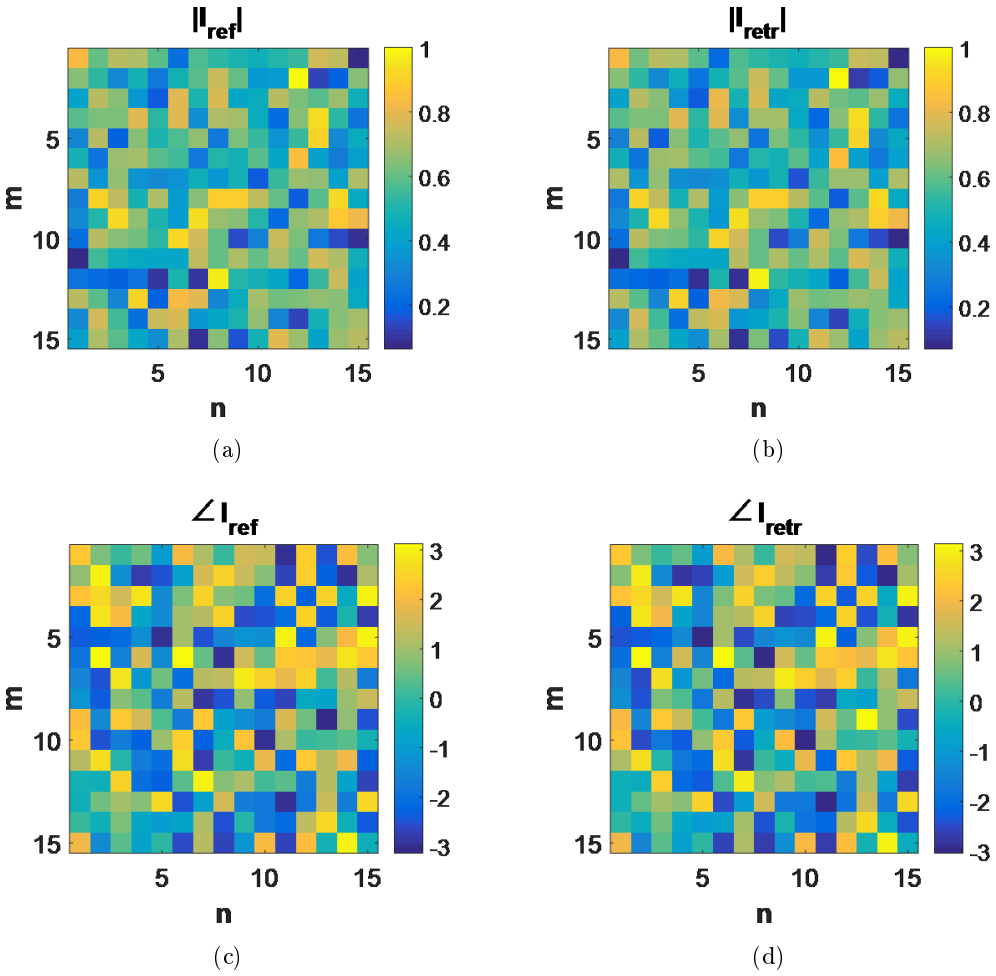

Fig. 5.5: Example 1: (a) Amplitude of the reference excitations; (b) Amplitude of the retrieved excitations; (c) Phase of the reference excitations; (d) Phase of the retrieved excitations.

5.2.4 The exploitation of 'collapsed' distributions, special cases of actual interest, and final remarks

As just stated, the triggering/initialization of the procedure is the most critical part of the proposed approach. Interestingly, there are a couple of interesting applications where the initialization can take advantage from the intrinsic nature of the signal to be retrieved, or from some available a-priori information. This is for example the case where the signal $f(\mathbf{x})$ is known to be *real* or *real and positive* (which is the case of crystallography, diffraction microscopy, and so on, since such a kind of signal corresponds for instance to the density of microparticles [44] or to nanotubes' atomic dimensions [124]). In such a case, in fact, the property of being real (and positive)

of the 2-D signal implies that the corresponding collapsed distribution [see (5.2) and (7.2)] is also real (and positive) as well.

Hence, such a property can be conveniently used in solving the 1-D PR problem along all the strips passing through the origin in the transformed domain in order to discard a number of outcomes of the corresponding SF problem, and hence hopefully simplifying the correct initial setting of the procedure. In fact, for example, when $\bar{u} = 0$ or $\widehat{v} = 0$, the equations (5.a) and (7.a) simply become respectively:

$$\bar{C}_m(\bar{u} = 0) = \sum_{n=-\tilde{N}}^{\tilde{N}} C_{n,m} \tag{10.a}$$

and

$$\widehat{C}_n(\widehat{v} = 0) = \sum_{m=-\tilde{M}}^{\tilde{M}} C_{n,m} \tag{10.b}$$

Consequently, the unknown coefficients at the left hand member of (10.a) and (10.b) have to be real and positive, and hence all the solutions that do not meet this requirement can be automatically discarded.

In case of (very peculiar) support information, a similar reasoning is possible. For example, the support information depicted in fig. 5.3 implies that the corresponding collapsed distribution along the $u = v$ direction has to be generated by a linear array where a number of excitations has to be equal to zero. Obviously, such a circumstance implies that one can hopefully have a univocal phase distribution along the $u = v$ direction, which simplifies the following steps.

As a final comment concerning all the different possible procedures described above, it is worth noting that a suitable alternative to the general solution procedure (i.e., solving the auxiliary 1-D PR problems along all the different rows and columns and then exploiting these latters in order to discriminate amongst admissible or inadmissible words) is available. In fact, once a sufficient number of rows and columns have been retrieved, one can conveniently switch to a least square fitting procedure as in [127]. In fact, the already retrieved samples of the spectrum can be used as linear constraints in a more classical PR procedure. Then, provided the number of these constraints is sufficiently large, false solutions can be safely avoided [23, 127].

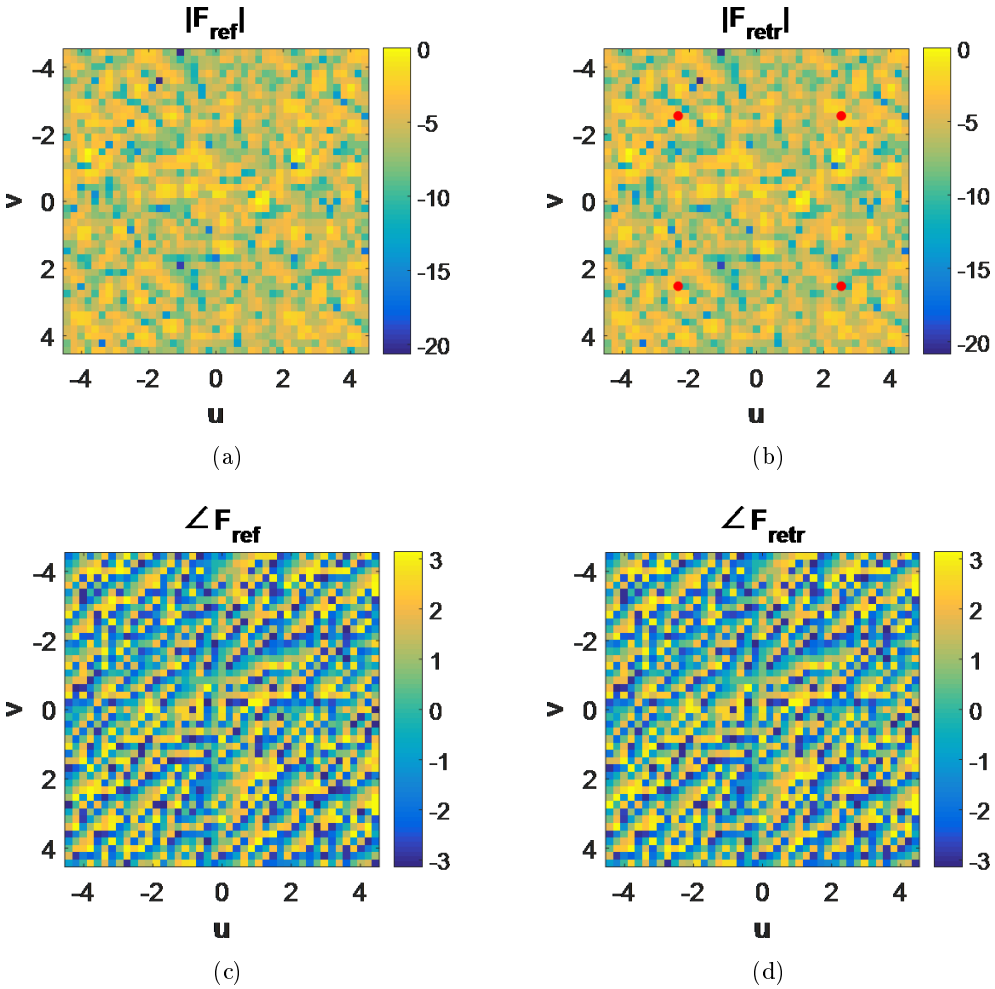

Fig. 5.6: Example 2: (a) Amplitude of the reference field; (b) Amplitude of the retrieved field; (c) Phase of the reference field; (d) Phase of the retrieved field. The red circle markers are those point wherein the complex field is supposed a-priori known (in amplitude and phase), and correspond to $(u_1, v_1) = (-2.33, -2.54)$, $(u_2, v_2) = (2.54, -2.54)$, $(u_3, v_3) = (-2.33, 2.54)$, $(u_4, v_4) = (2.54, 2.54)$.

5.3 Numerical results

As a proof of concept of the above proposed strategy, this Section shows some numerical examples for antenna problems. In particular, the 2-D signal to be retrieved corresponds to the excitations of a planar array, while measured data $A^2(u, v)$ corresponding to amplitude samples of the corresponding radiated power pattern. Accordingly, $u = \beta d_x sin\theta cos\Phi$ and $v = \beta d_y sin\theta sin\Phi$, where $\beta = 2\pi/\lambda$ denotes the wavenumber (λ being the operative wavelength), d_x, d_y are the element spacings along

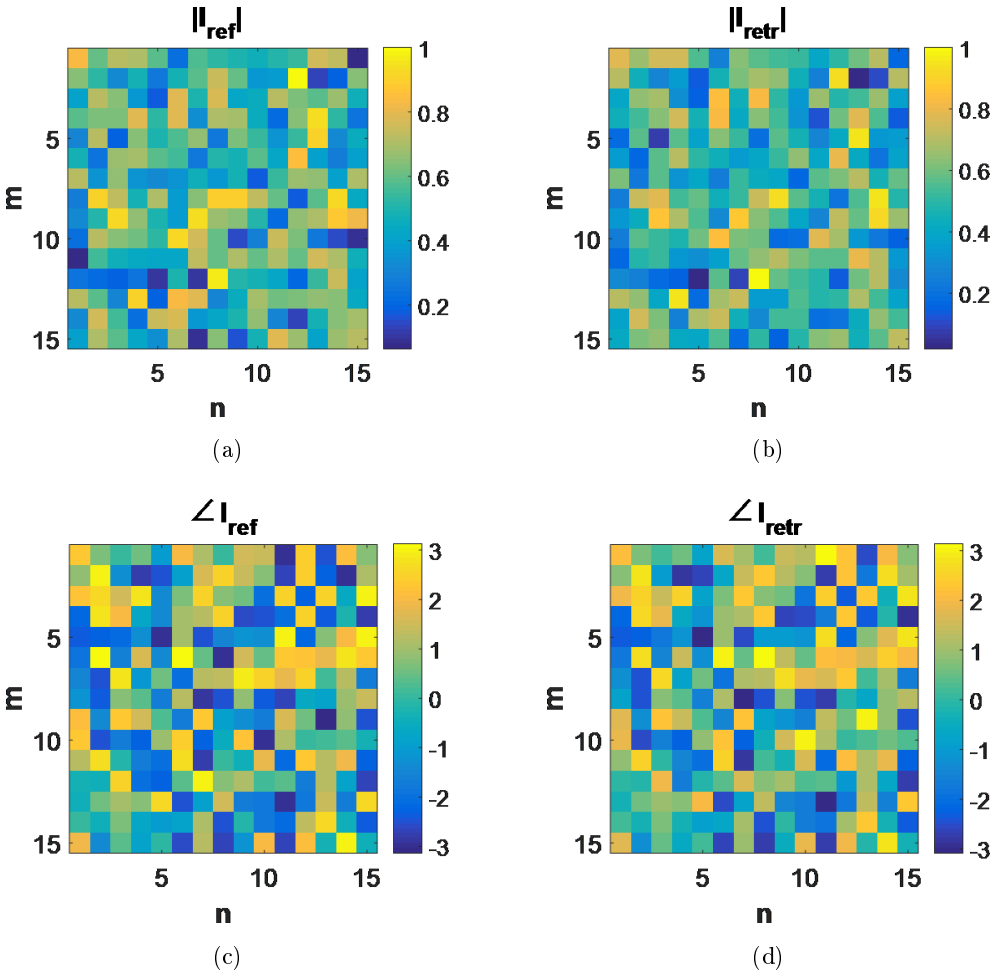

Fig. 5.7: Example 2: (a) Amplitude of the reference excitations; (b) Amplitude of the retrieved excitations; (c) Phase of the reference excitations; (d) Phase of the retrieved excitations.

the x and y axis, and θ, Φ respectively denote the elevation and azimuth aperture angles with respect to boresight.

In order to make the whole periodicity range of the power pattern available for measurements (see [42] for more details), an inter-element spacing of $d_x = d_y = 0.707\lambda$ has been adopted for all the following examples.

By indicating with $\mathbf{I}$=$[I_1, I_2, \ldots, I_{NM}]$ the vector containing the NM array excitations, the Normalized Mean Square Error (NMSE) is computed to quantitatively evaluate the accuracy of the PR procedure:

$$NMSE = \frac{\|\mathbf{I} - \mathbf{I}_{retr}\|^2}{\|\mathbf{I}\|^2} \tag{10}$$

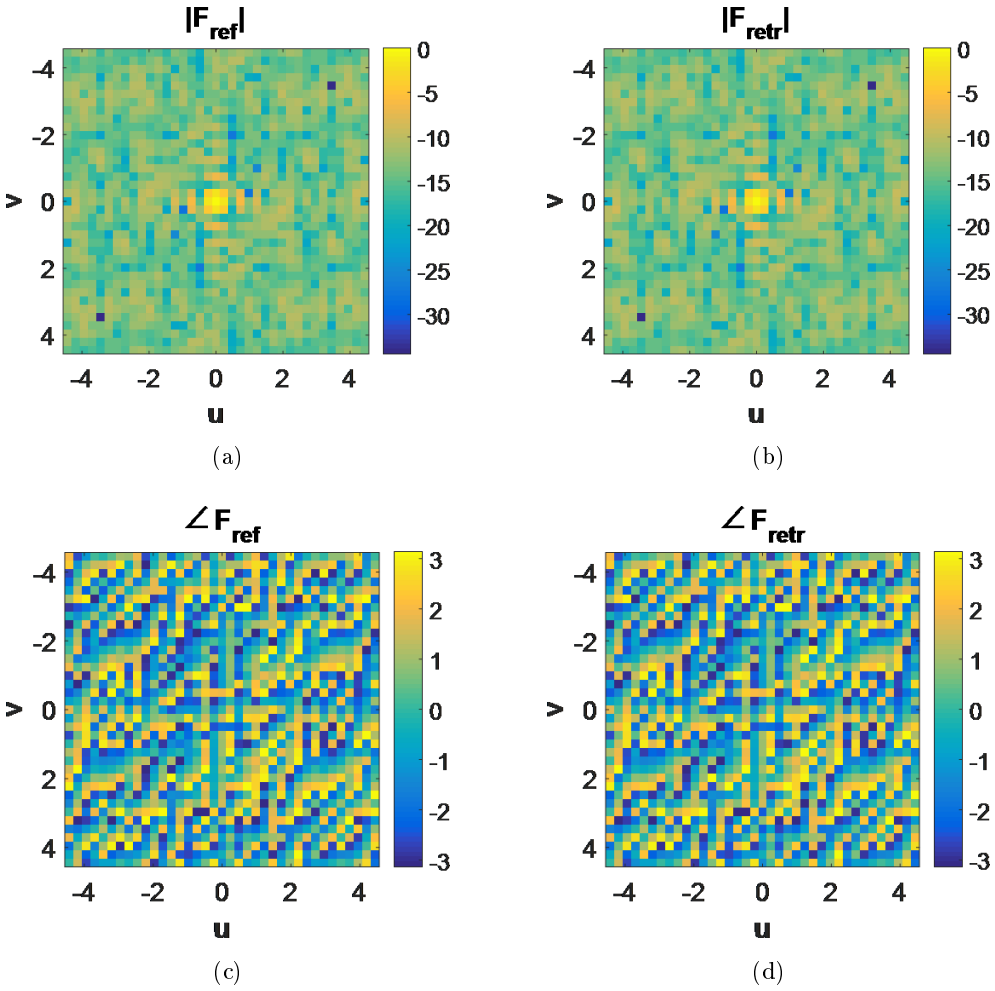

Fig. 5.8: Example 3: (a) Amplitude of the reference field; (b) Amplitude of the retrieved field; (c) Phase of the reference field; (d) Phase of the retrieved field.

$\mathbf{I}_{retr}$ being the vector containing the NM retrieved array excitations.

The first numerical example deals with a 15×15 elements equally spaced square array with *complex* random excitations. The power pattern has been measured over an equally spaced grid made of 43×43 points in the u-v plane (which is restricted to the $[-\pi, \pi; -\pi, \pi]$ periodicity range), and has been assumed completely known in four points of the spectral plane in order to properly trigger the recovery procedure and give us the momentum to keep going, see fig. 5.4. Consequently, these points allow us to recover the four lines passing through them (two vertical and two horizontal lines), and each point of the retrieved lines becomes a "known" word of our crossword puzzle.

It is easy to understand that this allows us to considerably reduce the search space for subsequent words. In fact, once you have solved some of the easiest clues

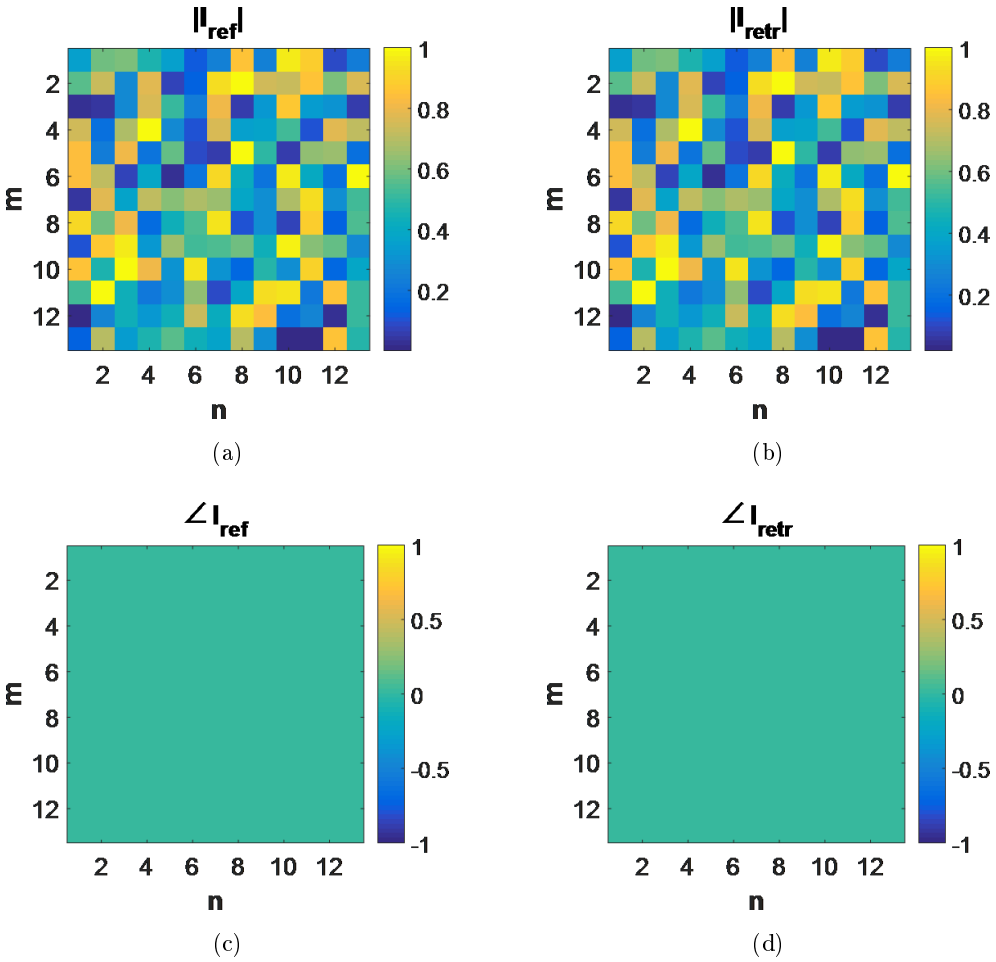

Fig. 5.9: Example 3: (a) Amplitude of the reference excitations; (b) Amplitude of the retrieved excitations; (c) Phase of the reference excitations; (d) Phase of the retrieved excitations.

it is time to start working through systematically considering additional horizontal, vertical and oblique line of the radiation pattern in order to identify the correct field behavior amongst the very many possible ones.

A comparison between reference and reconstructed results is given in fig. 5.4 in terms of fields, and in fig. 5.5 in terms of excitations. As it can be seen, the proposed procedure led to a fully satisfactory excitations recovery. The effectiveness of the proposed approach is also testified by the very low NMSE value (i.e., $NMSE = 1.0767 \times 10^{-5}$).

In the second test case, we used the same signal source of the previous example but enhanced the PR difficulty by corrupting each measured field amplitude by

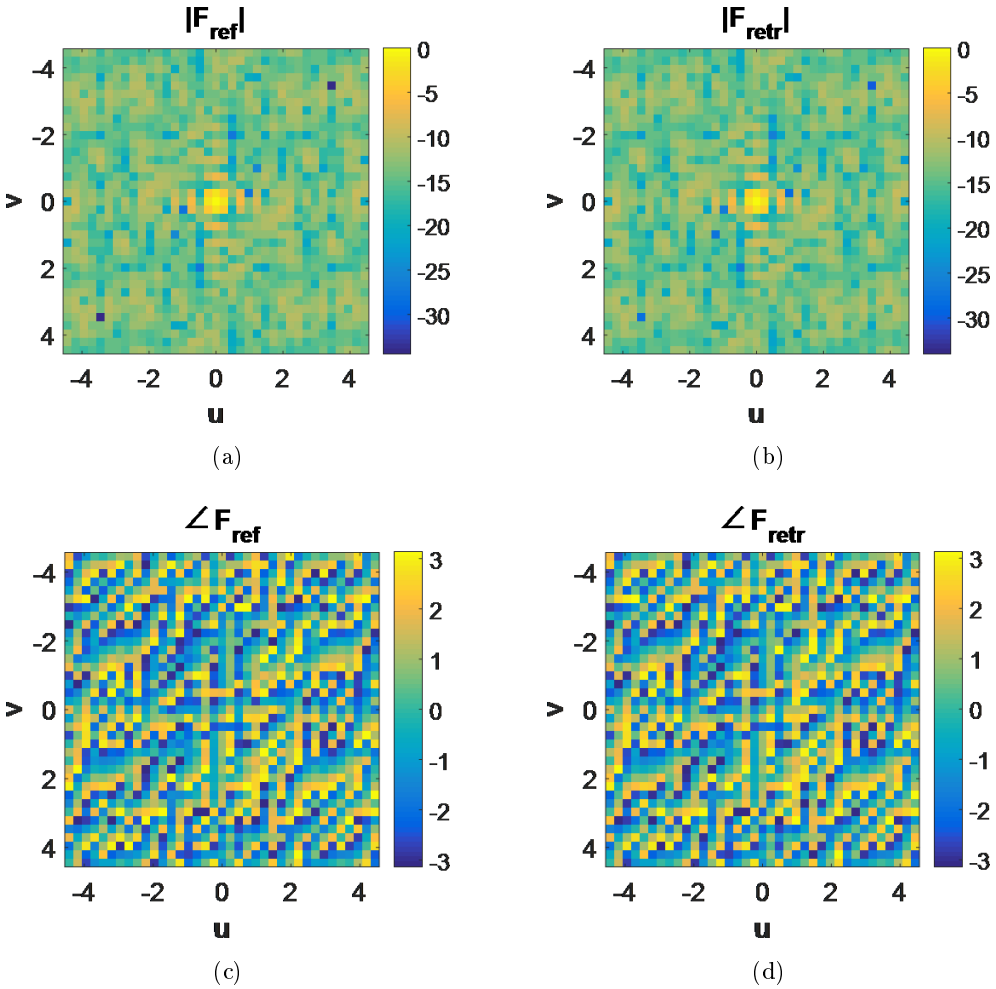

Fig. 5.10: Example 4: (a) Amplitude of the reference field; (b) Amplitude of the retrieved field; (c) Phase of the reference field; (d) Phase of the retrieved field.

white Gaussian noise with $SNR = 25dB$[8]. Also, the power pattern has been assumed completely known in the same four points of the spectral plane as before in order to properly trigger the recovery procedure.

A comparison between reference and reconstructed results is given in fig. 5.6 in terms of fields, and in fig. 5.7 in terms of excitations. As it can be seen, a satisfactory PR solution has been again achieved. The NMSE results equal to 0.0035.

In the third test case, we considered the case of a *real and positive* signal, in order to test the potentialities of the procedure described in Section 5.2.4. By still referring to antenna problems, we considered a 13×13-elements square array whose excitations have been set as real and positive random variables uniformly distributed in the range

[8] Notably, the square amplitude distribution is oversampled with respect to the minimal requirements, which allows a reduction of the overall measurement error.

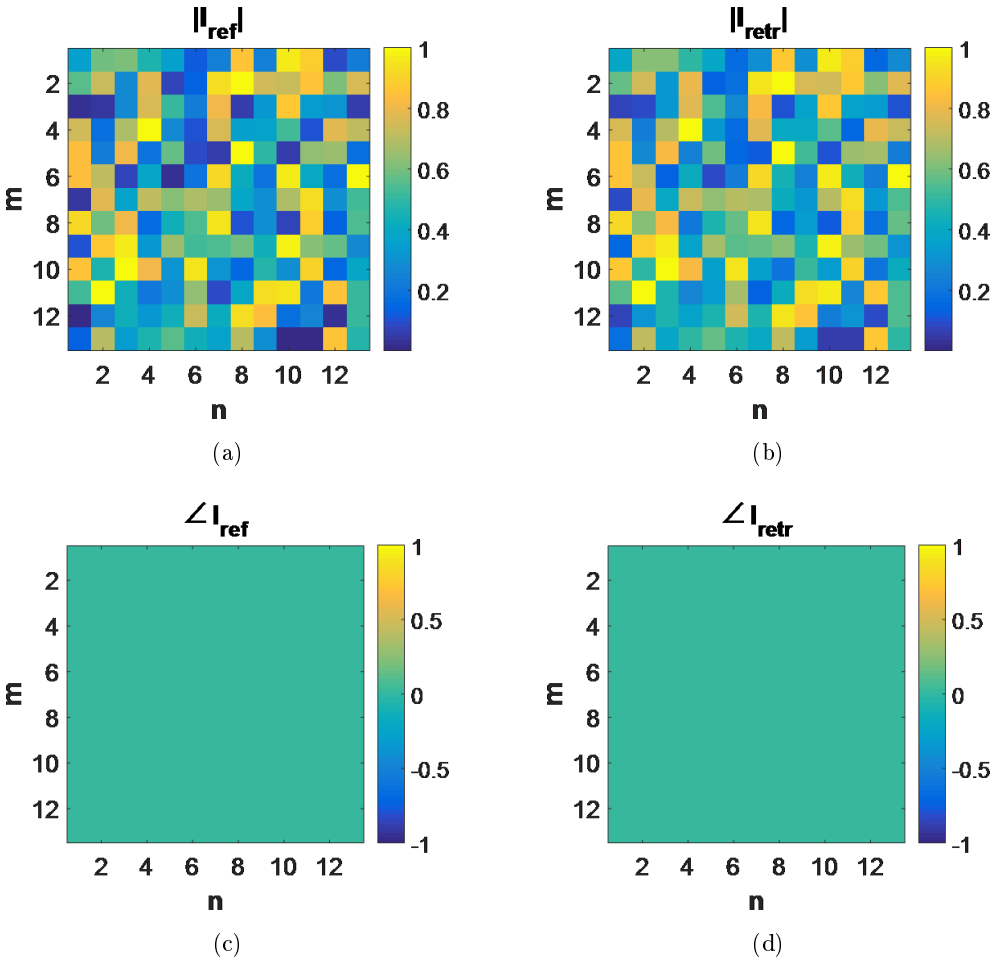

Fig. 5.11: Example 4: (a) Amplitude of the reference excitations; (b) Amplitude of the retrieved excitations; (c) Phase of the reference excitations; (d) Phase of the retrieved excitations.

$[0, 1]$. The corresponding power pattern has been measured over an equally spaced grid made of 37×37 points in the u-v plane, but no complex measurements have been added to data. In fact, as detailed in Section 5.2.4, dealing with real signals allows to resort to a *collapsed distribution* when $\bar{u} = 0$ and $\widehat{v} = 0$ are considered, with the consequent advantage of looking to real excitations sets amongst all gathered solutions through the SF. Once compatible 'words' have been retrieved along the u and v axes, one has the complex spectrum along two sides of a rectangle so that the recovery procedure can continue as in Section 5.2.3, i.e., by determining the complex values of $F(u, v)$ along a rectangle and then performing SF along the remaining rows, columns and diagonals (and enforcing coherence amongst their multiplicity of solutions to discard many of them).

The results for the third example are shown in fig. 5.8 and fig. 5.9 from which it is possible to observe the effectiveness of the proposed PR approach, as also witnessed by the $NMSE = 1.2790 \times 10^{-4}$.

In the last test case, we used the same signal source of the previous example but enhanced the PR difficulty by corrupting each measured field amplitude with $SNR = 25$ dB[9].

A comparison between reference and reconstructed results is given in fig. 5.10 in terms of fields, and in fig. 5.11 in terms of excitations. Also in this case, a satisfactory PR solution has been achieved. The NMSE results equal to 0.0018.

It is worth to underline that, although having been assessed in the case of array antennas and far field measurements, the given tools can be exploited for the phase recovery of whatever non-superdirective source, and can also be extended to the case of near-field measurements. In such a case, one can in fact exploit the 'reduced radiated field' concept, so that the near field still admits a Fourier series representation in terms of auxiliary variables and a fictitious array [82].

5.4 Concluding remarks

In this Chapter a new and original approach to the phase retrieval of two-dimensional complex signals has been presented which allows to set a deterministic and globally effective procedure for the retrieval of 2-D signals from phaseless and noiseless data. The characteristics of the approach have been discussed, emphasizing useful properties as well as the corresponding limitations in the actual case of noisy data. Also, some possible ways out from the limitations, suggesting for the antenna diagnostics problem the possible exploitation of hybrid measurement schemes using a (very) reduced number of amplitude and phase measurements, have been suggested. We have also shown that the basic approach (using just amplitude information) can be of immediate usefulness in those (many) cases where the starting signal is known to be real, or real and positive.

Notably, while (almost) all the existing approaches to antenna characterization problems require the exploitation of two different amplitude distributions [119], or two different probes [40], or two different defocusing conditions [38] in order to avoid the occurrence of false solutions, the proposed one just requires a single measurement surface and few additional information with respect to the one strictly needed for theoretical uniqueness. Also, it is not based in its present version on global optimization.

[9] Again, the procedure takes advantage from some oversampling of the square amplitude distribution.

While having indeed a number of drawbacks, we have shown by means of examples that the approach can be of interest in case of moderate dimension sources, and we are confident that the hybridization of the proposed 'congruence' point of view with other more classical approaches can give rise to further convenient solution procedures.

Another interesting research direction is the application of the above strategy based on 1-D decompositions to antenna synthesis problem and, in particular, to the optimal synthesis of mask constrained power patterns by means of planar arrays. In such a case, in fact, although considerable progress has been made in Chapter 3, a provably globally optimal synthesis procedure (opposite to the linear case) is still lacking.

6

PHASE RETRIEVAL FOR CIRCULARLY SYMMETRIC SOURCES: A CONCENTRIC CROSSWORDS-LIKE PROCESSING

6.0 Summary

This Chapter presents a PR strategy applied to the field radiated by continuous aperture sources for the detection of shape deformations on reflector antennas. It is based on a decomposition of the 2-D problem into subsequent 1-D PR problems along rings and diameters through the Spectral Factorization method, and a crosswords-like scheme is followed to discard multiple solutions and complete the retrieval of the field matrix. The proposed hybrid three steps procedure is assessed for the retrieving of realistic phase distortions on the reflector aperture field. Numerical examples concerning the retrieval of realistic phase distortions on the reflector aperture field support the given theory and confirm the effectiveness of the developed solution strategies[1].

[1] Some contents of this Chapter have been published in references [13, 15] of the "Publications List of G. M. Battaglia" reported at the end of the Thesis.

6.1 Introduction

In the framework of reflector antennas, deviations of the surface from the ideal reflector surface caused by gravity, wind, load, temperature play an important role, because they can cause decreases in observation efficiency of the antenna [128, 129]. To achieve acceptable efficiency, the root-mean-square-error (RMSE) deviation of the reflector surface from the ideal surface should be less than $\lambda/15$ to obtain more than 50% aperture efficiency [128]. Therefore, the challenge is to retrieve the shape in an accurate fashion and quickly, so that possible countermeasures can be adopted.

In 1985, Rahmat-Samii [129] introduced a simple and widely adopted model relating the shape deformation to the phase of the aperture field. More recently, a deformation-amplitude relationship has also been introduced in [130]. In both cases it is argued that the knowledge of the aperture field would provide the desired information.

In the literature, several approaches have been proposed for reflector surface diagnostics. A simple classification can be done by considering strategies based on the processing of both amplitude and phase of the radiated FF, which is typical of microwave-holography-based techniques (see for example [19, 131–134]), and strategies exploiting just the FF power pattern [28, 38, 135–138]. However, with increasing frequencies collecting phase measurements can be very difficult, or excessively expensive, so the second kind of strategy is indeed of interest. Accordingly, the problem of surface shape detection in reflector antennas can be conveniently linked to a PR problem [129, 139].

By considering an unknown complex function $f(\underline{x})$ and an operator T such that $F(\underline{k}) = T[f(\underline{x})] = |F(\underline{k})|e^{(j\angle F(\underline{k})}$, the PR problem deals with the determination the complex quantity $F(\underline{k})$ from the knowledge of $|F(\underline{k})|$, plus some additional information.

A very popular approach for such a kind of problems has been given by Misell in [38]. As in all PR methods available in literature for antenna (or other devices) characterization (but for [42]), a certain diversity in collecting data (e.g., two or more power patterns, probes, measurement surfaces, defocus conditions, or the like) is required [38, 40, 119]. In particular, the Misell algorithm requires two or more far-field amplitude patterns to be measured: one with the antenna in focus (i.e., with the probe at the parabola focus) and the other with the antenna defocused (or even with two defocused patterns) [38]. While being very fast to converge to the final solution, the major drawback of this procedure is that it can converge to a local minimum if the initial estimation of the aperture distribution is far from the ground truth. A

smart way to overcome such a problem, at least from a practical point of view, is the so-called 'hybrid input-output' procedure [140], which is still very popular and adopted widespread [44].

Another benchmark and well-assessed approach, based on GLO, is proposed in [120]. However, since the computational complexity of GLO procedures is expected to exponentially grow with the number of unknowns [96], it can prevent the actual attainment of the global optimum in case of very large number of unknowns.

As a contribution towards effective solution strategies for such a problem, this Chapter presents a novel approach for PR, which requires only one measurement surface in the far field in combination with the knowledge of the source' support and of the field' phase in a very reduced number of sampling points.

Note that avoiding different kinds of measurements collections is indeed a relevant asset, since it allows a great simplification in the measurement procedure and acquisition time [42].

The proposed approach relies on three basic bricks.

The first, and more obvious one, is the aperture antenna theory, which allows for simple relationships amongst the aperture field and the far field from one side, and the aperture field and reflector deformations from the other side.

The second brick, related indeed to the previous one, is given by the expansions of the aperture and far field in terms of the so called 'Orbital Angular Momentum' (OAM) modes, where the far field is given in terms of suitable Hankel transforms of the aperture modes (see [106, 141]).

The third ingredient is a recent approach to PR problems for the case of 2-D discrete signals (with particular attention to array antennas and hence periodic spectra) [123]. In this latter, an analogy amongst filling the rows and columns of the spectrum and completing a 'crosswords' scheme is introduced and discussed. In a nutshell, the approach exploits the capability to solve in a deterministic fashion 1-D PR problem in order to recast the 2-D PR problem as a combination of 1-D PR problems, and congruence/discrimination criteria in order to establish the correct behavior along the different (horizontal, vertical and diagonal) strips covering the 2-D scenario [123].

Basically, the proposed procedure consists of two main steps. In the first one, as in [123], we solve 1-D PR problems through the SF technique [2], and use congruence/discrimination arguments in order to select the correct behavior amongst the possible 'words'. However, two basic differences are present with respect to [123]. In fact, we solve PR problems along circles and diameters (rather than horizontal, verti-

cal and diagonal strips), with a number of advantages. These latters include a much simpler inizialization (and hence a much better computational efficiency), and the capability to deal with continuous sources. To this end, we also take full advantage from effective representations based both on OAM modes [106] and singular value decompositions (SVD) [142] of the fields corresponding to each mode order.

In the second step, once the field has been determined in a number of circles and diameters, the overall scheme is completed by solving a fitting problem that takes into account both the starting data (i.e., the square amplitude of the far field) and the complex field retrieved in the first step for a subset of sampling points. Notably, by virtue of the chosen representations, such a second step also contemporarily determines the aperture field.

Notably, in the second step the presence of a purely quadratic term allows, along the guidelines of [23, 127] to avoid the occurrence of false solutions.

The method is herein presented in case of generic planar continuous sources contained within a circle of given dimension and exhibiting no particular symmetries and, because of its generality, it applies to whatever related PR problem, so that similar tools may be eventually applied to synthesis (rather than recovery) problems.

The remainder of the Chapter is as follows. In Section 6.2 we briefly recall mathematical backgrounds on aperture antenna theory. Then, the rational of the proposed strategy is presented in Section 6.3 and formally described in Section 6.4. Finally, Section 6.5 is devoted to the assessment in case of reflector antennas deformation. Conclusions follow.

6.2 Mathematical Background and Formulation of the PR Problem

Let us consider a continuous aperture field $f(\rho', \phi')$ with circular support. By denoting with ρ', ϕ' the radial and angular variable spanning the aperture, respectively, this latter can be expanded in a multipole series as [106]:

$$f(\rho', \phi') = \sum_{\ell=-\infty}^{+\infty} f_\ell(\rho') e^{j\ell\phi'} \tag{1}$$

where

$$f_\ell(\rho') = \frac{1}{2\pi} \int_0^{2\pi} f(\rho', \phi') e^{-j\ell\phi'} \, d\phi' \tag{2}$$

Then, by denoting with $k^{'}$, ϕ the radial and azimuth coordinates in the spectral domain[2], the Fourier transform of the source (1) is [106]:

$$F(k^{'},\phi) = \frac{1}{2\pi}\int_{0}^{2\pi}\int_{0}^{\infty} f(\rho^{'},\phi^{'})e^{-jk^{'}\rho^{'}cos(\phi^{'}-\phi)}\rho^{'}\,d\rho^{'}d\phi^{'} \tag{3}$$

that can be also expanded in a multipole series as [141]:

$$F(k^{'},\phi) = \sum_{\ell=-\infty}^{+\infty} F_{\ell}(k^{'})e^{j\ell\phi} \tag{4}$$

wherein

$$F_{\ell}(k^{'}) = \frac{1}{2\pi}\int_{0}^{2\pi} F(k^{'},\phi)e^{-j\ell\phi}\,d\phi \tag{5}$$

Let now consider the problem of reconstructing the 2-D source $f(\rho^{'},\phi^{'})$ from the knowledge (e.g., measurements) of a sufficient number [80] of square amplitude samples of its Fourier transform, named M^2.

By denoting with $B[\cdot]$ the operator performing the square amplitude operation, i.e.:

$$B\left[F(k^{'},\phi)\right] = F(k^{'},\phi)F^{*}(k^{'},\phi) = |F(k^{'},\phi)|^2 = M^2 \tag{6}$$

the PR problem can be stated as the retrieving of $\widehat{F}(\underline{k}^{'},\underline{\phi})$ such that:

$$B\left[\widehat{F}(\underline{k}^{'},\underline{\phi})\right] = M^2(\underline{k}^{'},\underline{\phi}) \tag{7}$$

in the sampled spectral domain with $\underline{k}^{'} = [k_1^{'},\ldots,k_K^{'}]$, $\underline{\phi} = [\phi_1,\ldots,\phi_Q]$, K and Q being the number of discretization points for the radial and azimuth variable, respectively.

[2] By denoting θ as the elevation angle with respect to the boresight and adopting the usual correspondence with spectral variables $u = \beta sin\theta cos\phi$ and $v = \beta sin\theta sin\phi$, it will be: $k^{'} = \sqrt{u^2+v^2} = \beta sin\theta$, β being the wavenumber.

6.3 Rational of the PR strategy: Concentric-Crosswords-like Scheme

As already done in the Previous Chapter, we can see the FF matrix to be retrieved exactly like a particular kind of crossword puzzle (see Figs. 6.2a).

In this respect, the 2-D PR problem is turned into a collection of auxiliary 1-D PR problems and each of them is solved by adopting the SF method [2].

As it is well known, besides trivial ambiguities described below, 1-D PR problem does not admit unique solution. This is due to the fact that, the FF square amplitude can be written (but for a constant) as the product of factors of the kind $e^{ju} - z_i$, and any 'flipping'[3] of zeros z_i (which are organized in couples) corresponds to a different solution [2].

Therefore, for each 1-D PR problem we have a collection of possible solutions for the pertaining part of the spectrum.

As 2-D polynomials are not factorable (but for a zero-measure set of cases), ambiguities due to spectrum factorization do not generally occur in 2-D PR problems. Accordingly, the solution of a number of 1-D PR problems and their correct intersection according to congruence/discrimination arguments may allow to get the actual solution, the only residual problem being the so called 'trivial ambiguities'.

These latter ambiguities affecting uniqueness consist in

i) a constant phase on the far field/aperture source;

ii) a linear phase on the FF, corresponding to a translation of the source;

iii) a conjugation of the complex ff, corresponding to a reflection (and conjugation) of the aperture field;

iv) any combination of the above.

In fact, each of the above situations result in the same identical square amplitude distribution.

While the first two ambiguities can be faced by fixing a reference phase and supposing the support of the source to be known, respectively, the third one still remains. Hence, even neglecting possible factorizations of the 2-D spectrum, some additional a-priori information is anyway needed in order to get a theoretically unique solution even in the 2-D case.

To this aim, besides the exact source support, we suppose to exactly know the complex FF in a limited number of points, resulting in a 'facilitated' crossword puzzle,

[3] Unless the two elements of the couple have unitary amplitude.

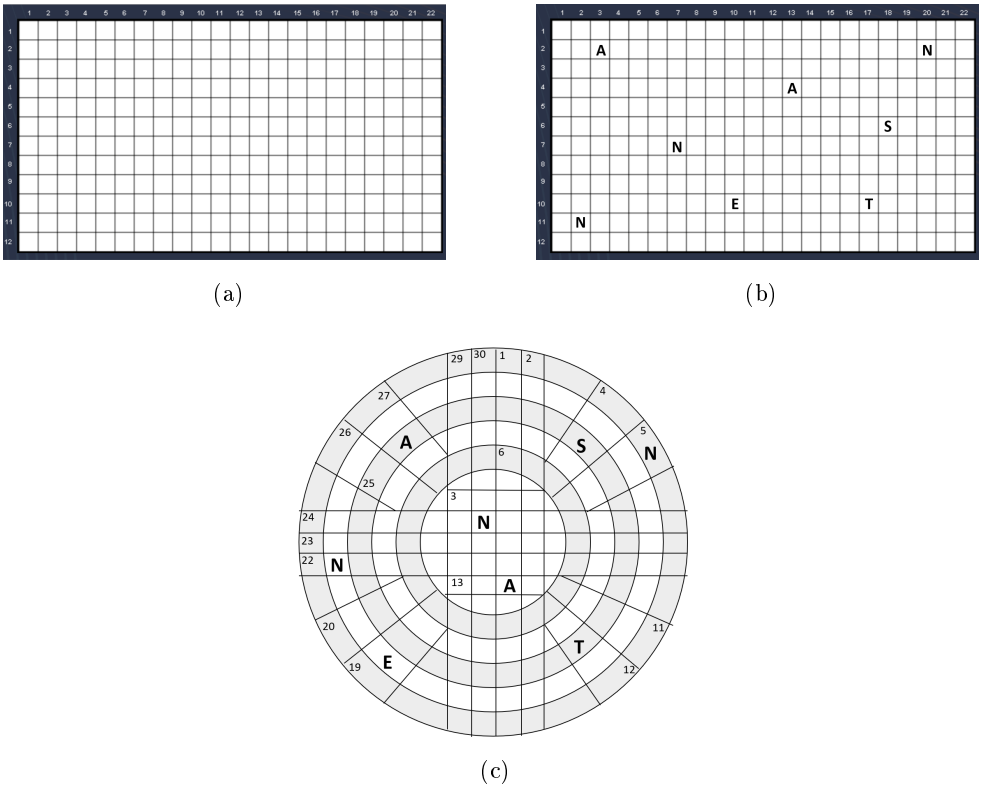

Fig. 6.1: Rational of the proposed PR strategy based on a crossword puzzle scheme: (a) Fill-in crossword; (b) Facilitated fill-in crossword; (c) Facilitated concentric crossword

see Fig. 6.1(b). In fact, such a configuration will allow a better discrimination amongst multiple solutions.

Since we are dealing with circularly supported aperture sources, we will consider 1-D PR problems along rings and diameters of the spectrum. For this reason, we refer to our approach as 'concentric' crosswords-like scheme (Fig. 6.1(c)).

The approach is general and applies to whatever continuous aperture source, and it overcomes some of the issues associated to the previous approach [123]. In this latter, in fact, a horizontal, a vertical and a diagonal cut were needed to have three intersections and initialize the solution of the puzzle, resulting in a cumbersome combinatorial problem[4]. Herein, the 'concentric' scheme allows to start with just one ring and one diameter (and hence with a reduced order combinatorial problem)[5]. Accordingly, the 'concentric' scheme leads to a considerably reduced computational burden

[4] In fact, the first two intersection just normalizes the phase along the second and third strip, and the third intersection allows for discrimination.

[5] In fact, they have two intersection points and the second one already allows for discarding incongruent solutions amongst the chosen diameter and ring.

with respect to the previous approach. Moreover (see sect. 6.4 below) one can take advantage from convenient representations of the radiated fields.

Finally, let us note that by following the suggested puzzle solution strategy, also in the PR problem there is a convenience in first retrieving the 'easiest' part of the spectrum. In particular, it is convenient to select 1-D cuts in correspondence of high intensity field amplitude and avoid nulls of the field wherein the phase would make no sense [14]. Also, cuts where many zeroes are present are preferred to reduce the number of multiple solutions in the corresponding 1-D SF problem, and hence the computational burden of the combinatorial problem at hand.

Hence, once the easiest cuts have been solved, it goes on systematically. Completion of the scheme is rather intuitive for crosswords' solvers.

6.4 A convenient representation for the far-field

To give an accurate representation of the field, we exploit the SVD of the radiation operator relating the source $f_\ell(\rho')$ to the field $F_\ell(k')$.

If Eq. (1) is substituted into Eq. (3) and then Eq. (4) is used, the radiated field can be written as [106]:

$$F_\ell(k') = \int_0^\infty f_\ell(\rho') J_\ell(k'\rho')\rho' d\rho' = H_\ell\{f_\ell(\rho')\} \tag{8}$$

wherein $J_\ell(\cdot)$ is the ℓ-th order Bessel function and the integral expression is the Hankel transform [141] of order ℓ of the function $f_\ell(\rho')$.

By normalizing ρ', k' such that the normalized variables ρ, k belong to the interval $[0,1]$, Eq. (8) becomes in an operator form as follows:

$$F_\ell = A_\ell f_\ell \tag{9}$$

A_ℓ being a compact notation for the radiation operator. We can now perform the SVD of A_ℓ, that is $\{v_{\ell,n}, \sigma_{\ell,n}, u_{\ell,n}\}$, such that:

$$A_\ell v_{\ell,n} = \sigma_{\ell,n} u_{\ell,n} \tag{10.a}$$

$$A_\ell^+ u_{\ell,n} = \sigma_{\ell,n} v_{\ell,n} \tag{10.b}$$

with $\sigma_{\ell,n}$, $v_{\ell,n}$, $u_{\ell,n}$ denoting the *n-th* singular value, right-hand and left-hand singular function, respectively, associated to the ℓ-th order, while A_ℓ^+ is the adjoint

operator. Since the singular functions $v_{\ell,n}$ and $u_{\ell,n}$ are orthonormal in the space of source and field, respectively, they can be used as representation bases in the respective domains. Therefore, we can represent the field as follows:

$$F_\ell(k) = \sum_{n=1}^{\infty} b_{\ell,n} u_{\ell,n}(k) \tag{11}$$

and, by substituting Eq. (11) into Eq. (4), we finally achieve:

$$F(k,\phi) = \sum_{\ell=-\infty}^{+\infty} \sum_{n=1}^{\infty} b_{\ell,n} u_{\ell,n}(k) e^{j\ell\phi} \tag{12}$$

Then, expansion (12) can be conveniently truncated on the basis of the properties in [106]. By so doing, one achieves

$$F(k,\phi) = \sum_{\ell=-\beta a}^{\beta a} \sum_{n=1}^{N_\ell} b_{\ell,n} u_{\ell,n}(k) e^{j\ell\phi} \tag{13}$$

where $N_\ell = \frac{2a}{\lambda} - \frac{|\ell|}{\pi}$.

Finally, a further advantage can be taken from the fact that the singular functions $u_{\ell,n}$ must exhibit a 'hole' of the order L in the $k = 0$ direction, so that for a given value of k the external summation on L can be further limited. Notably, this means that when considering a ring of radius k, the field can be conveniently written in terms of a trigonometric polynomial whose order depends indeed on k (the lower k, the lower the order of the polynomial).

6.5 The proposed procedure

As already stated, the key point of the proposed PR strategy is to recast the 2-D problem into a combinatorial problem over 1-D instances.

Ideally, one has to solve 1-D problems as long as the entire far field matrix is retrieved thank to subsequent solutions intersections. However (see below) a more effective scheme is possible once a sufficient number of rings and diameters have been solved.

In the first step, a reduced number of 1-D PR problems is solved by properly choosing rings and diameters cuts as suggested in Section 6.3. In such a step, advantage is taken from the fact that the source has a limited dimension, so that its spectrum is bandlimited. As a consequence, a finite number of cuts (and rings) can

be considered, and all quantities can also be safely sampled along the corresponding domains. Moreover, once the ratio between the number of retrieved overall field samples and the total number of field samples is sufficiently high [80], one can move to a faster mixed fitting procedure. This latter amounts in the minimization of the sum of two functionals, enforcing respectively a fitting over the residual square amplitude data, and over the already retrieved field data.

Notably (see above), because of the chosen (SVD based) representation of the spectrum, such a step also implicitely retrieves the aperture distribution.

The three steps of the PR procedure are detailed in the following subsections.

6.5.1 Step 1: 1-D PR via SF and crosswords

Let define with ξ the generic independent variable depending on the 1-D field curve at hand, that is:

$$F(\xi) = \begin{cases} F(k^{'}) \ for \ \phi = \bar{\phi} \ (i.e., a \ diameter) \\ F(\phi) \ for \ k^{'} = \bar{k^{'}} \ (i.e., a \ ring) \end{cases} \tag{14}$$

According to [2], the square amplitude distribution of Eq. (14) can be expressed in terms of auxiliary coefficients D_p such that:

$$|F(\xi)|^2 = P(\xi) = \sum_{p=-2P}^{2P} D_p e^{jp\xi} \tag{15}$$

where, because of the fact that the left-hand member is a real quantity, D_p is a Hermitian sequence of $4P+1$ complex coefficients, that is $D_p = D^*_{-p}$[6].

By considering the measured square amplitude data, that is $\tilde{P}(\underline{\xi})$ with $\underline{\xi} = [\xi_1, \ldots, \xi_N]$, N being the number of measurements taken according to [80], the sequence D_p can be determined in such a way that:

$$\tilde{P}(\underline{\xi}) = \sum_{p=-2P}^{2P} D_p e^{jp\underline{\xi}} \tag{16}$$

Once coefficients D_p have been determined, the SF technique developed in [2] is applied in order to get the multiplicity of solutions for the pertaining 1-D cut of the power pattern.

[6] Note that the square amplitude distribution has a (spatial) bandwidth which is twice the one pertaining to the corresponding complex field. Moreover, the number of DoF of the field along a diameter and a ring is generally different.

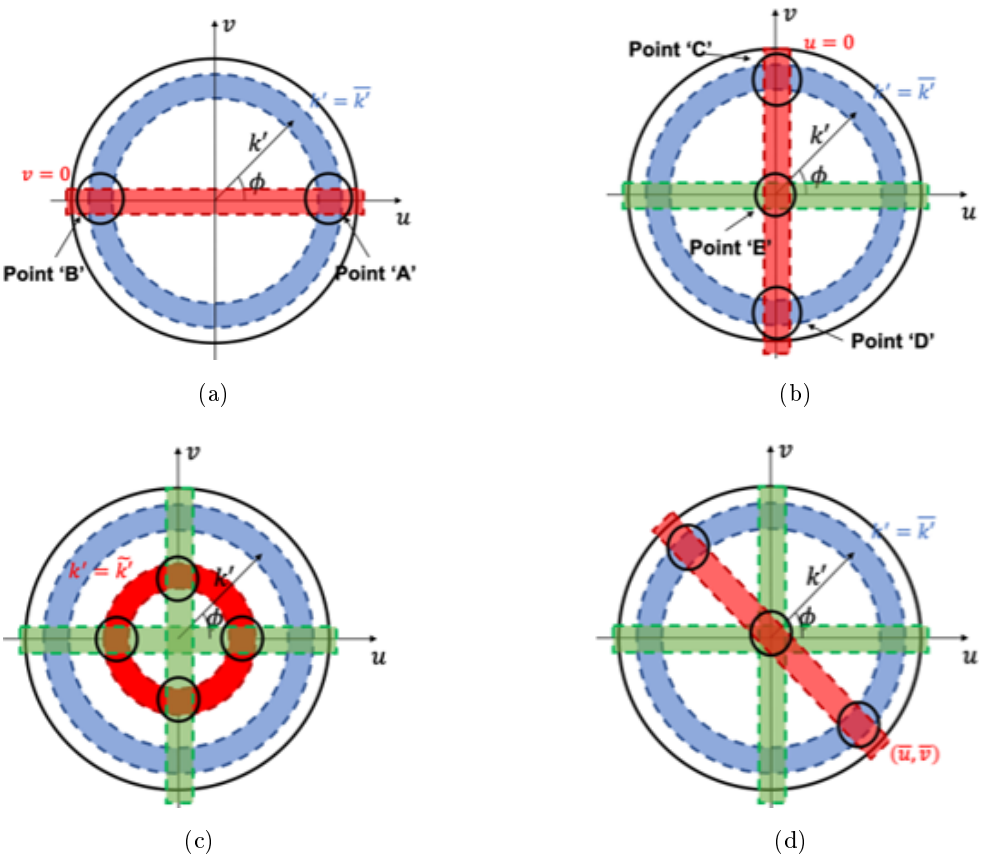

Fig. 6.2: Concentric Crosswords-like scheme of the proposed PR strategy. (a) Intersection amongst diameter at $v = 0$ and ring at $k^{'} = \bar{k'}$; complex field known in Point 'A' for phase normalization and in Point 'B' for solutions discard. (b) Intersection amongst diameter at $u = 0$, ring at $k^{'} = \bar{k'}$ and point ($u = 0$,$v = 0$); complex field known in Point 'C' for phase normalization, in Point 'D' for solutions discard and in Point 'E' from previous intersection. (c) Intersection amongst ring at $k^{'} = \widetilde{k'}$ and diameters at $u = 0$ and $v = 0$; all the intersection Points are known from previous intersections. (d) Intersection amongst diagonal ($u = \bar{u}$,$v = \bar{v}$) and ring at $k^{'} = \bar{k'}$. The continuous black circle indicates the contour of the visible part of the spectrum.

For the sake of simplicity, let suppose to have applied the SF to the horizontal diameter and to a generic ring, as depicted in Fig. 6.2(a). Hence, for each of them, a number of possible solutions are available. In order to discover the correct one, let apply the 'crossword' approach and consider the intersection between two field values (i.e., points 'A' and 'B') which are supposed known. In particular, point 'A' acts as a

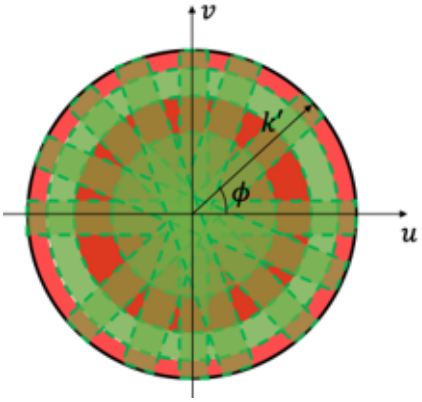

Fig. 6.3: Pictorial view of the field in the spectral domain after Step1. The green zone is relative to points where the complex field has been retrieved. The red zone is relative to point where field has yet to be recovered.

normalization point[7], while point 'B' is used to discard a number of possibilities and hopefully identify the correct field along the diameter and the ring.

Now, it is possible to move to another cut, for instance the vertical diameter (see Fig. 6.2(b)), solve Eq. (16) for D_p and evaluate the multiplicity of solutions. Then, the 'crossword' approach is applied once again. At this time, point 'E' is known from the previous intersection, while point 'C' and 'D' can be used to normalize the fields and discard solutions, respectively.

The procedure is iterated by considering, for instance, a new ring as in Fig. 6.2(c), or a new diameter as in Fig. 6.2(d).

In summary, every time a crossword approach is applied the PR requires that the complex field is known in the two intersection points, in order to have a reference field value for all the multiple solutions and to discard all of them that are far from the actual one. In case two points are not enough to discriminate the actual solution, it is possible to consider more intersections. For instance, if the scenario in Fig. 6.2(a) cannot allow the retrieving of the field, one can move to scenario of Fig. 6.2(b) and adopt points 'B', 'C' and 'D' to discover the solution.

As it can be easily guessed, as the procedure goes on, the number of points in which the complex field becomes known and usable grows, so the 1-D PR problems at hand become easier and easier.

[7] A normalization procedure is performed to avoid the trivial ambiguity due to a linear phase superimposed on the field itself. Hence, the normalization process makes the field value of all multiple solutions in the point at hand $(k_N^{'}, \Phi_N)$ equal to the actual field in that point. By denoting with J the total number of multiple solutions, it means that: $F_j(k_N^{'}, \phi) = F_j(k_N^{'}, \phi) \frac{F_{actual}(k_N^{'}, \phi)}{F_j(k_N^{'}, \phi)}$, $j = 1, ..., J$.

6.5.2 Step2: PR Completion

After that a number of rings and diameters of the FF have been retrieved through the procedure detailed in Section 6.5.1, the scenario at hand will appear as depicted in fig. 3. In the figure, the retrieved field is highlighted in green while the red part indicates those points where just the amplitude of the field is still unknown. Hence, to run out the PR procedure, we need to recover those points.

To accomplish such a goal, two possibilities come out. The first one is a simple interpolation of the available field. Undoubtedly, phase errors in the reconstructed points are expected in this case.

As a second and more accurate possibility, we can solve a fitting problem in the overall spectral domain such that a proper field representation must fit the already retrieved field in the 'green points' and the available data in the 'red points'.

Let split the spectral domain in two parts: $\widehat{\prod} \equiv (\widehat{k}, \widehat{\phi})$ relative to points with already retrieved field (i.e., complex values $M_{\widehat{k},\widehat{\phi}}$) and $\widetilde{\prod} \equiv (\widetilde{k}, \widetilde{\phi})$ where just amplitude data (i.e., $\widetilde{M}^2_{\widetilde{k},\widetilde{\phi}}$) are still known.

The PR completion is performed by solving the following optimization problem:

$$\min_{\mathbf{b}} \psi(\mathbf{b}) = w_1^2 \psi_1(\mathbf{b}) + w_2^2 \psi_2(\mathbf{b}) \tag{17}$$

where $\mathbf{b}$ is the vector containing the representation coefficients $b_{\ell,n}$, w_1^2 and w_2^2 are positive constants properly weighting the two functionals ψ_1 and ψ_1, which are defined as [127]:

$$\psi_1(\mathbf{b}) = \left\| \frac{|F_{\widetilde{k},\widetilde{\phi}}|^2 - M^2_{\widetilde{k},\widetilde{\phi}}}{M^2_{\widetilde{k},\widetilde{\phi}}} \right\|^2_{\widetilde{\prod}} = \sum_{\widetilde{k}} \sum_{\widetilde{\phi}} \frac{\left[|F_{\widetilde{k},\widetilde{\phi}}|^2 - M^2_{\widetilde{k},\widetilde{\phi}} \right]^2}{M^2_{\widetilde{k},\widetilde{\phi}}} \tag{18.a}$$

$$\psi_2(\mathbf{b}) = \left\| F_{\widehat{k},\widehat{\phi}} - M_{\widehat{k},\widehat{\phi}} \right\|^2_{\widehat{\prod}} = \sum_{\widehat{k}} \sum_{\widehat{\phi}} |F_{\widehat{k},\widehat{\phi}} - M_{\widehat{k},\widehat{\phi}}|^2 \tag{18.b}$$

Accordingly, the optimization problem (17) aims at determining coefficients $b_{\ell,n}$ such that amplitude data are fitted through Eq. (18a) and the already retrieved field from Step 1 are fitted through Eq. (18b). Note that while functional (18b) is quadratic with respect to unknowns, functional (19a) is indeed quartic.

To perform the optimization, a gradient-based minimization scheme is adopted. As known, this kind of deterministic solution algorithm converges to the closest local minimum of the cost functional. However, thanks to Step 1, and hence to the quadratic

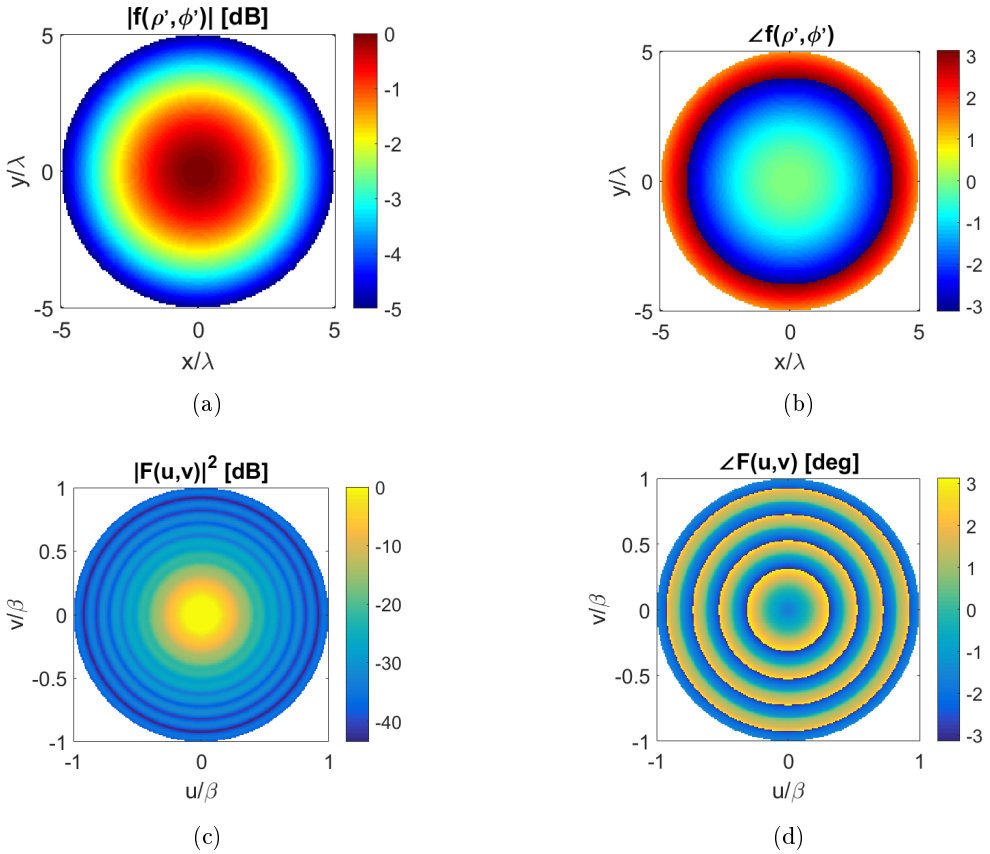

Fig. 6.4: Example 1. Amplitude (a) and phase (b) of the nominal aperture field distribution. Square amplitude (c) and phase (d) of the corresponding far field.

part of the functional, such a drawback is reduced or avoided at all. Moreover, also the adoption of a normalization factor in Eq. (18a) for the enhancement of low data values guarantee more robustness against local minima [127].

Details about the implementation of the gradient-based solution algorithm are given in Appendix C.

6.5.3 Step3: Aperture Field Retrieval

While the usual PR problem can be considered accomplished with Step 2, the diagnostic problem we are interested in will end with the retrieving of the aperture field distribution since, as extensively said previously, contains within itself information about reflector shape deformations.

To this aim, we exploit the available SVD of the radiation operator $A_{\ell}l$. In fact, the singular functions $v_{(\ell,n)}$ can be used as representation basis for the source:

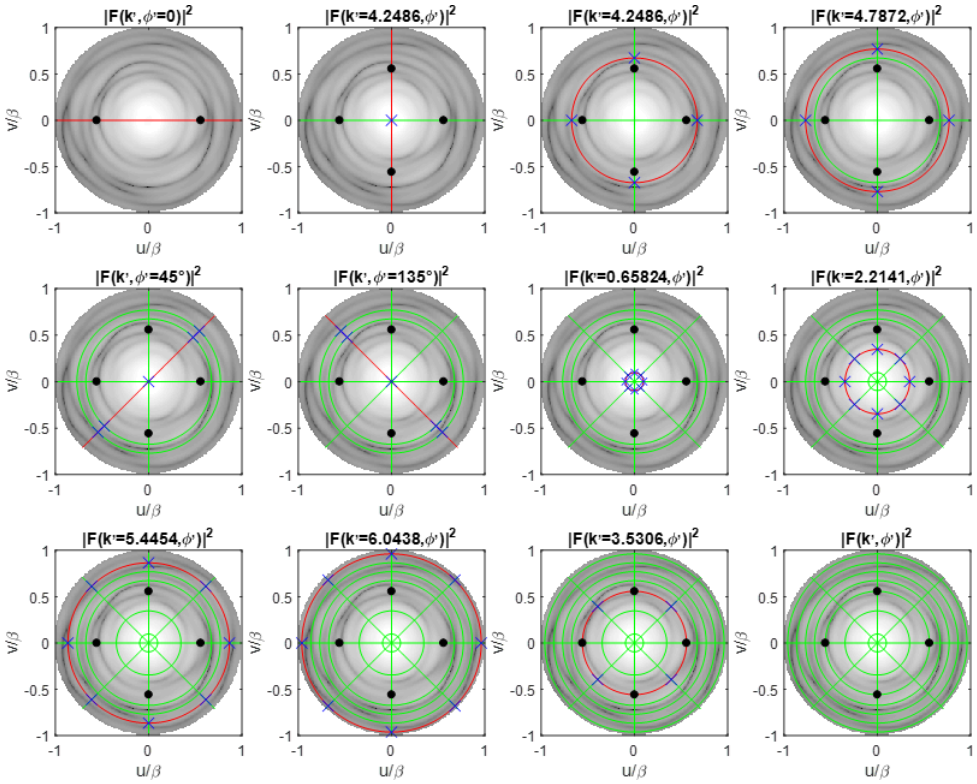

Fig. 6.5: Example 1: diameters and rings retrieved in Step 1. The continuous red line indicates the 1-D field to be retrieved through SF; the continuous green line indicates the field known (in amplitude and phase) from previous 1-D PR problems. The black circle markers are those points wherein the complex field is supposed a-priori know; the blue star markers indicate intersection points wherein the complex field is known from previous 1-D PR problems. The last figure represents the final configuration of the retrieved far field at the end of Step 1.

$$f_\ell(\rho) = \sum_{n=1}^{N_\ell} \alpha_{\ell,n} v_{\ell,n}(\rho) \tag{19}$$

and the source representation coefficients $\alpha_{\ell,n}$ can be directly evaluated through singular values by means of [142]:

$$b_{\ell,n} = \sigma_{\ell,n} \alpha_{\ell,n} \tag{20}$$

where the adopted truncations of the different SVD allows for a safe and robust recovery of $\alpha_{\ell,n}$ coefficents. Then, the aperture field is finally retrieved by substituting Eq. (19) into Eq. (1).

6.6 Numerical Examples

This section is devoted to the assessment of the proposed hybrid PR strategy for the diagnosis of surface deformations on a reflector antenna in case of different kinds of distortions.

As nominal source, we considered a continuous aperture field with a circular support whose nominal expression is the following:

$$f(\rho^{'},\phi^{'}) = |f|e^{j\phi f} \tag{21.a}$$

$$|f| = \frac{4FL}{4FL^2 + \rho^{'2}} \tag{21.b}$$

$$\phi_f = \beta\left[2FL + \frac{\Delta z}{\rho}\left(\frac{4FL^2 - x^{'2} - y^{'2}}{4FL}\right)\right] \tag{21.c}$$

wherein FL is the focal length, while $\frac{\Delta z}{\rho}$ is a constant factor.

In the first example, we supposed a surface deformation $\delta(\rho^{'},\phi^{'})$ [137] on the reflector that turns into a phase distortion on $f(\rho^{'},\phi^{'})$ which add up to the quadratic phase, i.e.:

$$f(\rho^{'},\phi^{'}) = |f|e^{j\phi_f + \Delta} \tag{22}$$

with:

$$\Delta = \frac{8FL^2\beta}{4FL^2 + \rho^{'2}}\delta \tag{23}$$

Relationship (23), relating the aperture phase linearly with the surface deformation has been derived in [129]. According to [137], we set δ randomly in the range $[-\lambda/30, \lambda/30]$.

The nominal source with the corresponding FF are shown in fig. 6.4. The radius of the source is 5λ, $FL = 4\lambda$, $\frac{\Delta z}{\rho} = 0.5$ and the amplitude $|f|$ has been scaled such to exhibit a taper of 5dB.

Step 1 of the PR procedure provides for a subsequent recovery of 1-D complex fields in correspondence of significant diameters and rows of the data matrix. In particular,

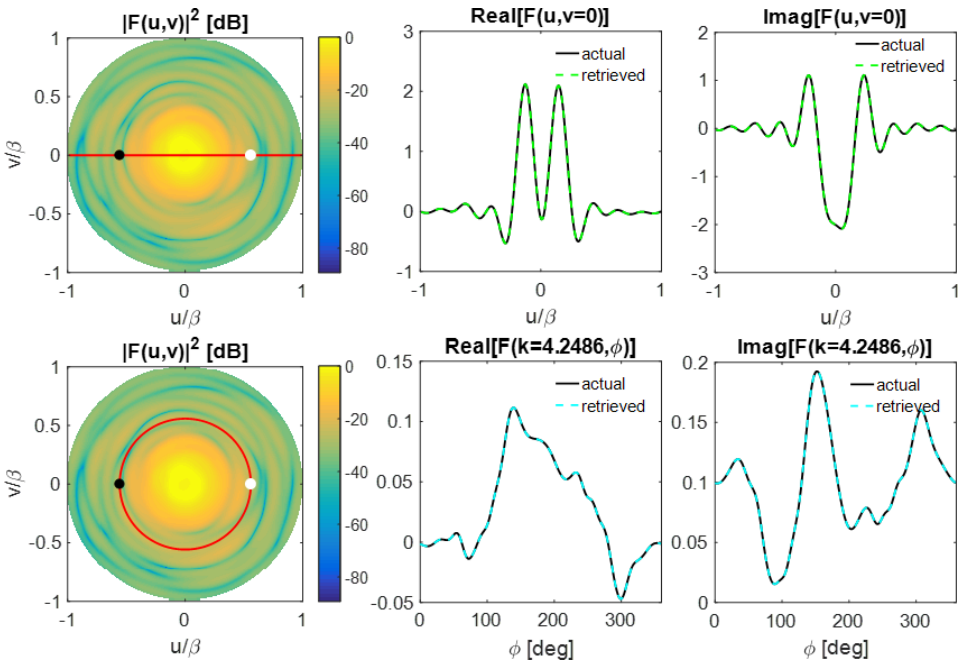

Fig. 6.6: Step 1 of the PR procedure. Outcome of 1-D PR problem through Spectral Factorization for: (top) diameter at $v = 0$; (bottom) ring at $k^{'} = 4.2486$. In the 2-D image the continuous red line indicates the considered diameter and ring; the circle markers indicate points where the complex field is supposed known: the white point is used for fields normalizations and the black point is used for discarding multiple solutions.

we have chosen 7 rings passing through points with high intensity amplitude, and 4 diameters ($u = 0$, $v = 0$, diagonals at 45° and 135°). In fig. 6.5 the sequence of 1-D PR problems dealt with in Step 1 are shown by highlighting with a continuous red line the 1-D field to be retrieved, with a continuous green line the field already gathered in a previous PR problem, while with blue and black markers coordinates of the spectrum wherein the complex field is known due to previous recovery or for a-priori knowledge, respectively. In this respect, it is worth to note that only 4 complex measurements are needed to trigger the overall procedure, which is a very reduced number with respect to a-priori information or diversity conditions required in other strategies.

For the sake of brevity, in fig. 6.6 the retrieved fields by means of the SF for the diameter at $v = 0$ and the ring at $k^{'} = 4.2486$ are reported.

Thereafter, the procedure for the PR completion has been undertaken. In fig. 6.7b is shown the result achieved by just interpolating the field retrieved in Step 1, while in fig. 6.8b improved results achieved from the fitting problem (18) can be appraised. The

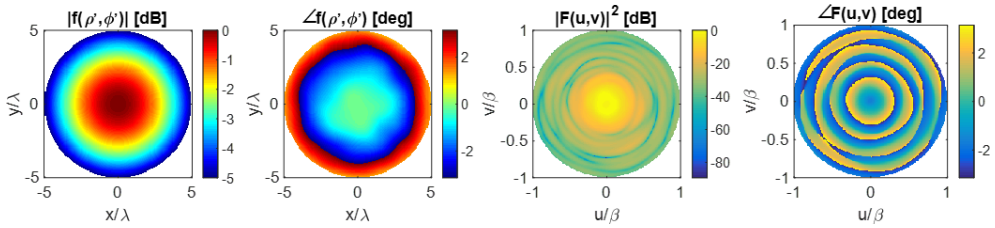

(a)

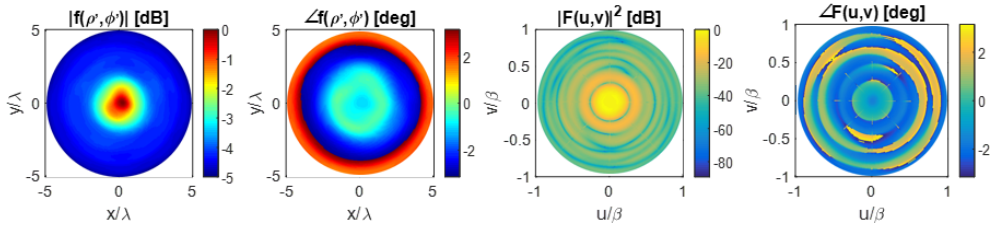

(b)

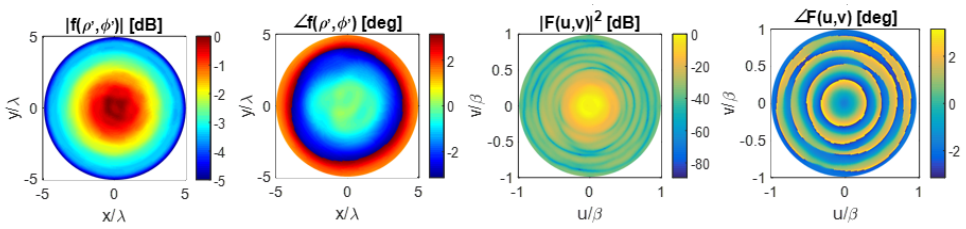

(c)

Fig. 6.7: Step 2 and 3 for Example 1. From left to right: amplitude and phase of the continuous aperture source, square amplitude and phase of the corresponding far field. From top to bottom: actual distributions (a); retrieved distributions through interpolation (b); retrieved distributions through the proposed hybrid strategy (c).

weighting parameters w_1^2 and w_2^2 have been set equal to the energy of the pertaining data.

To quantitatively appraise the improvement brought from the hybrid approach, we introduced the following normalized mean square error metric, for both the radiated ($NMSE_{rf}$) and the aperture ($NMSE_{af}$) field:

$$NMSE_{rf} = \frac{\left\| F^{actual}(k',\phi) - F^{recovered}(k',\phi) \right\|^2}{\left\| F^{actual}(k',\phi) \right\|^2} \tag{24.a}$$

$$NMSE_{af} = \frac{\left\| f^{actual}(\rho',\phi') - f^{recovered}(\rho',\phi') \right\|^2}{\left\| f^{actual}(\rho',\phi') \right\|^2} \tag{24.b}$$

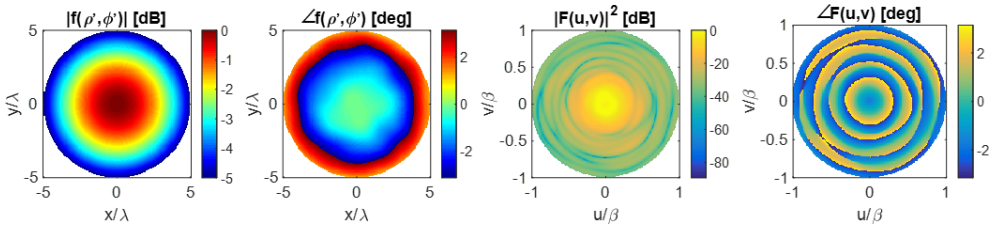

(a)

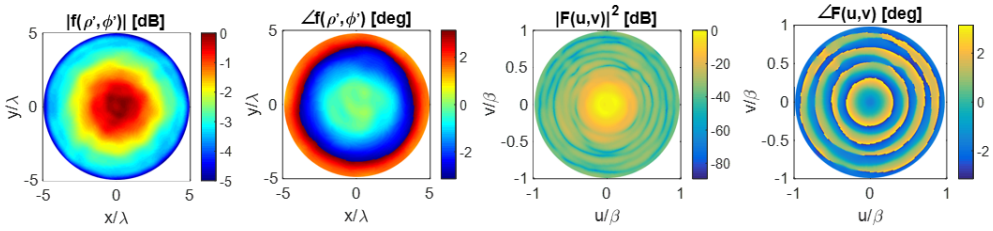

(b)

Fig. 6.8: Step 2 and 3 for Example 1 with $SNR = 30dB$. From left to right: amplitude and phase of the continuous aperture source, square amplitude and phase of the corresponding far field. From top to bottom: actual distributions (a); retrieved distributions through the proposed hybrid strategy (b).

The attained metrics for the example at hand are summarized in Table 6.1.

The proposed PR strategy has been also successfully tested in case of data corrupted by white gaussian noise with a given SNR. Fields and sources retrieved in the noisy condition are shown in fig. 6.8 for $SNR = 30dB$, while error synthetic parameters are summarized in Table 6.2. Instead, in fig. 6.9 the retrieved fields by means of the SF for the diameter at $v = 0$ and the ring at $k^{'} = 4.2486$ are reported.

Table 6.1: Comparison of NMSE for Example 1

	$NMSE_{rf}$	$NMSE_{af}$
Interpolation	0.1310	0.6662
Fitting Problem (18)	$2.2302 \cdot 10^{-4}$	$5 \cdot 10^{-3}$

Table 6.2: NMSE for Example 1 with $SNR = 30dB$

	$NMSE_{rf}$	$NMSE_{af}$
Fitting Problem (18)	0.0014	0.0065

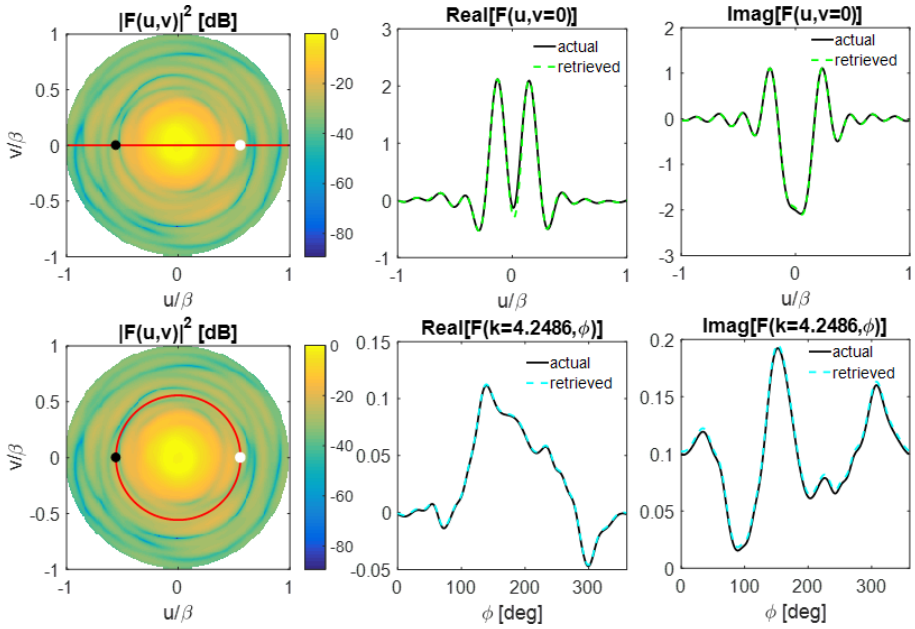

Fig. 6.9: Step 1 of the PR procedure. Outcome of 1-D PR problem through Spectral Factorization for: (top) diameter at $v = 0$; (bottom) ring at $k^{'} = 4\dot{2}486$. In the 2-D image the continuous red line indicates the considered diameter and ring; the circle markers indicate points where the complex field is supposed known: the white point is used for fields normalizations and the black point is used for discardimg multiple solutions.

As a second assessment case, we considered an optical path disturbance (OPD) represented by means of Zernike polynomials [143] up to the $7-th$ degree (36 expansion coefficients), as suggested in [138]. Accordingly:

$$f(\rho^{'}, \phi^{'}) = |f| e^{j\phi_f + 2\beta OPD} \tag{25}$$

with:

$$OPD(\rho^{'}, \phi^{'}) = \sum_n \sum_m c_{nm} z_n^m(\rho^{'}, \phi^{'}) \tag{26}$$

wherein polynomials Z are orthonormal over the unitary circle and coefficients c_{nm} have been randomly chosen in the interval [-1,1] [14]. The adopted $OPD(\rho^{'}, \phi^{'})$ function is shown in fig. 6.10. In this case, the radius of the aperture is 4λ, $FL = 1.65\lambda$, $\frac{\Delta z}{\rho} = 0.5$ and the amplitude $|f|$ has been scaled such to provide a tapering of 10dB at the reflector edge.

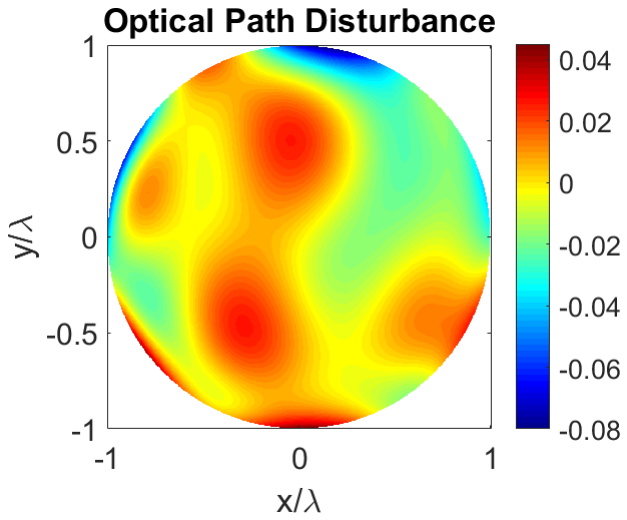

Fig. 6.10: Optical Path Disturbance adopted in Example 2.

Also in this case, we have chosen 7 rings passing through points with high intensity amplitude, and 4 diameters ($u = 0$, $v = 0$, diagonals at 45° and 135°), and only 4 complex measurements are needed to trigger the overall procedure.

For the sake of brevity, in fig. 6.11 the retrieved fields by means of the SF for the diameter at $v = 0$ and the ring at $k^{'} = 3.4109$ are reported.

Thereafter, the procedure for the PR completion has been undertaken. In fig. 6.12b results achieved from the fitting problem (18) can be appraised, while error synthetic parameters are summarized in Table 6.3. Also in this case, the weighting parameters w_1^2 and w_2^2 have been set equal to the energy of the pertaining data.

Table 6.3: Comparison of NMSE for Example 2

	$NMSE_{rf}$	$NMSE_{af}$
Fitting Problem (18)	$1.6164 \cdot 10^{-5}$	0.0282

Also in this case, the proposed PR strategy has been also successfully tested in case of data corrupted by white gaussian noise with a given SNR. Fields and sources retrieved in the noisy condition are shown in fig. 6.8 for $SNR = 30dB$, while error synthetic parameters are summarized in Table 6.4. Instead, in fig. 6.9 the retrieved fields by means of the SF for the diameter at $v = 0$ and the ring at $k^{'} = 3.4109$ are reported.

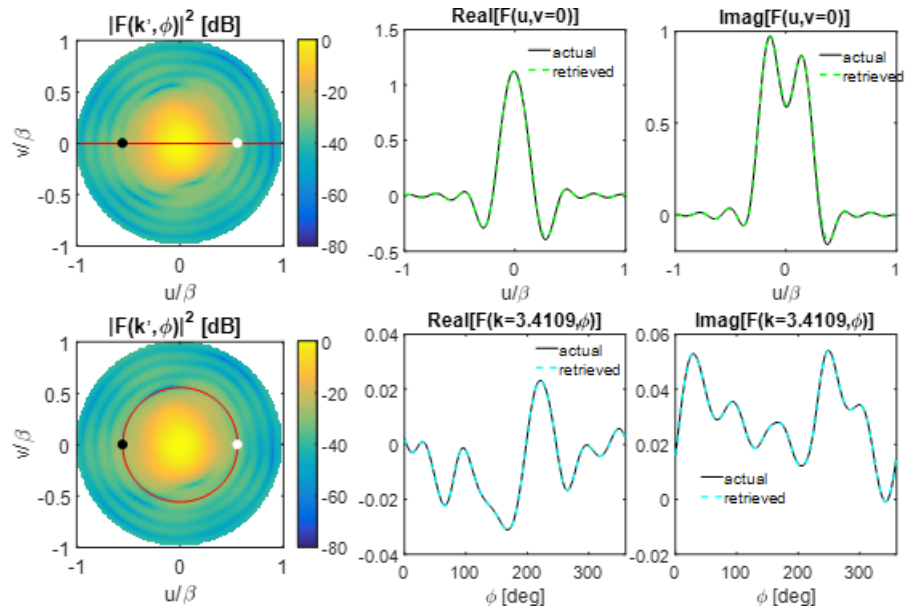

Fig. 6.11: Step 1 of the PR procedure. Outcome of 1-D PR problem through Spectral Factorization for: (top) diameter at $v = 0$; (bottom) ring at $k^{'} = 3\dot{4}109$. In the 2-D image the continuous red line indicates the considered diameter and ring; the circle markers indicate points where the complex field is supposed known: the white point is used for fields normalizations and the black point is used for discarding multiple solutions.

Table 6.4: NMSE for Example 2 with $SNR = 30dB$

	$NMSE_{rf}$	$NMSE_{af}$
Fitting Problem (18)	$2.2302 \cdot 10^{-4}$	$5 \cdot 10^{-3}$

6.7 Final remarks

This Chapter dealt with contributions to the 2-D PR problem. In particular, like the method presented in the previous Chapter, the 2-D PR problem can be seen as a proper combination of 1-D problems. Moreover, also in this case, the proposed technique (opposite to almost all available methods) requires measurements (plus some minimal a-priori information) over just one plane and avoids the exploitation of GLO algorithms. However, similarities end here. In fact, differently from the method proposed in the previous Chapter, the present one considers circular "continuous" aperture sources instead of antenna arrays. Then, by exporting the multipole expansion of the FF (and of the corresponding power pattern), it enables one to perform the above 'crosswords' PR procedure by acting, this time, just on diameters and concentric-

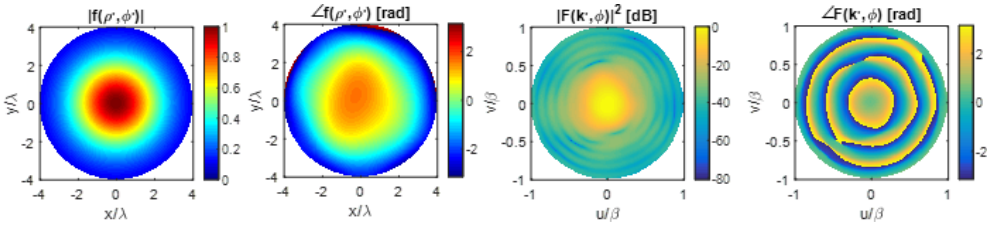

(a)

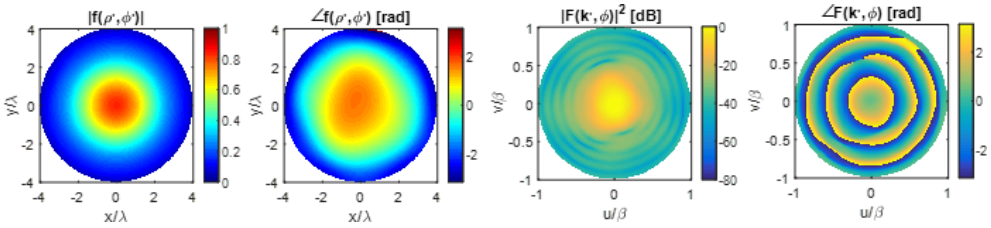

(b)

Fig. 6.12: Step 2 and 3 for Example 2. From left to right: amplitude and phase of the continuous aperture source, square amplitude and phase of the corresponding far field. From top to bottom: actual distributions (a); retrieved distributions through the proposed hybrid strategy (b).

ring (rather than horizontal, vertical and oblique) cuts of the pattern. In this case, in order to identify the correct field instances among all the ones provided by the SF, it is sufficient considering the intersection between two field values (rather than three field values) improving the previous procedure. In fact, the need of just two intersections will lead to a considerably reduced computational burden with respect to the first approach. Finally, this technique does not require any symmetry (e.g., a circularly-symmetric behavior) of the field in order to properly work.

As a demonstration of the interest and effectiveness of the proposed approaches, applications to array diagnostics as well as to reflectors' surface deformations are given.

The bottleneck of the proposed technique is the computational burden. In fact, as long as SF method is used, this latter grows as the number of array elements increases. However, one can develop some smart strategy in order to reduce the number of combinations to be explored. For instance, starting from a line where many zeroes are present reduces the number of ambiguities on the corresponding 1-D PR problems.

7

CONCLUSIONS AND POSSIBLE FUTURE DEVELOPMENTS

In this Thesis, novel contributions to phaseless inverse source problems and applications have been presented. The most common goal of an inverse source problem is to retrieve (and infer useful information about) a source starting from the knowledge of some data and of the model describing the electromagnetic phenomenon at hand.

In this respect, completely new point of views to phaseless inverse source problems have been considered in the Thesis.

More in detail, the contributions of the Thesis can be summarized as it follows.

After a brief recall of phaseless inverse source problem formulation and properties, the Thesis is composed by two different parts.

In PART I, electromagnetic fields shaping problems are dealt with. In particular, the problem of maximize the field intensity in a given point or direction as well as the problem of shaping the field within a given region have been considered. Coming to details, by taking advantages from a previously developed focusing method, called FOCO (FOcusing via Constrained Optimization), the aim was to delineate a general and unitary mathematical framework identifying the causes of non-convexity (and hence difficulties) and to propose an effective ways out. In particular, two up to now unsolved canonical problems have been successfully tackled.

The second Chapter has been devoted to shaping problem by means of 1-D arrays o 2-D planar arrays. In particular, the proposed approach combines the adoption of several 'control points' with the FOCO method in order to address both issues related to the occurrence of undesired side field peaks and to the field intensity uniformity in the target region. Moreover, the proposed approach is able to exploit all the DoF of the problem by looking for complex patterns, and it allows identifying (if any) a multiplicity of substantially-different excitation sets all fulfilling the assigned power-pattern mask. Finally, the approach seems to be the first one able to grant, at the same time, all the above features plus the capability of dealing with completely-arbitrary

array layouts and element patterns (including aperiodic planar and conformal arrays where mounting-platform and mutual-coupling effects are present). In fact, for any set of phase shifts the problem becomes essentially identical to FOCO, so that one just needs to optimize the phase shifts.

By taking advantage from the same circumstance, the third Chapter has been devoted to shaping problem by means of large and arbitrary arrays. In fact, a hybrid approach based on nested optimizations has been proposed, where the external GLO acts on the field's phase shifts over a minimal number of 'control points' located into the target region whereas the internal optimization acts instead on excitations. As discussed and validated through examples, the approach is very effective even in those cases where methods based on either enumerative strategies (Chapter 2) or GLO on all the excitations (or field samples) result too heavy under the computational point of view. In fact, the GLO is here performed on a minimal number of unknowns (which are conveniently identified as the field phase in a low number of control points). By so doing, the computational burden required for optimizing the synthesis is reduced as much as possible.

The fourth Chapter provides a very simple extension of the basic FOCO approach to the vector fields. In particular, it is shown that the non-convex part of the synthesis problem consists in the selection of the field polarization in the target point which provides the highest intensity of the overall field herein. In fact, once the optimal polarization is known, the focusing problem becomes a simple CP one. This interesting result allows the development of a possible solution strategy. In fact, one can search the optimal polarization by means of GLO procedure. In this case, GLO algorithms would be applied to a very small number of parameters (i.e., the five components of the polarization vector) so that the issues related to the number of variables, such as the actual optimality of the solution found and the computational burden, are avoided.

It has to be noted that the common strategy in Chapter 3 and 4 is that of identifying the causes of non-convexity of the problem and formulate its solution in such a way that the (required) GLO procedures only have to deal with the minimal number of unknowns, with the inherent benefits.

In Part II, the PR problem is dealt with. In particular, the developed approaches to PR require only one measurement surface plus the knowledge of the source's support and a few additional informations. Moreover, they deal with 2-D problems, i.e., with the retrieving of planar sources or excitations of planar arrays. As in PART I,

the proposed approaches are based on a proper combination of the solution of simpler problems, which are herein 1-D PR problems, and each of them can be solved through the SF [2] method obtaining, for each 1-D PR problem, a collection of possible solutions. Hence, the final actual solution of the 2-D PR problem is gathered by following a procedure which resembles the solution of crosswords puzzles, where one has to guarantee the congruence amongst the solutions amongst across and up-down possible words.

The fifth Chapter has been devoted to the case of antenna arrays, where the spacing is greater than (or equal to) $\frac{\sqrt{2}}{2}\lambda$. In fact, in such a case phaseless measurement allow collection of the square amplitude of the spectrum in the overall periodicity interval. Coming to details, the developoed approach is able to perform the 'crosswords' PR procedure by acting on horizontal, vertical and oblique cuts of the pattern. In order to identify the correct field instances among all the ones provided by the SF, it will be sufficient considering the intersection between three field values. As a distinguishing feature, opposite to almost all available techniques, the proposed one requires measurements (plus some minimal a-priori information) over just one plane and does not need to recur to computationally-expensive global-optimization algorithms.

The sixth Chapter has been devoted to continuous aperture sources. The proposed procedure is able to perform the above 'crosswords' PR procedure by acting, this time, just on diameter and concentric-ring cuts of the pattern (rather than horizontal, vertical and oblique) cuts of the radiation pattern. In this case, in order to identify the correct field instances among all the ones provided by the SF, it will be sufficient considering the intersection between two field values. The need of just two intersections in order to discard the unsuitable field distributions will lead to a considerably reduced computational burden with respect to the approach introduced in Chapter 5. Also, one is able to deal with whatever planar source.

Both results in PART I ans PART II allow to devise a series of possible developments.

First, a simple joining of results of Chapters 2 and 3 from one side, and Chapter 4 from the other side, will allow a convenient procedure for field intensity shaping. Second, the shaping procedures which have been developed can also be used in near field or non-homogeneous regions of space, which is of interest in very many applications including the shimming of the B_1^+ field in Magnetic Resonance Imaging applications. As a matter of fact, this possibility for realizing B_1^+ fields as uniform as possible in the region of interest is being considered at LEMMA/UNIRC.

As far as the second part is concerned, “expert systems” environments for X-words solutions are being developed. The case where one knows a-priori that the source is real and positive can be interestingly dealt with using the so-called "collapsed distribution" as a convenient starting, which is also in progress. Finally, all results can be hopefully extended, or they are at least of interest, for turning back to the first problem, i.e., antenna power pattern synthesis.

A

Appendix A

Analytic expression for Ripple function

This Appendix is aimed at showing how the R function (2) [and correspondingly the cost function (3)] can be accurately approximated as a positive semi-definite quadratic function of the excitations. To this end, as a linear transformation does not affect convexity properties, let us consider a sampling representation of the field. By so doing, one can rewrite expression (1) as follows:

$$|F(\underline{r})|^2 = \left| \sum_{m=1}^{L} F_m S(\underline{r} - \underline{r}_m) + \sum_{k=1}^{Q} F_k S(\underline{r} - \underline{r}_k) \right|^2 \tag{A.1}$$

wherein Q is the number of Nyquist samples located in $\Omega \setminus \Lambda$, $S(\underline{r} - \underline{r}_m)$ are the chosen sampling functions, and F_i denotes the value of the field in the sampling point $\underline{r}_i$. Notably, the first addendum [say $F_{DOM}(\underline{r})$] is known (as field samples have been fixed) while the second addendum [say $F_{RES}(\underline{r})$] is the one actually containing the unknowns.

Moreover, in the shaped zone, by virtue both of the typical behavior of sampling functions as well as of the fact that it depends on the (low-amplitude) sidelobes' samples, the second term can be considered to be negligible (residual) with respect to the first one. Then, by further elaborating (A.1), one finds:

$$|F(\underline{r})|^2 = |F_{DOM}(\underline{r})|^2 + 2\Re\{F_{DOM}(\underline{r})F^*_{RES}(\underline{r})\} + |F_{RES}(\underline{r})|^2 \tag{A.2}$$

wherein the first (and dominant) term is constant, the second term is a linear function of the unknowns, and the third one is a quadratic form of the unknowns. Hence, as long as the quadratic part can be neglected with respect to the previous ones, one can conclude that (A.2) is well approximated (within a controlled accuracy)

by a positive semidefinite quadratic form, and hence by a convex function. Also note that the third and last term can be made smaller and smaller (paying a price in terms of number of samples) by a proper use of the self-truncating sampling functions discussed in [98].

B

Appendix B

This Appendix is aimed at illustrating the meaning of the five parameters we have used to encode polarization.

The total complex *vector* field in (1) is expressed by:

$$\mathbf{E}(\underline{r}) = E_x(\underline{r})i_x + E_y(\underline{r})i_y + E_z(\underline{r})i_z \tag{B.1}$$

i_x, i_y, i_z denoting the unit vectors of the Cartesian coordinate system. As a common phase constant does not alter polarization, a convenient choice is to assume that one component of the field, say $E_x(\underline{r}_t)$, is purely real in the target point. By so doing, a field having a generic polarization and amplitude can be represented by five real quantities, i.e.:

$$\Re\{E_x(\underline{r}_t)\}, \Re\{E_y(\underline{r}_t)\}, \Im\{E_y(\underline{r}_t)\}, \Re\{E_z(\underline{r}_t)\}, \Im\{E_z(\underline{r}_t)\} \tag{B.2}$$

In such a space, every point lying on a single half-line departing from the origin has the same identical polarization, so that the unit vector along the half line univocally identifies the polarization. Hence, if

$$p_1 = \frac{\Re\{E_x(\underline{r}_t)\}}{|\mathbf{E}|}, p_2 = \frac{\Re\{E_y(\underline{r}_t)\}}{|\mathbf{E}|}, p_3 = \frac{\Im\{E_y(\underline{r}_t)\}}{|\mathbf{E}|}, p_4 = \frac{\Re\{E_z(\underline{r}_t)\}}{|\mathbf{E}|}, p_5 = \frac{\Im\{E_z(\underline{r}_t)\}}{|\mathbf{E}|} \tag{B.3}$$

then the unit vector associated to the polarization which is needed in (7) can be finally written as:

$$\mathbf{p} = p_1 i_x + \{p_2 + jp_3\}i_y + \{p_4 + jp_5\}i_z \tag{B.4}$$

so that $\mathbf{E} = |\mathbf{E}|\mathbf{p}$. Note that, in view of definition and expected properties, the parameters p_1,...,p_5 (have to) satisfy the constraint:

$$p_1^2 + p_2^2 + p_3^2 + p_4^2 + p_5^2 = 1 \tag{B.5}$$

This latter property implies that the space of possible polarizations can be regarded as a 5-sphere.

Appendix C

Analytic expression of the gradient

This appendix is devoted to report the expressions of the gradient and the line search parameter related to the cost functional ψ in (18) within a conjugate gradient scheme.

In fact, the conjugate-gradient-based solution of (18) reads:

$$b^{(i+1)} = b^{(i)} + \mu_i A_i \nabla\psi_i \tag{C.1}$$

where i and $i+1$ denotes the i^{th} and $(i+1)^{th}$ iteration, respectively, $\nabla\psi$ is the gradient of ψ and μ_i is a scalar value chosen at each step such to guarantee the maximum decrease along the direction defined by $A\nabla\psi$. Finally, the matrix A characterizes the kind of the adopted minimization.

Herein, we adopted the Polak-Ribiere scheme [58].

Considering that $\Delta\psi_b = \langle \Delta\psi_b, \Delta b \rangle$, the gradient is given by [127]:

$$\begin{aligned} \Delta\psi_{b_{\ell,n}} =& 4w_1^2 \sum_{\widetilde{k}} \sum_{\widetilde{\phi}} \frac{\left(u_{\ell,n}(\widetilde{k}) e^{j\ell\widetilde{\phi}}\right)^* F_{\widetilde{k},\widetilde{\phi}} \left[|F_{\widetilde{k},\widetilde{\phi}}|^2 - \widetilde{F}^2_{\widetilde{k},\widetilde{\phi}} \right]}{\widetilde{F}^2_{\widetilde{k},\widetilde{\phi}}} + \\ & 2w_2^2 \sum_{\widehat{k}} \sum_{\widehat{\phi}} \left(u_{\ell,n}(\widehat{k}) e^{j\ell\widehat{\phi}}\right)^* \left(F_{\widehat{k},\widehat{\phi}} - \widehat{F}_{\widehat{k},\widehat{\phi}}\right) \end{aligned} \tag{C.2}$$

where the superscript $*$ denotes the complex conjugation operation.

The line minimization step is evaluated as:

$$\mu_i = argmin\psi\left(b^{(i)} + \mu_i \nabla b^{(i)}\right) \tag{C.3}$$

where $\nabla b^{(i)}$ is the descent research direction considered at the i^{th} iteration.

Due to the nature of the functional ψ_1 and ψ_2, the overall functional can be rewritten as a fourth-degree algebraic polynomial:

$$\psi_i(\mu) = a\mu^4 + b\mu^3 + c\mu^2 + d\mu + e \tag{C.4}$$

whose coefficients are the following:

$$a = w_1^2 \sum_{\widetilde{k}} \sum_{\widetilde{\phi}} \frac{|f_{\widetilde{k},\widetilde{\phi}}|^4}{\widetilde{F}^2_{\widetilde{k},\widetilde{\phi}}} \tag{C.5}$$

$$b = 4w_1^2 \sum_{\widetilde{k}} \sum_{\widetilde{\phi}} \frac{\left[|f_{\widetilde{k},\widetilde{\phi}}|^2 \cdot \Re\left(F_{\widetilde{k},\widetilde{\phi}} f^*_{\widetilde{k},\widetilde{\phi}}\right)\right]}{\widetilde{F}^2_{\widetilde{k},\widetilde{\phi}}} \tag{C.6}$$

$$\begin{aligned} c =& w_1^2 \sum_{\widetilde{k}} \sum_{\widetilde{\phi}} \frac{4|\Re\left(F_{\widetilde{k},\widetilde{\phi}} f^*_{\widetilde{k},\widetilde{\phi}}\right)|^2}{\widetilde{F}^2_{\widetilde{k},\widetilde{\phi}}} + w_1^2 \sum_{\widetilde{k}} \sum_{\widetilde{\phi}} \frac{2\left[|f_{\widetilde{k},\widetilde{\phi}}|^2 \left(|F_{\widetilde{k},\widetilde{\phi}}|^2 - \widetilde{F}^2_{\widetilde{k},\widetilde{\phi}}\right)\right]}{\widetilde{F}^2_{\widetilde{k},\widetilde{\phi}}} + \\ & w_2^2 \sum_{\widetilde{k}} \sum_{\widetilde{\phi}} |f_{\widetilde{k},\widetilde{\phi}}|^2 \end{aligned} \tag{C.7}$$

$$d = 4w_1^2 \sum_{\widetilde{k}} \sum_{\widetilde{\phi}} \frac{\left[\Re\left(F_{\widetilde{k},\widetilde{\phi}} f^*_{\widetilde{k},\widetilde{\phi}}\right)\left(|F_{\widetilde{k},\widetilde{\phi}}|^2 - \widetilde{F}^2_{\widetilde{k},\widetilde{\phi}}\right)\right]}{\widetilde{F}^2_{\widetilde{k},\widetilde{\phi}}} + 2w_2^2 \sum_{\widetilde{k}} \sum_{\widetilde{\phi}} \Re\left[\left(F_{\widetilde{k},\widetilde{\phi}} - \widetilde{F}^2_{\widetilde{k},\widetilde{\phi}}\right) f^*_{\widetilde{k},\widetilde{\phi}}\right] \tag{C.8}$$

$$e = w_1^2 \sum_{\widetilde{k}} \sum_{\widetilde{\phi}} \frac{\left[|F_{\widetilde{k},\widetilde{\phi}}|^2 - \widetilde{F}^2_{\widetilde{k},\widetilde{\phi}}\right]^2}{\widetilde{F}^2_{\widetilde{k},\widetilde{\phi}}} + w_2^2 \sum_{\widetilde{k}} \sum_{\widetilde{\phi}} |F_{\widetilde{k},\widetilde{\phi}} - \widetilde{F}_{\widetilde{k},\widetilde{\phi}}|^2 \tag{C.9}$$

where:

$$f_{\widetilde{k},\widetilde{\phi}} = \sum_{\ell} \sum_{n} \nabla b_{\ell,n} u_{\ell,n}(k) e^{j\ell\phi} \tag{C.10}$$

for the pertaining (k, ϕ) points.

References

1. J.-Y. Li, Y.-X. Qi, and S.-G. Zhou, "Shaped beam synthesis based on superposition principle and taylor method," *IEEE Transactions on Antennas and Propagation*, vol. 65, no. 11, pp. 6157–6160, 2017.
2. T. Isernia, O. Bucci, and N. Fiorentino, "Shaped beam antenna synthesis problems: Feasibility criteria and new strategies," *Journal of Electromagnetic Waves and Applications*, vol. 12, no. 1, pp. 103–138, 1998.
3. H. Orchard, R. S. Elliott, and G. Stern, "Optimising the synthesis of shaped beam antenna patterns," in *IEE Proceedings H (Microwaves, Antennas and Propagation)*, vol. 132, pp. 63–68, IET, 1985.
4. Y. Liu, Z.-P. Nie, and Q. H. Liu, "A new method for the synthesis of non-uniform linear arrays with shaped power patterns," *Progress In Electromagnetics Research*, vol. 107, pp. 349–363, 2010.
5. B. Fuchs, "Synthesis of sparse arrays with focused or shaped beampattern via sequential convex optimizations," *IEEE Transactions on Antennas and Propagation*, vol. 60, no. 7, pp. 3499–3503, 2012.
6. Y. Liu, X. Huang, K. Da Xu, Z. Song, S. Yang, and Q. H. Liu, "Pattern synthesis of unequally spaced linear arrays including mutual coupling using iterative fft via virtual active element pattern expansion," *IEEE Transactions on Antennas and Propagation*, vol. 65, no. 8, pp. 3950–3958, 2017.
7. A. Rodriguez, R. Munoz, H. Estevez, E. Ares, and E. Moreno, "Synthesis of planar arrays with arbitrary geometry generating arbitrary footprint patterns," *IEEE transactions on antennas and propagation*, vol. 52, no. 9, pp. 2484–2488, 2004.
8. Y.-X. Qi and J.-Y. Li, "Superposition synthesis method for 2-d shaped-beam array antenna," *IEEE Transactions on Antennas and Propagation*, vol. 66, no. 12, pp. 6950–6957, 2018.
9. B. Fuchs, L. Le Coq, and M. D. Migliore, "Fast antenna array diagnosis from a small number of far-field measurements," *IEEE Transactions on Antennas and Propagation*, vol. 64, no. 6, pp. 2227–2235, 2016.

10. H.-T. Chou, N.-N. Wang, H.-H. Chou, and J.-H. Qiu, "An effective synthesis of planar array antennas for producing near-field contoured patterns," *IEEE transactions on antennas and propagation*, vol. 59, no. 9, pp. 3224–3233, 2011.
11. G. G. Bellizzi, D. A. Iero, L. Crocco, and T. Isernia, "Three-dimensional field intensity shaping: The scalar case," *IEEE Antennas and Wireless Propagation Letters*, vol. 17, no. 3, pp. 360–363, 2018.
12. M. Bertero, "Linear inverse and iii-posed problems," in *Advances in electronics and electron physics*, vol. 75, pp. 1–120, Elsevier, 1989.
13. N. Bleistein and J. K. Cohen, "Nonuniqueness in the inverse source problem in acoustics and electromagnetics," *Journal of Mathematical Physics*, vol. 18, no. 2, pp. 194–201, 1977.
14. A. Morabito, R. Palmeri, and T. Isernia, "A compressive-sensing-inspired procedure for array antenna diagnostics by a small number of phaseless measurements," *IEEE Transactions on Antennas and Propagation*, vol. 64, no. 7, pp. 3260–3265, 2016.
15. R. G. Yaccarino and Y. Rahmat-Samii, "Phaseless bi-polar planar near-field measurements and diagnostics of array antennas," *IEEE Transactions on Antennas and Propagation*, vol. 47, no. 3, pp. 574–583, 1999.
16. R. Palmeri, T. Isernia, and A. F. Morabito, "Diagnosis of planar arrays through phaseless measurements and sparsity promotion," *IEEE Antennas and Wireless Propagation Letters*, vol. 18, no. 6, pp. 1273–1277, 2019.
17. J. Laviada, A. Arboleya-Arboleya, Y. Alvarez-Lopez, C. Garcia-Gonzalez, and F. Las-Heras, "Phaseless synthetic aperture radar with efficient sampling for broadband near-field imaging: Theory and validation," *IEEE Transactions on Antennas and Propagation*, vol. 63, no. 2, pp. 573–584, 2014.
18. J. Laviada, Y. Álvarez-López, C. García-González, C. Vázquez-Antuña, S. Ver-Hoeye, M. Fernández-García, G. Hotopan, R. Camblor, and F. Las-Heras, "A novel phaseless frequency scanning based on indirect holography," *Journal of Electromagnetic Waves and Applications*, vol. 27, no. 4, pp. 430–438, 2013.
19. G. Mazzarella, G. Montisci, and G. Serra, "A microwave holographic procedure for large symmetric reflector antennas using a fresnel-zone field data processing," *International Journal of Antennas and Propagation*, vol. 2012, 2012.
20. R. Subrahmanyan, "Photogrammetric measurement of the gravity deformation in a cassegrain antenna," *IEEE transactions on antennas and propagation*, vol. 53, no. 8, pp. 2590–2596, 2005.
21. G. Mazzarella, G. Montisci, N. Schirru, and G. Serra, "A backus-gilbert approach to the reflector surface reconstruction," in *2006 IEEE Antennas and Propagation Society International Symposium*, pp. 1053–1056, IEEE, 2006.
22. O. Bucci, A. Capozzoli, and G. D'elia, "Diagnosis of array faults from far-field amplitude-only data," *IEEE Transactions on Antennas and Propagation*, vol. 48, no. 5, pp. 647–652, 2000.

23. T. Isernia, F. Soldovieri, G. Leone, and R. Pierri, "On the local minima in phase reconstruction algorithms," *Radio Science*, vol. 31, no. 6, pp. 1887–1899, 1996.
24. A. Anderson, G. Junkin, and J. McCormack, "Near-field far-field predictions from single-intensity-planar-scan phase retrieval," *ElL*, vol. 25, p. 519, 1989.
25. T. Isernia, G. Leone, and R. Pierri, "Radiation pattern evaluation from near-field intensities on planes," *IEEE Transactions on Antennas and Propagation*, vol. 44, no. 5, p. 701, 1996.
26. O. M. Bucci, G. D'Elia, and M. D. Migliore, "An effective near-field far-field transformation technique from truncated and inaccurate amplitude-only data," *IEEE Transactions on Antennas and Propagation*, vol. 47, no. 9, pp. 1377–1385, 1999.
27. B. Fuchs and L. Le Coq, "Excitation retrieval of microwave linear arrays from phaseless far-field data," *IEEE Transactions on Antennas and Propagation*, vol. 63, no. 2, pp. 748–754, 2014.
28. D. Morris, "Phase retrieval in the radio holography of reflector antennas and radio telescopes," *IEEE transactions on antennas and propagation*, vol. 33, no. 7, pp. 749–755, 1985.
29. D. A. Iero, T. Isernia, A. F. Morabito, I. Catapano, and L. Crocco, "Optimal constrained field focusing for hyperthermia cancer therapy: A feasibility assessment on realistic phantoms," *Progress In Electromagnetics Research*, vol. 102, pp. 125–141, 2010.
30. M. I. Dessouky, H. A. Sharshar, and Y. A. Albagory, "Design of high altitude platforms cellular communications," *Progress In Electromagnetics Research*, vol. 67, pp. 251–261, 2007.
31. A. F. Morabito, A. R. Lagana, and L. Di Donato, "Satellite multibeam coverage of earth: Innovative solutions and optimal synthesis of aperture fields," *Progress In Electromagnetics Research*, vol. 156, pp. 135–144, 2016.
32. M. Mosalanejad, S. Brebels, C. Soens, I. Ocket, and G. A. Vandenbosch, "Millimeter wave cavity backed microstrip antenna array for 79 ghz radar applications," *Progress In Electromagnetics Research*, vol. 158, pp. 89–98, 2017.
33. F. Soldovieri, R. Solimene, and R. Pierri, "Reconstructing the contour of metallic planar objects from only intensity scattered field data over a single plane," *Optics Express*, vol. 16, no. 13, pp. 9468–9479, 2008.
34. C. Fienup and J. Dainty, "Phase retrieval and image reconstruction for astronomy," *Image recovery: theory and application*, vol. 231, p. 275, 1987.
35. R. P. Millane, "Phase retrieval in crystallography and optics," *JOSA A*, vol. 7, no. 3, pp. 394–411, 1990.
36. T. Isernia and G. Panariello, "Optimal focusing of scalar fields subject to arbitrary upper bounds," *Electronics letters*, vol. 34, no. 2, pp. 162–164, 1998.
37. A. Capozzoli, C. Curcio, G. D'Elia, and A. Liseno, "Phaseless antenna characterization by effective aperture field and data representations," *IEEE Transactions on Antennas and Propagation*, vol. 57, no. 1, pp. 215–230, 2009.

38. D. Misell, "A method for the solution of the phase problem in electron microscopy," *Journal of Physics D: Applied Physics*, vol. 6, no. 1, p. L6, 1973.
39. B. Fuchs, M. Mattes, S. Rondineau, and L. Le Coq, "Phaseless near-field antenna measurements from two surface scans—numerical and experimental investigations," *IEEE Transactions on Antennas and Propagation*, vol. 68, no. 3, pp. 2315–2322, 2019.
40. R. Pierri, G. D'Elia, and F. Soldovieri, "A two probes scanning phaseless near-field far-field transformation technique," *IEEE Transactions on Antennas and Propagation*, vol. 47, no. 5, pp. 792–802, 1999.
41. A. Laganà, A. Morabito, and T. Isernia, "Phase retrieval by constrained power inflation and signum flipping," *Radio Science*, vol. 51, no. 12, pp. 1855–1863, 2016.
42. A. F. Morabito, R. Palmeri, V. A. Morabito, A. R. Laganà, and T. Isernia, "Single-surface phaseless characterization of antennas via hierarchically ordered optimizations," *IEEE Transactions on Antennas and Propagation*, vol. 67, no. 1, pp. 461–474, 2018.
43. T. Isernia and A. Morabito, "Mask-constrained power synthesis of linear arrays with even excitations," *IEEE Transactions on Antennas and Propagation*, vol. 64, no. 7, pp. 3212–3217, 2016.
44. S. Marchesini, "Invited article: A unified evaluation of iterative projection algorithms for phase retrieval," *Review of scientific instruments*, vol. 78, no. 1, p. 011301, 2007.
45. C. A. Balanis, *Antenna Theory, Analysis, and Design*. Harper & Row Publishers Inc., NewYork, 1982.
46. R. S. Elliot, *Antenna theory and design*, vol. 7632. Prentice-Hall Inc., Englewood Cliffs, New Jersey, 1981.
47. E. C. Jordan and K. G. Balmain, *Electromagnetic Waves and Radiating Systems*. Prentice Hall, Englewood Cliffs, New Jersey, 1968.
48. T. Isernia, P. Di Iorio, and F. Soldovieri, "An effective approach for the optimal focusing of array fields subject to arbitrary upper bounds," *IEEE Transactions on Antennas and Propagation*, vol. 48, no. 12, pp. 1837–1847, 2000.
49. L. Caccavale, F. Soldovier, and T. Isernia, "Methods for optimal focusing of microstrip array antennas including mutual coupling," *IEE Proceedings-Microwaves, Antennas and Propagation*, vol. 147, no. 3, pp. 199–202, 2000.
50. O. M. Bucci, L. Caccavale, and T. Isernia, "Optimal far-field focusing of uniformly spaced arrays subject to arbitrary upper bounds in nontarget directions," *IEEE Transactions on Antennas and Propagation*, vol. 50, no. 11, pp. 1539–1554, 2002.
51. A. F. Morabito, A. R. Lagana, and T. Isernia, "On the optimal synthesis of ring symmetric shaped patterns by means of uniformly spaced planar arrays," *Progress In Electromagnetics Research*, vol. 20, pp. 33–48, 2010.
52. O. M. Bucci, T. Isernia, and A. F. Morabito, "Optimal synthesis of circularly symmetric shaped beams," *IEEE Transactions on Antennas and Propagation*, vol. 62, no. 4, pp. 1954–1964, 2014.
53. A. Nemirovsky, *Problem complexity and method efficiency in optimization*.

54. G. G. Bellizzi, L. Crocco, G. M. Battaglia, and T. Isernia, "Multi-frequency constrained sar focusing for patient specific hyperthermia treatment," *IEEE Journal of Electromagnetics, RF and Microwaves in Medicine and Biology*, vol. 1, no. 2, pp. 74–80, 2017.

55. A. Buffi, A. Serra, P. Nepa, G. Manara, and M. Luise, "Near field focused microstrip arrays for gate access control systems," in *2009 IEEE Antennas and Propagation Society International Symposium*, pp. 1–4, IEEE, 2009.

56. I. Iliopoulos, M. Casaletti, R. Sauleau, P. Pouliguen, P. Potier, and M. Ettorre, "3-d shaping of a focused aperture in the near field," *IEEE Transactions on Antennas and Propagation*, vol. 64, no. 12, pp. 5262–5271, 2016.

57. Y. Nesterov, H. Wolkowicz, and Y. Ye, "Semidefinite programming relaxations of nonconvex quadratic optimization," in *Handbook of semidefinite programming*, pp. 361–419, Springer, 2000.

58. D. G. Luenberger, Y. Ye, *et al.*, *Linear and nonlinear programming*, vol. 2. Springer, 1984.

59. G. G. Bellizzi, M. M. Paulides, T. Drizdal, G. C. van Rhoon, L. Crocco, and T. Isernia, "Selecting the optimal subset of antennas in hyperthermia treatment planning," *IEEE Journal of Electromagnetics, RF and Microwaves in Medicine and Biology*, vol. 3, no. 4, pp. 240–246, 2019.

60. E. Zastrow, S. C. Hagness, B. D. Van Veen, and J. E. Medow, "Time-multiplexed beamforming for noninvasive microwave hyperthermia treatment," *IEEE transactions on biomedical engineering*, vol. 58, no. 6, pp. 1574–1584, 2011.

61. G. G. Bellizzi, T. Drizdal, L. Crocco, G. C. van Rhoon, T. Isernia, and M. M. Paulides, "Multi-target foco for head&neck hyperthermia treatment planning: A feasibility study," in *2018 IEEE International Symposium on Antennas and Propagation & USNC/URSI National Radio Science Meeting*, pp. 577–578, IEEE, 2018.

62. E. Zastrow, S. C. Hagness, and B. D. Van Veen, "3d computational study of noninvasive patient-specific microwave hyperthermia treatment of breast cancer," *Physics in Medicine & Biology*, vol. 55, no. 13, p. 3611, 2010.

63. G. G. Bellizzi, M. M. Paulides, T. Drizdal, G. C. van Rhoon, L. Crocco, and T. Isernia, "Sparsity promoted antenna selection in hyperthermia treatment planning," in *2018 EMF-Med 1st World Conference on Biomedical Applications of Electromagnetic Fields (EMF-Med)*, pp. 1–2, IEEE, 2018.

64. G. M. Battaglia, G. G. Bellizzi, A. F. Morabito, G. Sorbello, and T. Isernia, "A general effective approach to the synthesis of shaped beams for arbitrary fixed-geometry arrays," *Journal of Electromagnetic Waves and Applications*, vol. 33, no. 18, pp. 2404–2422, 2019.

65. G. M. Battaglia, A. F. Morabito, G. Sorbello, and T. Isernia, "Mask-constrained power synthesis of large and arbitrary arraysas a few-samples global optimization," *Progress In Electromagnetics Research*, vol. 98, pp. 69–81, 2020.

66. G. Battaglia, A. Morabito, R. Palmeri, and T. Isernia, "Constrained focusing of vector fields intensity in near zone and/or complex scenarios as a low-dimensional global optimization," *Journal of Electromagnetic Waves and Applications*, vol. 34, no. 15, pp. 1977–1989, 2020.

67. P. Woodward and J. Lawson, "The theoretical precision with which an arbitrary radiation-pattern may be obtained from a source of finite size," *Journal of the Institution of Electrical Engineers-Part III: Radio and Communication Engineering*, vol. 95, no. 37, pp. 363–370, 1948.

68. R. Elliott and G. Stern, "A new technique for shaped beam synthesis of equispaced arrays," *IEEE Transactions on Antennas and Propagation*, vol. 32, no. 10, pp. 1129–1133, 1984.

69. T. Isernia, "Problemi di sintesi in potenza: criteri di esistenza e nuove strategie," *Proceedings X Riunione di Elettromagnetismo*, pp. 533–536, 1994.

70. S.-P. Wu, S. Boyd, and L. Vandenberghe, "Fir filter design via spectral factorization and convex optimization," in *Applied and computational control, signals, and circuits*, pp. 215–245, Springer, 1999.

71. R. S. Elliott, "Criticisms of the woodward-lawson method," *IEEE Antennas and Propagation Society Newsletter*, vol. 30, no. 3, pp. 43–43, 1988.

72. D. W. Boeringer and D. H. Werner, "Particle swarm optimization versus genetic algorithms for phased array synthesis," *IEEE Transactions on antennas and propagation*, vol. 52, no. 3, pp. 771–779, 2004.

73. Y. Liu, Q. H. Liu, and Z. Nie, "Reducing the number of elements in the synthesis of shaped-beam patterns by the forward-backward matrix pencil method," *IEEE Transactions on Antennas and Propagation*, vol. 58, no. 2, pp. 604–608, 2009.

74. B. Fuchs, "Application of convex relaxation to array synthesis problems," *IEEE Transactions on Antennas and Propagation*, vol. 62, no. 2, pp. 634–640, 2013.

75. O. M. Bucci, T. Isernia, and A. F. Morabito, "An effective deterministic procedure for the synthesis of shaped beams by means of uniform-amplitude linear sparse arrays," *IEEE Transactions on Antennas and Propagation*, vol. 61, no. 1, pp. 169–175, 2012.

76. A. F. Morabito and P. G. Nicolaci, "Optimal synthesis of shaped beams through concentric ring isophoric sparse arrays," *IEEE Antennas and Wireless Propagation Letters*, vol. 16, pp. 979–982, 2016.

77. A. Morabito, A. Massa, P. Rocca, and T. Isernia, "An effective approach to the synthesis of phase-only reconfigurable linear arrays," *IEEE Transactions on Antennas and Propagation*, vol. 60, no. 8, pp. 3622–3631, 2012.

78. A. F. Morabito, "Synthesis of maximum-efficiency beam arrays via convex programming and compressive sensing," *IEEE Antennas and Wireless Propagation Letters*, vol. 16, pp. 2404–2407, 2017.

79. S. E. Nai, W. Ser, Z. L. Yu, and H. Chen, "Beampattern synthesis for linear and planar arrays with antenna selection by convex optimization," *IEEE Transactions on Antennas and Propagation*, vol. 58, no. 12, pp. 3923–3930, 2010.
80. O. M. Bucci, C. Gennarelli, and C. Savarese, "Representation of electromagnetic fields over arbitrary surfaces by a finite and nonredundant number of samples," *IEEE Transactions on Antennas and Propagation*, vol. 46, no. 3, pp. 351–359, 1998.
81. C. A. Balanis, *Ansoft High Frequency Structural Simulator (HFSS)*. Pittsburgh (PA): Ansoft Cor, Ver. 13, 2010.
82. O. Bucci and M. D'urso, "Power pattern synthesis of given sources exploiting array methods," 2007.
83. G. Bellizzi and O. M. Bucci, "On the optimal synthesis of sum or difference patterns of centrosymmetric arrays under arbitrary sidelobe constraints," *IEEE Transactions on Antennas and Propagation*, vol. 66, no. 9, pp. 4620–4626, 2018.
84. T. Zhang and W. Ser, "Robust beampattern synthesis for antenna arrays with mutual coupling effect," *IEEE transactions on antennas and propagation*, vol. 59, no. 8, pp. 2889–2895, 2011.
85. P. Cao, J. S. Thompson, and H. Haas, "Constant modulus shaped beam synthesis via convex relaxation," *IEEE Antennas and Wireless Propagation Letters*, vol. 16, pp. 617–620, 2016.
86. B. Fuchs, "Shaped beam synthesis of arbitrary arrays via linear programming," *IEEE antennas and wireless propagation letters*, vol. 9, pp. 481–484, 2010.
87. S. Ho and S. Yang, "Multiobjective synthesis of antenna arrays using a vector tabu search algorithm," *IEEE Antennas and Wireless Propagation Letters*, vol. 8, pp. 947–950, 2009.
88. A. F. Morabito and P. Rocca, "Reducing the number of elements in phase-only reconfigurable arrays generating sum and difference patterns," *IEEE Antennas and Wireless Propagation Letters*, vol. 14, pp. 1338–1341, 2015.
89. O. Bucci, T. Isernia, A. Morabito, S. Perna, and D. Pinchera, "Aperiodic arrays for space applications: An effective strategy for the overall design," in *2009 3rd European Conference on Antennas and Propagation*, pp. 2031–2035, IEEE, 2009.
90. O. Bucci, M. D'Urso, and T. Isernia, "Optimal synthesis of difference patterns subject to arbitrary sidelobe bounds by using arbitrary array antennas," *IEE Proceedings-Microwaves, Antennas and Propagation*, vol. 152, no. 3, pp. 129–137, 2005.
91. L. Poli and G. Oliveri, "Optimal sub-arraying of compromise planar arrays through an innovative aco-weighted procedure," 2010.
92. A. F. Morabito, T. Isernia, and L. Di Donato, "Optimal synthesis of phase-only reconfigurable linear sparse arrays having uniform-amplitude excitations," *Progress In Electromagnetics Research*, vol. 124, pp. 405–423, 2012.

93. G. K. Mahanti, A. Chakraborty, and S. Das, "Phase-only and amplitude-phase only synthesis of dual-beam pattern linear antenna arrays using floating-point genetic algorithms," *Progress In Electromagnetics Research*, vol. 68, pp. 247–259, 2007.

94. W.-B. Wang, Q. Feng, and D. Liu, "Application of chaotic particle swarm optimization algorithm to pattern synthesis of antenna arrays," *Progress In Electromagnetics Research*, vol. 115, pp. 173–189, 2011.

95. D. Liu, Q. Feng, W.-B. Wang, and X. Yu, "Synthesis of unequally spaced antenna arrays by using inheritance learning particle swarm optimization," *Progress In Electromagnetics Research*, vol. 118, pp. 205–221, 2011.

96. C. A. Floudas and P. M. Pardalos, *State of the art in global optimization: computational methods and applications*, vol. 7. Springer Science & Business Media, 2013.

97. A. F. Morabito, A. Di Carlo, L. Di Donato, T. Isernia, and G. Sorbello, "Extending spectral factorization to array pattern synthesis including sparseness, mutual coupling, and mounting-platform effects," *IEEE Transactions on Antennas and Propagation*, vol. 67, no. 7, pp. 4548–4559, 2019.

98. O. M. Bucci and G. Di Massa, "The truncation error in the application of sampling series to electromagnetic problems," *IEEE transactions on antennas and propagation*, vol. 36, no. 7, pp. 941–949, 1988.

99. R. G. Compton, B. A. Coles, and F. Marken, "Microwave activation of electrochemical processes at microelectrodes," *Chemical communications*, no. 23, pp. 2595–2596, 1998.

100. J. P. O'Callaghan and K. Sriram, "Focused microwave irradiation of the brain preserves in vivo protein phosphorylation: comparison with other methods of sacrifice and analysis of multiple phosphoproteins," *Journal of neuroscience methods*, vol. 135, no. 1-2, pp. 159–168, 2004.

101. A. F. Morabito, "Power synthesis of mask-constrained shaped beams through maximally-sparse planar arrays.," *Telkomnika*, vol. 14, no. 4, 2016.

102. A. Buffi, A. Serra, P. Nepa, G. Manara, *et al.*, "A focused planar microstrip array for 2.4 ghz rfid readers," *IEEE Transactions on Antennas and Propagation*, vol. 58, no. 5, pp. 1536–1544, 2010.

103. H.-T. Chou, T.-M. Hung, N.-N. Wang, H.-H. Chou, C. Tung, and P. Nepa, "Design of a near-field focused reflectarray antenna for 2.4 ghz rfid reader applications," *IEEE Transactions on Antennas and Propagation*, vol. 59, no. 3, pp. 1013–1018, 2010.

104. H.-T. Chou, M.-Y. Lee, and C.-T. Yu, "Subsystem of phased array antennas with adaptive beam steering in the near-field rfid applications," *IEEE Antennas and Wireless Propagation Letters*, vol. 14, pp. 1746–1749, 2015.

105. D. M. Sheen, D. L. McMakin, T. E. Hall, and R. H. Severtsen, "Active millimeter-wave standoff and portal imaging techniques for personnel screening," in *2009 IEEE Conference on Technologies for Homeland Security*, pp. 440–447, IEEE, 2009.

106. A. F. Morabito, L. Di Donato, and T. Isernia, "Orbital angular momentum antennas: Understanding actual possibilities through the aperture antennas theory," *IEEE Antennas and Propagation Magazine*, vol. 60, no. 2, pp. 59–67, 2018.

107. J. Alvarez, R. Ayestarán, and F. Las-Heras, "Design of antenna arrays for near-field focusing requirements using optimisation," *Electronics letters*, vol. 48, no. 21, pp. 1323–1325, 2012.

108. D. A. M. Iero, "Constrained power focusing in inhomogeneous media as a polarization optimization," *International Journal of Antennas and Propagation*, vol. 2015, 2015.

109. D. A. Iero, L. Crocco, and T. Isernia, "Constrained power focusing of vector fields: an innovative globally optimal strategy," *Journal of Electromagnetic Waves and Applications*, vol. 29, no. 13, pp. 1708–1719, 2015.

110. S. J. Yang, Y. D. Kim, D. W. Yi, N. H. Myung, *et al.*, "Antenna modeling using sparse infinitesimal dipoles based on recursive convex optimization," *IEEE Antennas and Wireless Propagation Letters*, vol. 17, no. 4, pp. 662–665, 2018.

111. G. Franceschetti, *Electromagnetics: theory, techniques, and engineering paradigms*. Springer Science & Business Media, 2013.

112. R. M. Von Bunau, H. Fukuda, and T. Terasawa, "Phase retrieval from defocused images and its applications in lithography," *Japanese journal of applied physics*, vol. 36, no. 12S, p. 7494, 1997.

113. T. Isernia, A. R. Laganà, D. A. M. Iero, A. F. Morabito, A. Carlström, and G. Toso, "Optimization of the array element layout for a rotating imaging interferometer," *IEEE transactions on antennas and propagation*, vol. 61, no. 10, pp. 5057–5067, 2013.

114. A. Grjasnow, A. Wuttig, and R. Riesenberg, "Phase resolving microscopy by multi-plane diffraction detection," *Journal of microscopy*, vol. 231, no. 1, pp. 115–123, 2008.

115. F. Üstüner, E. Aydemir, E. Güleç, M. İlarslan, M. Çelebi, and E. Demirel, "Antenna radiation pattern measurement using an unmanned aerial vehicle (uav)," in *2014 XXXIth URSI General Assembly and Scientific Symposium (URSI GASS)*, pp. 1–4, IEEE, 2014.

116. G. Junkin, "Planar near-field phase retrieval using gpus for accurate thz far-field prediction," *IEEE transactions on antennas and propagation*, vol. 61, no. 4, pp. 1763–1776, 2012.

117. K. Knopp, "Theory of functions parts i and ii, two volumes bound as one, part i," 1996.

118. R. Pierri and R. Moretta, "On data increasing in phase retrieval via quadratic inversion: flattening manifold and local minima," *IEEE Transactions on Antennas and Propagation*, 2020.

119. F. Soldovieri, A. Liseno, G. D'Elia, and R. Pierri, "Global convergence of phase retrieval by quadratic approach," *IEEE transactions on antennas and propagation*, vol. 53, no. 10, pp. 3135–3141, 2005.

120. P. Netrapalli, P. Jain, and S. Sanghavi, "Phase retrieval using alternating minimization," in *Advances in Neural Information Processing Systems*, pp. 2796–2804, 2013.

121. E. J. Candès and X. Li, "Solving quadratic equations via phaselift when there are about as many equations as unknowns," *Foundations of Computational Mathematics*, vol. 14, no. 5, pp. 1017–1026, 2014.

122. A. Morabito, P. Nicolaci, R. Palmeri, and T. Isernia, "Two-dimensional phase retrieval as a 'crosswords' problem," in *2019 13th European Conference on Antennas and Propagation (EuCAP)*, pp. 1–4, IEEE, 2019.

123. A. Morabito, R. Palmeri, and T. Isernia, "Phase retrieval of scalar fields radiated by finite-dimensional sources through single-surface measurements and a crosswords-like processing," in *2019 PhotonIcs & Electromagnetics Research Symposium-Spring (PIERS-Spring)*, pp. 540–546, IEEE, 2019.

124. J.-M. Zuo, I. Vartanyants, M. Gao, R. Zhang, and L. Nagahara, "Atomic resolution imaging of a carbon nanotube from diffraction intensities," *Science*, vol. 300, no. 5624, pp. 1419–1421, 2003.

125. J. Illade-Quinteiro, J. Rodriguez-González, and F. Ares-Pena, "Shaped-pattern synthesis by spreading out collapsed distributions," *IEEE Antennas and Propagation Magazine*, vol. 52, no. 6, pp. 110–114, 2010.

126. E. W. Hansen, *Fourier transforms: principles and applications*. John Wiley & Sons, 2014.

127. T. Isernia, G. Leone, R. Pierri, and F. Soldovieri, "Role of support information and zero locations in phase retrieval by a quadratic approach," *JOSA A*, vol. 16, no. 7, pp. 1845–1856, 1999.

128. J. Ruze, "Antenna tolerance theory—a review," *Proceedings of the IEEE*, vol. 54, no. 4, pp. 633–640, 1966.

129. Y. Rahmat-Samii, "Microwave holography of large reflector antennas–simulation algorithms," *IEEE Transactions on antennas and Propagation*, vol. 33, no. 11, pp. 1194–1203, 1985.

130. J. Huang, H. Jin, Q. Ye, and G. Meng, "Surface deformation recovery algorithm for reflector antennas based on geometric optics," *Optics Express*, vol. 25, no. 20, pp. 24346–24361, 2017.

131. J. Bennett, A. Anderson, P. McInnes, and A. Whitaker, "Microwave holographic metrology of large reflector antennas," *IEEE Transactions on Antennas and Propagation*, vol. 24, no. 3, pp. 295–303, 1976.

132. P. F. Scott and M. Ryle, "A rapid method for measuring the figure of a radio telescope reflector," *Monthly Notices of the Royal Astronomical Society*, vol. 178, no. 4, pp. 539–545, 1977.

133. M. Godwin, A. Whitaker, J. Bennett, and A. Anderson, "Microwave diagnostics of the chilbolton 25m antenna using the ots satellite," in *icap*, pp. 232–236, 1981.

134. C. E. Mayer, J. H. Davis, W. L. Peters, and W. J. Vogel, "A holographic surface measurement of the texas 4.9-m antenna at 86 ghz," *IEEE Transactions on instrumentation and measurement*, vol. 32, no. 1, pp. 102–109, 1983.

135. R. K. Amineh, J. McCombe, and N. K. Nikolova, "Microwave holographic imaging using the antenna phaseless radiation pattern," *IEEE Antennas and Wireless Propagation Letters*, vol. 11, pp. 1529–1532, 2012.

136. Y. Xu, Q. Ye, and G. Meng, "Optimisation of phase factor in phase retrieval for reflector antennas with active surface," *IET Microwaves, Antennas & Propagation*, vol. 12, no. 15, pp. 2285–2291, 2018.

137. H. Jin, J. Huang, Q. Ye, G. Meng, B. Xiang, and N. Wang, "Surface shape detection with a single far-field intensity by combined amplitude and phase retrieval," *International Journal of Antennas and Propagation*, vol. 2019, 2019.

138. A. Capozzoli and G. D'Elia, "Global optimization and antenna synthesis and diagnosis, part two: applications to advanced reflector antennas synthesis and diagnosis techniques," *Progress In Electromagnetics Research*, vol. 56, pp. 233–261, 2006.

139. T. Isernia, G. Leone, and R. Pierri, "Phase retrieval of radiated fields," *Inverse Problems*, vol. 11, no. 1, p. 183, 1995.

140. J. R. Fienup, "Phase retrieval algorithms: a comparison," *Applied optics*, vol. 21, no. 15, pp. 2758–2769, 1982.

141. R. Piessens, "The transforms and applications handbook," 1996.

142. M. Bertero, *Introduction to inverse problems in imaging*. CRC press, 2020.

143. F. W. Born, M. Born, E. Wolf, and A. B. Bhatia, *Principles of optics: electromagnetic theory of propagation, interference and diffraction of light*. Pergamon, 1980.

Publications

1. G. G. Bellizzi, L. Crocco, G. M. Battaglia, T. Isernia, "Multi-frequency constrained SAR focusing for patient specific hyperthermia treatment," in *IEEE Journal of Electromagnetics, RF and Microwaves in Medicine and Biology*, 1(2), 74-80, 2017.
2. G. M. Battaglia, G. G. Bellizzi, A. F. Morabito, G. Sorbello, T. Isernia, "A General Effective Approach to the Synthesis of Shaped Beams for Arbitrary Fixed-Geometry Arrays," in *Journal of Electromagnetic Waves and Application*, 33.18 (2019): 2404-2422.
3. G. M. Battaglia, A. F. Morabito, G. Sorbello, T. Isernia, "Mask-Constrained Power Synthesis of Large and Arbitrary Arrays as a Few Samples Global Optimization," in *Progress In Electromagnetics Research*, 98 (2020): 69-81.
4. G. M. Battaglia, A. F. Morabito, R. Palmeri, T. Isernia, "Constrained focusing of vector fields intensity in near zone and/or complex scenarios as a low-dimensional global optimization," in *Journal of Electromagnetic Waves and Applications*, 34.15 (2020): 1977-1989.
5. G. G. Bellizzi, M. T. Bevacqua, G. M. Battaglia, L. Crocco, T. Isernia, "Advances in Target Conformal SAR Deposition For Hyperthermia Treatment Planning," in *2nd URSI AT-RASC*, Gran Canaria, 2018.
6. A. F. Morabito, G. M. Battaglia, G. G. Bellizzi, T. Isernia, "A General Approach To The Optimal Synthesis Of Shaped-Beams Through Fixed Geometry Arrays," in *IEEE AP-S International Symposium*, Boston, 2018.
7. G. M. Battaglia, G. G. Bellizzi, T. Isernia, A. F. Morabito, "Optimal Synthesis of Shaped Beams for Generic Fixed Geometry Arrays," in *XXII RiNEm*, Cagliari, 2018.
8. G. G. Bellizzi, G. M. Battaglia, M. T. Bevacqua, L. Crocco, T. Isernia, "FOCO: A Novel Versatile Tool in Hyperthermia Treatment Planning," in *1 3th European Conference on Antennas and Propagation (EuCAP) IEEE*, 2019, p. 1-4.
9. G. M. Battaglia, G. G. Bellizzi, A. F. Morabito, G. Sorbello, T. Isernia, "A Hybrid Approach for the Optimal Synthesis of Shaped-Beams Through Generic Arrays," in *13th European Conference on Antennas and Propagation (EuCAP) IEEE*, 2019, p. 1-4.

10. G. M. Battaglia, G. G. Bellizzi, A. F. Morabito, G. Sorbello, T. Isernia, "Synthesis of 2-D Shaped Beams through Generic Fixed-Geometry Arrays: A New Hybrid Approach," in *IEEE AP-S International Symposium*, Atlanta, 2019.
11. G. M. Battaglia, A. F. Morabito, T. Isernia, "Field intensity focusing and shaping in complex 3-D scenarios: A unitary perspective for actual optimality," in *Riunione Congiunta GTTI-SIEm*, Pavia, 2019.
12. G. M. Battaglia, T. Isernia, A. F. Morabito, "Optimal Antenna Array Pattern Synthesis via Hybrid Optimization," in 23^{rd} *International Conference on Applied Electromagnetics and Communications*, Croazia, 2019.
13. G. M. Battaglia, A. F. Morabito, R. Palmeri, T. Isernia, "Retrieval and Synthesis of Sources having a Circular Support and Generating Given Shaped Beams," in *URSI GASS*, 2020.
14. G. M. Battaglia, A. F. Morabito, R. Palmeri, T. Isernia, "Towards 3-D Vector Intensity Focusing of Near and Far Fields," in *14th European Conference on Antennas and Propagation (EuCAP) IEEE*, 2020, p. 1-3.
15. G. M. Battaglia, R. Palmeri, A. F. Morabito, T. Isernia, "Phase Retrieval for Reflector Antennas Diagnostics through a Concentric 'X-words-like' Approach," in *RiNEm 2020.*
16. G. M. Battaglia, R. Palmeri, A. F. Morabito, T. Isernia, "A New "X-Words Like" Approach to Two Dimensional Phase Retrieval Problems," in *15th European Conference on Antennas and Propagation (EuCAP) IEEE*, 2021 (accepted).
17. G. M. Battaglia, R. Palmeri, A. F. Morabito, P. G. Nicolaci, T. Isernia, "A Non-Iterative Crosswords-Inspired Approach to the Recovery of 2-D Discrete Signals from Phaseless Fourier Transform Data", IEEE Open Journal of Antennas and Propagation, 2020 (submitted).